CANADIAN THESES

THÈSES CANADIENNES

NOTICE

The quality of this microfiche is heavily dependent upon the quality of the original thesis submitted for microfilming. Every effort has been made to ensure the highest quality of reproduction possible.

If pages are missing, contact the university which granted the degree.

Some pages may have indistinct print especially if the original pages were typed with a poor typewriter ribbon or if the university sent us an inferior photocopy.

Previously copyrighted materials (journal articles, published tests, etc.) are not filmed.

Reproduction in full or in part of this film is governed by the Canadian Copyright Act, R.S.C. 1970, c. C-30.

AVIS

La qualité de cette microfiche dépend grandement de la qualité de la thèse soumise au microfilmage. Nous avons tout fait pour assurer une qualité supérieure de reproduction.

S'il manque des pages, veuillez communiquer avec l'université qui a conféré le grade.

La qualité d'impression de certaines pages peut laisser à désirer, surtout si les pages originales ont été dactylographiées à l'aide d'un ruban usé ou si l'université nous a fait parvenir une photocopie de qualité inférieure.

Les documents qui ~~font~~ déjà l'objet d'un droit d'auteur (articles de revue, examens publiés, etc.) ne sont pas microfilmés.

La reproduction, même partielle, de ce microfilm est soumise à la Loi canadienne sur le droit d'auteur, SRG 1970, c. C-30.

THIS DISSERTATION
HAS BEEN MICROFILMED
EXACTLY AS RECEIVED

LA THÈSE A ÉTÉ
MICROFILMÉE TELLE QUE
NOUS L'AVONS REÇUE

NL-339 (r.86/06)

Canada

A CHARACTERIZATION OF THE FREQUENCY SELECTIVE FADING OF THE MOBILE RADIO CHANNEL

by

PIERRE MELANÇON

A thesis
presented to the University of Ottawa
in partial fulfillment of the
requirements for the degree of
Master of Applied Science
in
Department of Electrical Engineering

OTTAWA, ONTARIO, 1986

ISBN 0-315-33290-5

The University of Ottawa requires the signatures of all persons using or photocopying this thesis. Please sign below and give address and date.

ABSTRACT

The aim of this thesis is to examine the characteristics of the mobile radio channel from the point-of-view of its frequency selectivity over its passband. The measurement technique used for the experiments is a multitone method. This technique probes the channel's transfer function by the simultaneous transmission of several tones. The statistical knowledge of the transfer function is particularly important for digital communications, where frequency selectivity increases the bit error probability due to the introduction of excessive intersymbol interference.

The results gathered show the presence of frequency selectivity even for bandwidths as small as 32 kHz. The most disturbing factor is the presence of hills, which diffracts the signals resulting in serious frequency selectivity. Moreover, multiple reflections, such as those encountered in an urban environment, are also the source of the frequency selectivity phenomenon, but have lesser effects than diffraction. The coherence bandwidth, a measure of the frequency selectivity, was found from more than 1000 kHz to less than 200 kHz in the experiments conducted here. The effect of this phenomenon on the probability of error is shown to range from 1.2×10^{-4} to 11.9×10^{-5} assuming differential phase shift keying modulation, infinite signal-to-noise ratio and a baud rate of 9600.

ACKNOWLEDGMENTS

This thesis has been realized in collaboration with the Communications Reasearch Centre. I wish to thank Dr. J.S. Belrose, director of the DRC section at the CRC for his support.

I am very thankful to Dr. J. LeBel who originally suggested the idea for the research done in this thesis. Throughout this project, he gave me much encouragement and useful suggestions.

I would like to thank Dr. P.Galko from the University of Ottawa and Dr. A.U.H.Sheikh from the Carleton University for their support and for the many interesting discussions we had.

I would like to express my appreciation to Dr. M. Burke who made many useful suggestions.

Finally, I wish to express my special appreciation to my wife Solange for her patience and support throughout this long project.

TABLE OF CONTENTS

LIST OF FIGURES

LIST OF TABLES

LIST OF SYMBOLS

$*a, b, c, d$	: Constant or represent a waveform s_0 or s_1.
$*B_r(\tau)$	: Variable.
$*B_c$	: Coherence bandwidth.
$*d$	: Normalized data rate $(1/TB_c)$.
D	: Average delay of an average power delay profile $P(\tau_n)$.
$*E$	: Transmitted signal power.
$E\{x\}$	: Expected value of x.
f	: Frequency (Hz).
f_c	: Carrier frequency.
$*F_L(\gamma)$	: $Pr(q > 0)$.
$*G_L(\gamma)$	: $Pr(q < 0)$.
$h(t)$	: Equivalent baseband impulse response of the channel.
$H(f)$	: Equivalent baseband frequency response of the channel.
H_I	: In phase component of $H(f)$.
H_Q	: Quadrature component of $H(f)$.
$I(\tau), Q(\tau)$	: Low-pass quadrature components obtained from the correlator.
$*L$	: Number of diversity branches.
m	: Mean of x_0.
$*m_{rs}$	: Moment of U_k and V_k.
n	: Index.
$n(t)$	: White gaussian noise.
$*N_0$	: Received noise power.
$p(\tau)$	: Power delay profile.
$p(x)$	: Density probability of amplitude x.
$*p_0$	: Error probability of receiving a bit 1 while a 0 is transmitted.
$*p_1$	: Error probability of receiving a bit 0 while a 1 is transmitted.
$*P$	: Matrix of value related to the received signal once demodulated by the receiver.
$*p_{abcd}$	: Probability of error caused by the sequence of symbols *abcd*.
$P(\tau_n)$	: Average power delay profile.
PER	: Probability of error.

$*Pr(q>0)$	: Probability that $q>0$.
$*Pr(q<0)$	: Probability that $q<0$.
r	: Envelope of $x(t)$.
$*r(\tau)$	: Time equivalent of $R(\Omega)$.
$R_f(\Omega), *R(\Omega)$	: Autocorrelation function of $T(f)$ for a frequency separation Ω.
$s(t)$	: Transmitted signal.
$*s_0(t), s_1(t)$	: Transmitted pulses.
$*S_0(f), S_1(f)$	: Spectrum of $s_0(t), s_1(t)$.
S	: Delay spread of an average power delay profile $P(\tau_n)$.
SNR	: Signal-to-Noise Ratio.
$*T$	: Duration of a symbol.
$*1/T$	: Data rate.
$T(f)$	: Tranfer function of the mobile radio channel.
$u(t)$	: Low-pass equivalent of $s(t)$.
$*U_k$	: Complex envelope of the sampled output of the delayed matched filter receiver.
V	: Velocity of the mobile unit (m/s).
$*V_k$	: Complex envelope of the sampled output of the undelayed matched filter receiver.
x	: Amplitude of h_I and h_Q.
x_0	: Variance of $p(x)$ or mean signal stength of the envelope r.
$x(t)$	: Received bandwidth signal.
$y(t)$	: Low-pass equivalent of $X(t)$.
$*y_k(t)$	: Complex envelope of the received signal.
$*Y_k(f)$	: Fourier transform of $y_k(t)$.
α_n	: Path strength associated with the path n.
$*\gamma$	: Parameter dependent upon the SNR and the type of receiver.
$*\rho(\tau)$	: Autocorrelation of $h(t)$.
$*\bar{\rho}$	: SNR ($\sigma^2 E/N_0$).
$*\rho_{ab\bar{b}c}, \rho_{abbc}$	: Equivalent SNR.
σ	: Standard deviation of X_0.
$*\sigma^2 E$	: Received signal power.
λ	: Wavelength of the signal (m).
$*\lambda_{rs}$	: Variable.

τ_0, τ_A : Minimum propagation path delay.

τ_n : Propagation path delay associated with the path n.

ϕ : Angle of arrival of a signal relatif to the direction of the receiving mobile unit.

ϕ_n : Phase shift associated to the path n.

Ω : Frequency separation between two tones.

* in the Appendix only.

PREFACE

The aim of this thesis is to examine the characteristics of the mobile radio channel from the point-of-view of its frequency selectivity. The mobile radio channel is characterized by multipath propagation and, of course, the different path lengths give rise to different propagation time delays. Typical spreads in time delays, depending on the type of environments range from a fraction of microseconds to many microseconds. The larger delay spreads are usually found in urban areas such as New York, whereas the shorter delay spreads usually occur in suburban areas [12-15,21]. The existence of different time delays and amplitude variations in the various waves that make up the total field causes the statistical properties of two signals of different frequencies to become essentially independent if the frequency separation is large enough. This phenomenon is often termed frequency selective fading. The maximum frequency difference for which the transfer function values of two frequencies are still strongly correlated is called the coherence bandwidth of the mobile radio transmission path. This parameter is important, the probability of error caused by frequency selectivity is based on the value of the coherence bandwidth.

The method selected here to investigate mobile radio frequency selective behaviour is the so-called multitone technique. It involves the simultaneous transmission of multiple tones. In the multitone technique, used during this experiment, a fixed station transmits a group of closely spaced tones to a mobile receiving system. By measuring each tone and comparing the relative effects of the mobile channel on each of them, it is possible to determine the frequency selective fading. A measure of this selectivity is the correlation between two tones, where a perfect correlation corresponds to the absence of frequency selective behaviour. In this perfect case, the two tones vary together as the mobile receiver moves through the interference pattern created by the multipath propagation of the signal. A low correlation indicates some independence of one tone with respect to the other. The multitone technique enables a precise measurement of both amplitude and phase behaviour.

Measurements were taken in the vicinity of Ottawa. Among the different environments tested there were rural environments with and without a line-of-sight propagation paths and also suburban and urban environments. No high urban density environment (e.g., New York) was available for study. During experiments the mobile laboratory which carried the receiving system, moved slowly following irregular paths into each zone in order to randomize the locations where measurements were taken.

Chapter 1 describes the mobile radio channel. The channel behaviour is first introduced in an informal approach, then a more complete and more formal description followed. The phenomenon of the frequency selectivite fading is defined and a review of previous works completes the chapter.

Chapter 2 covers the experiment itself. The multitone technique used to probe the channel is analysed. The practical implementation to generate and demodulate the signal are then fully described. The experimental procedure used to gather data ends the chapter.

Chapter 3 entirely describes the signal processing. This chapter is separated in mainly two parts; the amplitude and the phase behaviour. The method to compute the irreducable probability of error (PER) from the value of the coherence bandwidth is partly done along with the amplitude signal processing of the data.

Chapter 4 is an analysis of the results gathered both for amplitude and phase. Chapter 5 summerized the most important results obtained from this experiment. Finally, the Appendix is a complete description of the method to compute the PER for a DPSK signal.

CHAPTER 1

DESCRIPTION OF THE MOBILE RADIO CHANNEL

1.1 Introduction

The origin of mobile radio communications is as old as radio communications itself. Over the years, many applications of mobile communications have been developed with the result that the mobile radio communication spectrum have become very crowded. Since the allocated mobile radio bands cannot be expanded, it becomes very important to use the available frequency spectrum as efficiently as possible. Consequently, it is of a prime importance to study and understand the characteristics of the mobile radio channel.

There are two possible configurations for a mobile radio communication system: mobile to mobile and between a fixed station and a mobile unit in either direction. In either case, the atmosphere is used as the connecting medium between the receiver and the transmitter. This link has many characteristics that a system designer must know before the development of a mobile radio communication system. These characteristics will be considerably different when the mobile station is surrounded by high buildings or from when it is on the top of an isolated hill.

In order to describe the characteristics of a mobile radio channel, qualitatively, we may make use of a simplifying ray model of progation. In this model, the transmitted signal is viewed as being made up of a very large number of rays, each originating from the transmitting antenna and following a specific path away from the transmitter. If one considers the received signal as the sum of these rays and, as a first step, assumes a fixed receiver, the received signal undergoes modifications due entirely to the characteristics of the environment.

These modifications of the electromagnetic signals are attenuation, reflection, diffraction, local scattering, etc. (see Fig. 1.1). Many factors contribute to the attenuation of the signal: distance, absorption on reflecting surfaces, etc. Reflection occurs on the surface of the earth, on buildings, etc. Diffraction effects take place around building edges, over the top of hills, etc. Finally local scattering is the presence of multiple reflections within a short distance of the receiver.

A mobile station located at a fixed point receives a multitude of signals, each of them having followed a different path. This phenomenon termed multipath propagation leads to multipath fading. Each signal is modified independently and is defined by three different parameters; path

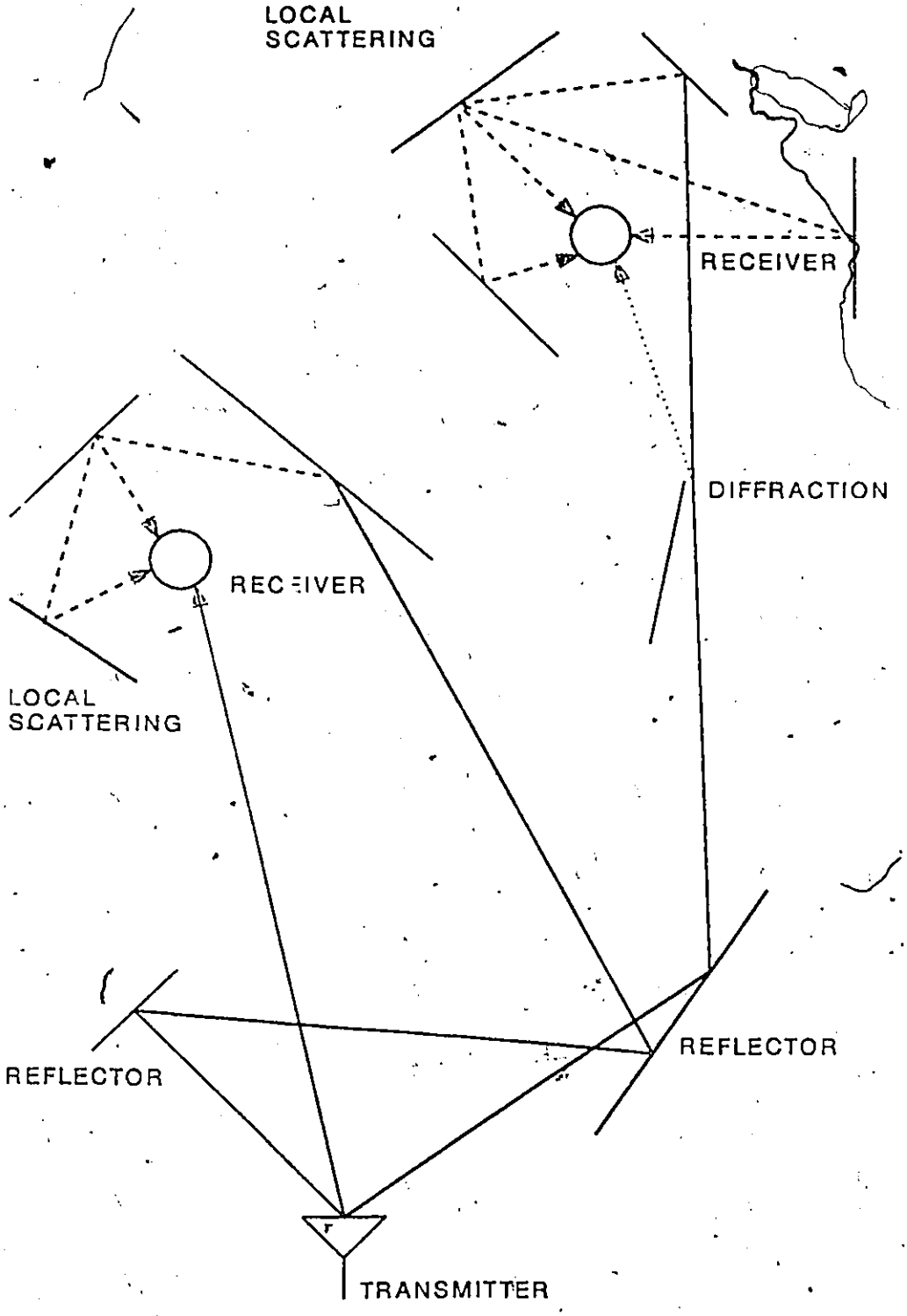

FIGURE 1.1 : A model of urban radio multipath channels (from [30]).

strength or attenuation of the signal, phase change, and propagation delay (note that phase change and propagation delay are closely related). The different signals combine together and form an interference pattern. The signal picked up by a mobile station moving through this pattern undergoes rapid and large changes. This fluctuation is known as 'fading', the region where signal is reduced being known as a fade.

This fading may be divided into slow and fast fading. The latter is a rapid variation of the received signal over a short distance. Typically, it can vary as much as 40 dB over a quarter wavelength of the signal. This fast fading is due to the interference pattern caused by the local scattering of the signal. It results in the combination of multiple reflections of about the same magnitude but of different phases. The signal strength is distributed about a relatively constant local mean. This local mean is the signal averaged over a short path (averaging over 20 to 40 wavelengths are typically used to measure the averaged signal within ± 1 DB [23], while this value is good for an area of about 200 wavelengths [22]) where the surrounding scatterers and obstacles have an influence. The slow fading refers to the variations of the local mean space over larger distances. This slow fading is primarily due to a change in the surrounding topography, mainly the presence of large objects (relative to the wavelength) such as buildings and hills, generally located at greater distances from the receiver.

If the receiver is moving, another phenomenon, called the Doppler effect enters the picture. This effect shifts the frequency of the signal. This shift is dependent upon the speed of the vehicle and the angle of arrival between the signals and the direction of the vehicle. Because the received signal is the combination of different rays from many directions, the Doppler shift is not uniform and spreads the signals over a bandwidth larger than originally transmitted.

Finally, if the bandwidth of the signal is wide enough, the propagation characteristics of the multipath medium will exhibit different characteristics upon the frequency observed. This phenomenon is often termed frequency selective fading. This is the channel characteristic which is studied experimentally in this thesis.

1.2 Signal Behaviour in a Mobile Radio Environment

A general representation of a transmitted bandpass signal $s(t)$ may be written as [27]:

$$s(t) = a(t)\cos[2\pi f_c t + \Phi(t)] = \mathrm{Re}[u(t)e^{j2\pi f_c t}] \qquad (1.1)$$

where $a(t)$ denotes the amplitude of $s(t)$, $\Phi(t)$ denotes the phase of $s(t)$ and $u(t)$ is a signal termed

the low-pass or baseband equivalent signal of $s(t)$ with respect to the carrier frequency f_c. We shall assume that there are $N+1$ propagation paths between the transmitter and the receiver. Associated with the n^{th} path is a propagation delay τ_n, an attenuation factor or path strength α_n and a phase shift θ_n. As shown by Fig. 1.1 the channel changes every path differently and therefore associates an attenuation and a phase shift different for each path. Thus the received bandpass signal $x(t)$ is the summation of $N+1$ different signals which follow $N+1$ different paths and it may be expressed in the form

$$\begin{aligned} x(t) &= \sum_{n=0}^{N} \alpha_n a(t-\tau_n) \cos[2\pi f_c(t-\tau_n) + \Phi(t-\tau_n) - \theta_n] \\ &= \mathrm{Re}\left[\sum_{n=0}^{N} \alpha_n u(t-\tau_n) e^{j2\pi f_c(t-\tau_n) - j\theta_n} \right] \end{aligned}$$

Note that the additive white Gaussian noise usually encountered in a mobile radio communication and any other types of noise are disregarded in this discussion. As the mobile station moves through the interference pattern created by multipath propagation, the number of contributive paths eventually changes.

If we let $y(t)$ be the low-pass equivalent of $x(t)$

$$\begin{aligned} y(t) &= \sum_{n=0}^{N} \alpha_n e^{-j(2\pi f_c \tau_n + \theta_n)} u(t-\tau_n) \\ &= \sum_{n=0}^{N} \alpha_n e^{-j\phi_n} u(t-\tau_n) \end{aligned} \tag{1.2}$$

where the carrier phase $\phi_n = 2\pi f_c \tau_n + \theta_n$ corresponds to a phase shift due to the delay τ_n and path phase shift θ_n. Comparing (1.1) and (1.2), the equivalent baseband impulse response of the channel $h(t)$ is expressed by

$$h(t) = \sum_{n=0}^{N} \alpha_n e^{-j\phi_n} \delta(t-\tau_n)$$

and the equivalent frequency response of the channel $H(f)$ is expressed by the Fourier transform of $h(t)$.

$$H(f) = \sum_{n=0}^{N} \alpha_n e^{-j(\phi_n + 2\pi f \tau_n)}$$

The propagation medium is then described by the set of three independent path variables

$$\{\alpha_n, \tau_n, \phi_n\}_0^N$$

The statistical behaviour of the path variables has been studied by numerous authors [21,31,32].

There is no difficulty in assuming *a priori* that the carrier phases $\{\phi_n\}_0^N$ of the various paths are mutually independent random variables which are uniformly distributed over $(0, 2\pi]$. This follows from the fact that the carrier phase is critically sensitive to path length, changing by 2π radians as the path length changes by a wavelength (in the present experiment the wavelength is about 35 cm). A typical distance between a transmitter and a receiver includes a very large number of wavelengths. This leads to a uniform distribution model for the phase ϕ_n. Also, the lack of a specific geometrical relationship between separate paths leads to an independence of ϕ_i and ϕ_j, $i \neq j$, and an uniform joint distribution of pairs of phases ϕ_i and ϕ_j.

Typical experimental values of $\{\alpha_n\}_0^N$ and $\{\tau_n\}_0^N$ were obtained by Turin et al.[32]. After transmitting a pulse via the urban radio propagation medium, a profile of the received waveform was obtained as a sequence of pulses due to reflections, diffractions and scattering (see Fig. 1.1).

The statistical behaviour of the path strength variable $\{\alpha_n\}_0^N$ combines with the uniform distribution of the carrier phase variable to determine the signal strength of the received signal. It is generally accepted that the path strength at any delay is Rayleigh distributed over a spacial dimension of a few tens of wavelength and the mean signal strength is log-normally distributed over areas whose dimensions are much larger [21,31,32]. This assumption is in fact not to be accepted uncritically, for there are always variations depending on the particular geography involved. It will not describe the large scale variations due to distance, hills, antenna heights, etc.

The frequency response of the channel $H(f)$ can be expressed by its quadrature and in phase components.

$$\begin{aligned} H(f) &= \sum_{n=0}^{N} \alpha_n e^{-j(\phi_n + 2\pi f \tau_n)} \\ &= \sum_{n=0}^{N} \alpha_n \cos(-\phi_n - 2\pi f \tau_n) + j \sum_{n=0}^{N} \alpha_n \sin(-\phi_n - 2\pi f \tau_n) \\ &= H_I(f) + j H_Q(f) \end{aligned}$$

If N is large enough, by the central limit theorem H_I and H_Q are Gaussian random variables. They have zero mean and equal variance. Moreover, they are uncorrelated and therefore independent.

The density probabilities for the amplitude x of H_I or H_Q for every frequency have the form

$$p(x) = \frac{1}{\sqrt{2\pi x_0}} \exp(-x^2/2x_0)$$

here x_0 is the variance of the variable x. The envelope r of the received signal for a transmitted signal $u(t) = e^{j2\pi f t}$ is proportional to

$$r = (H_I^2(f) + H_Q^2(f))^{1/2}$$

and as shown in Papoulis [25], the probability density of r is

$$p(r) = \frac{r}{x_0} e^{-r^2/2x_0} \quad r \geq 0$$
$$= 0 \qquad\qquad\quad r < 0$$

which is the Rayleigh density formula. Over a larger area, the mean signal strength x_0 ($E\{r^2\} = 2x_0$) varies following a log-normal density distribution:

$$p(x_0) = \frac{1}{x_0 \sigma \sqrt{2\pi}} \exp\left[\frac{-1}{2\sigma^2}(\log_{10} x_0 - m)^2\right] \quad x_0 \geq 0$$
$$= 0 \qquad\qquad\qquad\qquad\qquad\qquad\qquad\quad x_0 < 0$$

where σ is the standard deviation (in dB) of the density function and m is the mean also expressed in dB. The standard deviation is a function of the environment (e.g., London as a 4dB standard deviation [18]).

The Rayleigh density distribution is associated with the local scatterers (e.g. buildings) in an area of less than 200 wavelengths [22]. This phenomenon is usually refered to as fast fading. The log-normal density function covers a larger area. It is referred to as shadowing or slow fading. It is due to variations in size and localizations of large obstacles (relatively to the wavelength) in the area.

The following statistical model of the path strength for urban area explains the transition from the local distribution to the more global distribution of the path strength (Fig. 1.1).

The main wave arrives at a cluster of buildings. Before undergoing local scattering by the cluster, it has traversed a path which is subject to the influence of multiple reflections and/or diffractions by natural and made-man objects. The path strength, on arrival at the local cluster, will be a random variable. After arrival at the local cluster, the path undergoes a breaking up into local subpaths as a result of scattering from local objects. The subpaths all arrive at the receiver with roughly the same delay, but with different carrier phases. If we suppose a Rayleigh and a log-normal density distributions, the envelope of the signal is expressed as

$$p(r) = \int_0^\infty p(r|x_0) \cdot p(x_0) dx_0$$

where $p(r|x_0)$ is the local distribution of the envelope of the signal about the mean and $p(x_0)$ is the distribution of the mean over a larger area.

If we replace the density distributions in the equation

$$p(r) = \int_0^\infty \frac{r}{x_0} \exp(-r^2/2x_0) \cdot \frac{1}{\sqrt{2\pi x_0}\sigma} \exp\left(\frac{-(\log_{10} x_0 - m)^2}{2\sigma^2} \right) dx_0$$
$$= \frac{a}{2\sigma^2} \exp\left(ar - \frac{1}{2\sigma^2} \exp(ar) \right)$$

where $a = (\ln 10)/10$. According to Suzuki [31] this equation fits experimental data in many cases. Other distributions such as Rice distribution and Nakagami distribution have been tried [31]. They describe a more complex model of propagation (i.e., with a line of sight component) which will not be discussed here.

The last parameter to describe is the propagation delay $\{\tau\}$. Its statistical behaviour has been studied by many authors [9,12-15,29,31,32]. A simple and reasonable statistical model for the propagation delay sequence $\{\tau_n\}_0^N$ is a Poisson process [31] (a family of functions that describes the probability of having a defined number of arrivals in an interval of time), since the objects which cause this multipath propagation may be expected to be located randomly to a first approximation. More precisely, the excess delay time $\{\tau_n - \tau_0\}_0^N$ is a Poisson sequence on $(0, N)$ in this approximation, where τ_0 is the line-of-sight delay (the shortest possible delay). As observed by Suzuki there are considerable discrepencies between Poisson distributions and the empirical distributions gathered by experimentation.

To improve the description of the delay, a modified Poisson model with 2 states was then proposed. Whenever there is an event, i.e., a path occurs, the mean arrival rate (average number of paths per unit of time interval) is changed by a factor of K for the next Δ seconds, where K and Δ are parameters to be chosen, perhaps as a function of τ_n.

When $K = 1$ or $\Delta = 0$, the process returns to a standard Poisson sequence. For $K > 1$, the probability that there will be another path within the next Δ seconds increases, i.e., the process has a clustering property. For $K < 1$, the incidence of a path decreases the probability of having another path within the next Δ seconds, i.e., events have a tendency to arrive rather more equally spaced than in a pure Poisson model. The choice of K and Δ is also function of the type of environment. The modified Poisson model fits experimental data. Suzuki [31] concludes that paths tend to arrive in groups in suburban area. In urban areas, the path arrival time is almost homogeneous for initial paths but shows the clustering property for the late arrivals. To observe the different arrival times, an interesting function is the multipath intensity profile or delay power spectrum. A typical example is shown in figure 1.4. This plot shows the power of the signal

received if a pulse is transmitted through the channel. Assuming an infinite resolution in time, it is possible to observe each path delay. Furthermore, if we can determine the direction of the arrival, it is possible to separate each path.

Another phenomenon the signal experiences is the Doppler effect. It refers to the change in frequency caused by the movement of the receiver through the interference pattern. For a velocity of V m/s, an angle of arrival of ϕ rad (Fig. 1.2) and a wavelength λ m, the frequency shift of f Hz of a signal is expressed by

$$f = \frac{V\cos(\phi)}{\lambda}$$

For a multipath propagation environment, the occurence of multiple paths from different directions tends to spread the received signal in frequency.

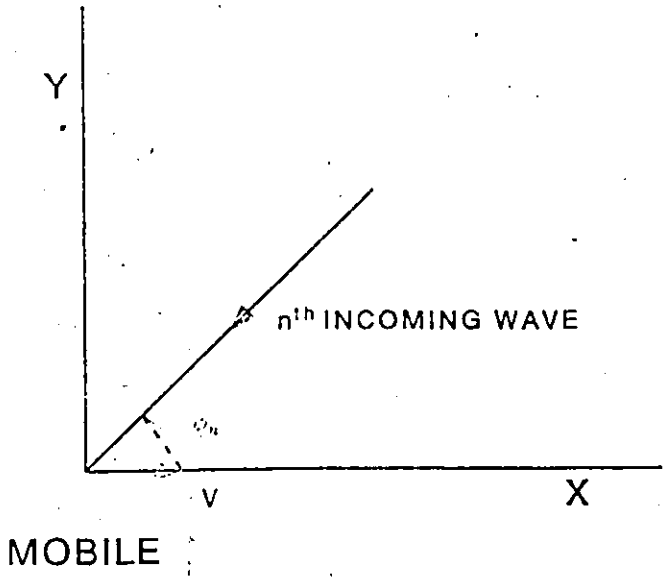

FIGURE 1.2 : A typical component wave incident on the mobile receiver (from [21])

1.3 Frequency selective fading

The mobile radio channel is characterized by multipath propagation and, of course, the different path lengths give rise to different propagation time delays. Typical spreads in time delays, depending on the type of environments range from a fraction of microseconds to many microseconds. The larger delay spreads are usually found in urban areas such as New York, whereas the shorter delay spreads usually occur in suburban areas [12-15,21]. The existence of different time delays and amplitude variations in the various waves that make up the total field causes the statistical properties of two signals of different frequencies to become essentially independent if the frequency separation is large enough. This phenomenon is often termed frequency selective fading.

Thus if the bandwidth is wide enough, the propagation characteristics of the multipath medium will exhibit a fade at some frequency within the band. These notches in the transfer function of the medium introduce distortions similar to filter distortions.

The maximum frequency difference for which the transfer function values of two frequencies are still strongly correlated is called the coherence bandwidth of the mobile radio transmission path. If we suppose the frequency transfer function is a wide sense stationary process with a Gaussian behaviour, the autocorrelation function will describe the channel statistical characteristics. By wide sense stationary it is meant that the average value of the frequency transfer function is constant and its autocorrelation depends only on the frequency difference. A Gaussian channel is defined as one whose output may be separated into a deterministic signal plus a random Gaussian signal when the input is deterministic.

If we define $T(f)$ as the transfer function of the channel, the correlation function is

$$R_f(f_1 - f) = \overline{T(f) \cdot T^*(f_1)}$$

and with the frequency separation defined as $\Omega = f_1 - f$

$$R_f(\Omega) = \overline{T(f) \cdot T^*(f + \Omega)}$$

where * denotes the complex conjugate and the overline an ensemble average. Here the coherence bandwidth is defined as the frequency separation between the two points where

$$R_f(\Omega)/R_f(0) = e^{-1}.$$

1.4 Previous Work

Several papers describe the frequency selective fading theoretically and experimentally [1-8,10,12-15,24,26-28]. Originally, the problem of frequency selective fading was studied for the case of reflections of electromagnetic signals by the ionosphere, which can change with time, both on a short term as well as diurnal basis. It was then assumed that this channel could be treated as a time-varying linear filter. A great deal of theoretical work has been done by P.A. Bello [3-8]. He described the different channel functions, and based a possible measurement method on the hypothesis of a quasi wide-sense stationary, ergodic process with Gaussian behaviour.

There is similarity between the ionospheric channel and the mobile radio channel. Both media suffer multipath propagations and scattering of the signals. However, the mobile radio channel exhibits a spacial variation rather than a time variation of the transfer function. Indeed, a vehicle moves through a relatively stable interference pattern, while the reflecting layers of the ionosphere move in time.

Several experiments have been performed to measure the transfer function characteristics of the mobile radio channel [2,10,12-15,28]. Several experimental techniques are possible. A simple technique is to transmit a narrow pulse and observe the received signal [28,31,32]. This method has been used to measure path strengths α_n and time delays τ_n. Unfortunately, it is practically difficult to implement such systems with a sufficiently large bandwidth.

A second technique that has been used by Cox [12-15], and later by Parsons and Bajwa [2,26], involves transmitting a carrier frequency modulated by pseudo-random sequences (PRS). Specifically, Cox transmitted a 910 MHz carrier frequency phase-reversal modulated by a certain binary pseudo-random sequence generated by a 9 delays shift-register with a 10 MHz clock rate. The pseudo-random sequence repeated itself every 511 clock periods or every 51.1 μs. The signal was transmitted from a based-station and received by an antenna located on the roof of a mobile vehicle. The signal received was correlated with a replica of the transmitted signal in two quadrature correlators. The PRS generated at the receiver and used in the correlator is clocked at a slightly (0.02%) slower rate then the transmitter sequence. The two correlator amplitude outputs in time represent the amplitude versus time delay τ for the low-pass quadrature components, $I(\tau)$ and $Q(\tau)$, of bandpass impulse response of the propagation paths.

The square envelope of the complex impulse response, $p(\tau) = I^2(\tau) + Q^2(\tau)$ is the same power-delay profile which would be received if a triangular pulse with base width of $0.2\mu s$ were transmitted

through all equipment filters and the propagation medium and detected with a square-law detector.

The Figure 1.3 shows the system used by Cox [12]. A weakness of this method is the time the correlation process takes. Indeed, as explained by Cox, the received signal is correlated by a copy of the transmitter signal. This copy is clocked at a slightly different frequency, 2 kHz for this specific case. Then, the correlation time is 0.5 ms for every bit. In order to respect the assumption of a measurement similar to the impulse technique, the vehicle must not move by more then 10% of a wavelength. Therefore, the pace of measurement is very slow. A faster clock difference was tried by Cox, but he observed distortions because as the clock difference increased, the signal used to compare with the received signal was increasingly different from the transmitted signal.

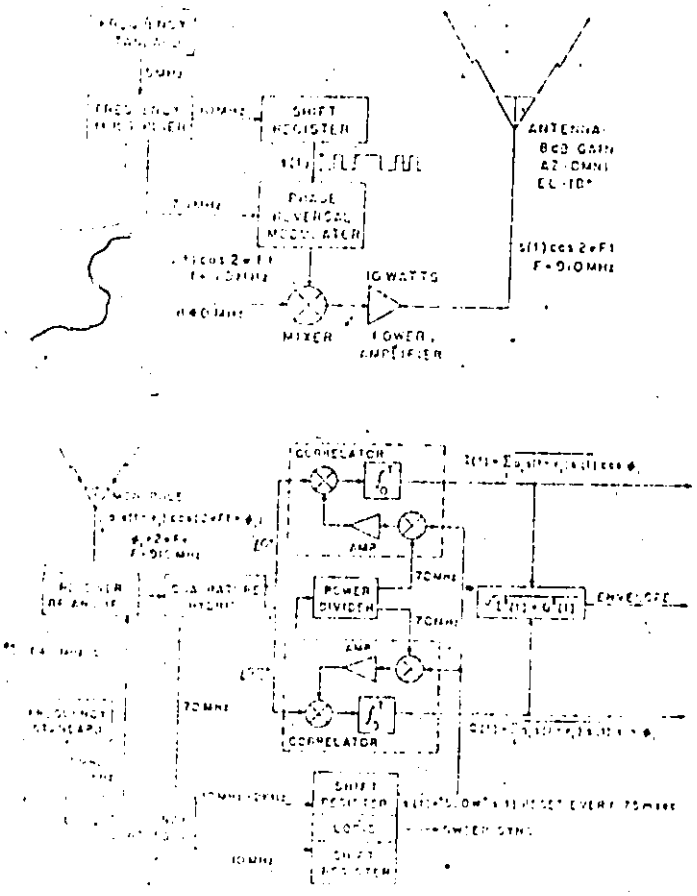

FIGURE 1.3 : (a) Time-delay measuring transmitter

(b) Time-delay measuring receiver (from [21]).

Cox computed individual power profiles defined as

$$p_i(\tau_n) = I_i^2(\tau_n) + Q_i^2(\tau_n)$$

where i identifies the set of profiles and n orders the delay sample within each profile. Figure 1.4 [from 12] shows some typical power delay profiles. The average power delay profile $P(\tau_n)$ for a set of K consecutive individual profiles is computed by the relation

$$P(\tau_n) = \frac{1}{K}\sum_{i=1}^{K} p_i(\tau_n) = \langle |h(\tau_n)|^2 \rangle \qquad (1.3)$$

where $h(\tau_n)$ is the impulse response of the medium. The distance travelled during the sampling of all K samples must exhibits wide sense stationarity. Cox took 210 samples for a total distance of 21 m [Fig. 1.4].

Two parameters are used by Cox to characterize the average power delay. The average delay D with respect to the first arrival delay τ_A.

$$D \triangleq \left\{ \left[\sum_{n=0}^{N} \tau_n P(\tau_n) \right] \Big/ \left[\sum_{n=0}^{N} P(\tau_n) \right] \right\} - \tau_A$$

τ_A is the minimum delay path chosen so that the profile amplitude is insignificant. Another parameter is the delay spread S defined as

$$S \triangleq \left\{ \left[\sum_{n=0}^{N} (\tau_n - D)^2 P(\tau_n) \right] \Big/ \left[\sum_{n=0}^{N} P(\tau_n) \right] \right\}^{1/2}$$

These parameters allow an easy comparison of different environments. The Fourier transform of the average delay profile $P(\tau_n)$ is the correlation function $R_f(\Omega)$ of the fluctuations in the complex transfer function $(h(\tau_n))$ multiplied by the transfer function of the instrumentation (probe). Once adjusted (without the probe), the final correlation function is equivalent to the correlation function of two signals separated (for this experiment) by 0 to 10 MHz (Fig. 1.5). The Table 1.1 gives the different parameters and the coherence bandwidth for two typical environments obtained by Cox [12-16].

Clearly, there is a relation between the average delay D, the delay spread S and the coherence bandwidth. However, this relation is not simple. The power delay profile is a saw-tooth function. Consequently, the correlation function is not monotonic, particularly for wide bandwidths (Fig. 1.5).

This method measures a very wide bandwidth, but with limited resolution. Indeed, the maximum resolution theoretically possible with the 511 bit PRS with a 10 MHz clock rate is about 20 kHz. Even then, this limited resolution is lost during the filtering in the correlators. A slower clock rate would give a better resolution, but the correlation process would be very long and the receiver would then have to move at a very slow pace.

The results of other investigations using the same method are available in the literature [2,10,26]. They usually yield similar results.

The subsequent chapters describe the multitone technique developed for this experiment. It measures the correlation function for different frequency separations. This technique offers the advantage of a sharp measurement of the correlation function at specific frequencies and a coherent demodulation of the signals, which allows the study of the phase behaviour from the point-of-view of the frequency selectivity.

TABLE 1.1 Statistical Parameters for Multipath Propagation
(from Cox experiments)

Statistical parameter	urban	sub-urban
Average of average delay D	1.1μs	0.15μs
Variance of average delay D	0.9μs	0.02μs
Maximum of average delay D	4μs	7μs
Average of delay spread S	1.3μs	0.24μs
Variance of delay spread S	0.6μs	1.4μs
Maximum of delay spread S	3.5μs	7μs
Minimum coherence bandwidth (B_c =0.9)	20 kHz	occasionally 40 kHz
Median coherence bandwidth (B_c =0.9)	70 kHz	usually > 250 kHz
Minimum coherence bandwidth (B_c =0.5)	55 kHz	occasionally 90 kHz
Median coherence bandwidth (B_c =0.5)		usually > 2000 kHz

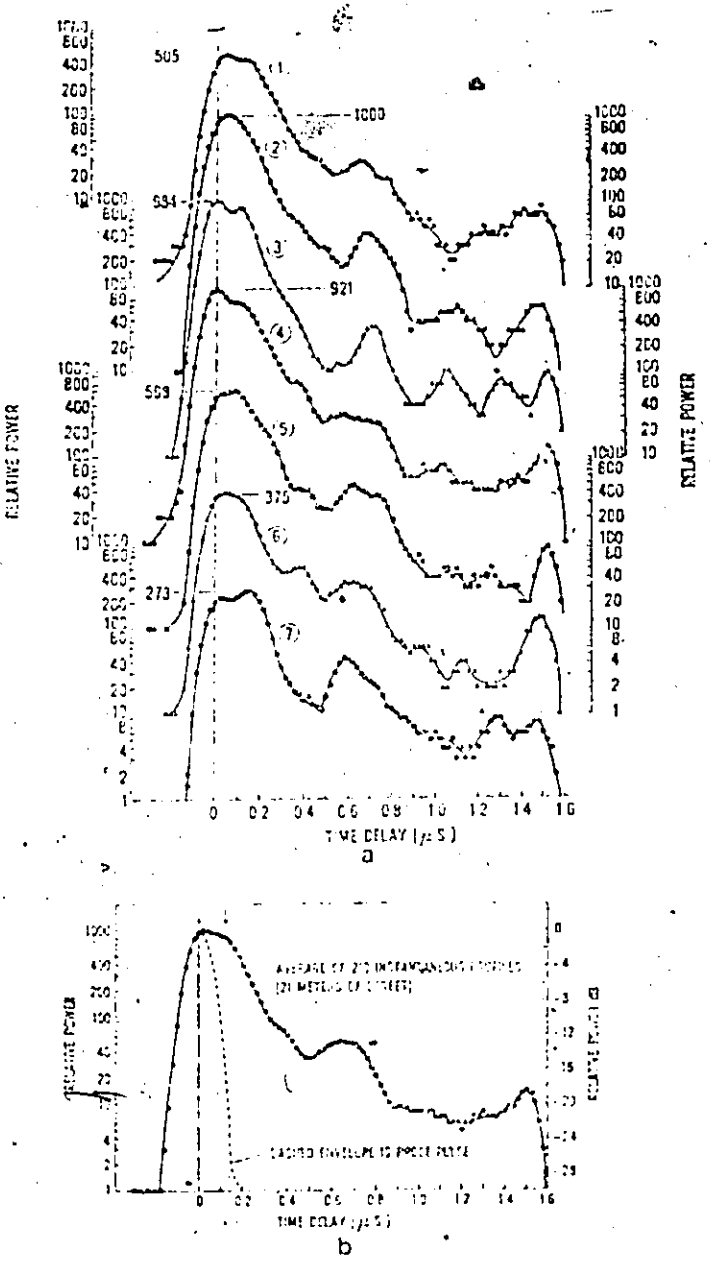

FIGURE 1.4 : (a) Average power delay profiles.
(b) Overall average of power delay profiles of (a) (from [12]).

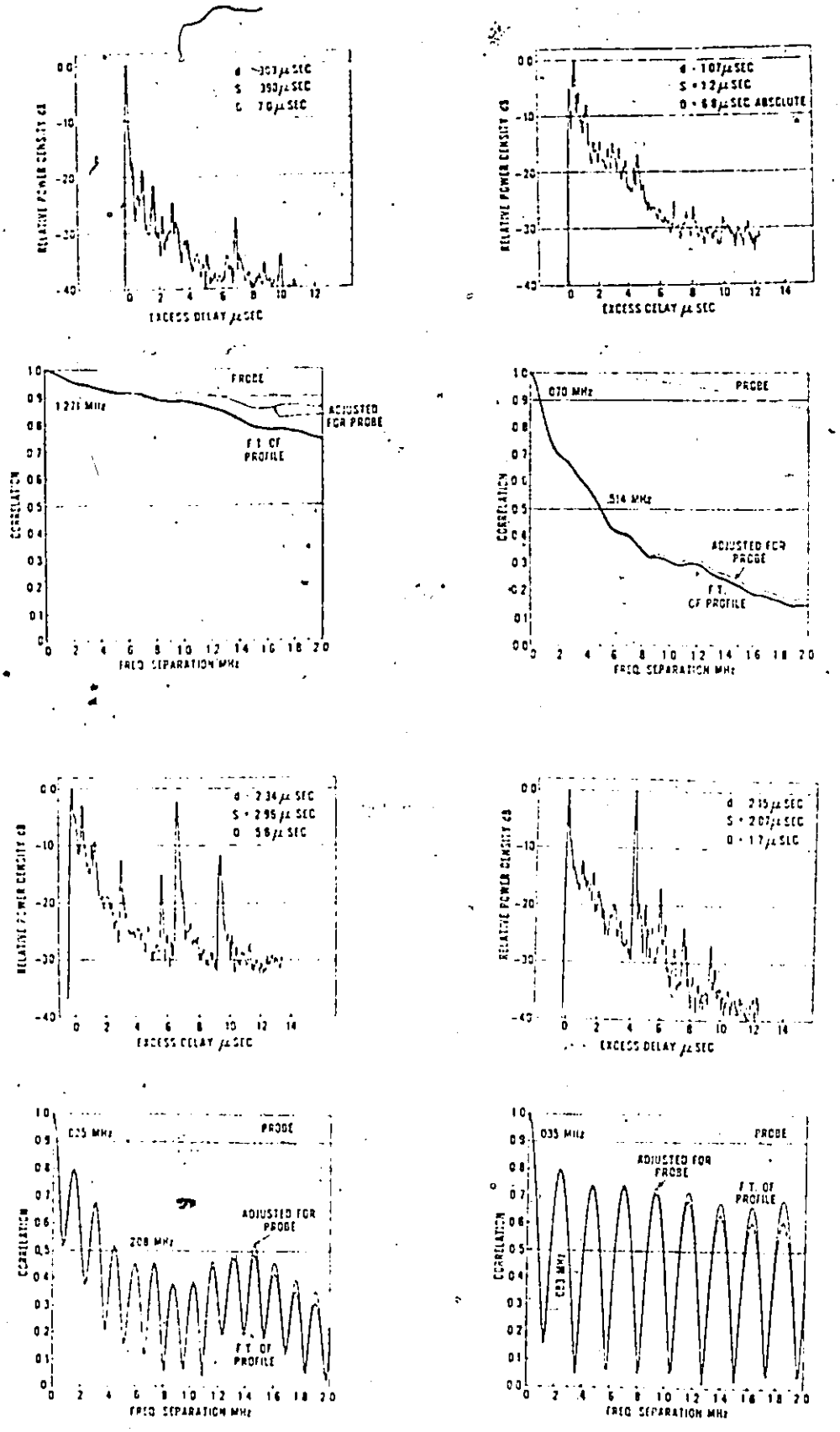

FIGURE 1.5 : (a)(c)(e)(g) Average power delays.
(b)(d)(f)(h) Magnitude of frequency correlation (from [13]).

CHAPTER 2

DESCRIPTION OF THE EXPERIMENT

2.1 Introduction

The aim of the experiment conducted was to measure the frequency selective fading characteristics of a mobile radio channel. For practical reasons, this characterization was limited to cover a medium bandwidth (128 kHz). The experiment was repeated in different areas under several environmental conditions to determine the main causes of frequency selectivity.

The method selected here to investigate mobile radio frequency selective behaviour is the so-called multitone technique. Bello described a multitone technique [7] to measure the characteristics of the ionospheric channel. It involves the simultaneous transmission of multiple tones. The implementation of this technique here differs from that of Bello although the basic concept is the same. In this multitone technique, a fixed station transmits a group of closely spaced tones to a mobile receiving system. By measuring each tone and comparing the relative effects of the mobile channel on each of them, it is possible to determine the frequency selective fading. A measure of this selectivity is the correlation between two tones, where a perfect correlation corresponds to the absence of frequency selective behaviour. In this perfect case, the two tones vary together as the mobile receiver moves through the interference pattern created by the multipath propagation of the signal. A low correlation indicates some independence of one tone with respect to the other. The multitone technique enables a precise measurement of both amplitude and phase behaviour, which is an advantage over the PRS technique. In fact, the methods are complementary, the PRS technique being able to probe a wide bandwidth while the multitone technique cannot.

2.2 The multitone technique

The transmission of a sinusoid through a mobile fading radio channel results in the reception of a narrow band random process. The received signal is slightly spread due to the doppler effect and represents the sum of multiple arrivals. The received waveform $x(t)$ of a sinusoid of unit amplitude located f Hz from the carrier f_c is:

$$x(t) = Re[T(f)e^{j2\pi(f_c+f)t}],$$

where $T(f)$ is the transfer function of the medium when measured with respect to the carrier frequency f_c. The correlation function of $T(f)$ is defined as :

$$R_f(\Omega) = \overline{T(f)T^*(f+\Omega)}$$

Assuming ergodicity, $R_f(\Omega)$ is later computed with the time average from the experimental data. For two transmitted sinusoids with frequencies f and f_1, the correlation function for a frequency separation $\Omega = f_1 - f$ is obtained. The complete determination of $R_f(\Omega)$ requires repeated measurements with different values of Ω. A simpler procedure is the simultaneous transmission of a set of sinusoids located at regular frequency intervals from the carrier. The frequency separation between two adjacent sinusoids is narrow enough (a few kHz) to render the correlation function smooth between two measured points. The assumption of smoothness is important, since these correlation measurements are discrete. This assumption is supported by the findings of others as explained below.

The correlation function $R_f(\Omega)$ is obtained from the received signal in its normalized form, the coefficient of correlation ρ. This normalization enables an easy comparison of two areas with a different mean power of the signal. The coefficient of correlation of $R_f(\Omega)$ is defined as

$$\rho = \frac{E\{XY\} - E\{X\}E\{Y\}}{\sqrt{(E\{X^2\} - E^2\{X\})(E\{Y^2\} - E^2\{Y\})}}$$

where X and Y are the received signals at two different frequencies.

$$X = T(f_X) \cdot S(f_X)$$

$$Y = T(f_Y) \cdot S(f_Y)$$

here E stands for the expected value and $S(f)$ is the transmitted signal.

Because the transmitted signal $S(f)$ is constant and independent of the transfer function of the channel $T(f)$, the expected values are expressed by

$$E\{X\} = S(f_X)E\{T(f_X)\}$$

$$E\{Y\} = S(f_Y)E\{T(f_Y)\}$$

$$E\{X^2\} = S^2(f_X)E\{T^2(f_X)\}$$

$$E\{Y^2\} = S^2(f_Y)E\{T^2(f_Y)\}$$

$$E\{XY\} = S(f_X)S(f_Y)E\{T(f_X)T(f_Y)\}$$

therefore ρ can be expressed by

$$\rho = \frac{E\{T(f_X)T(f_Y)\} - E\{T(f_X)\} \cdot E\{T(f_Y)\}}{\sqrt{(E\{T^2(f_X)\} - E^2\{T(f_X)\})(E\{T^2(f_Y)\} - E^2\{T(f_Y)\})}}$$

The correlation function is independent of the power of the transmitted signal.

2.3 Generation of the signal

The generation of multiple sinusoids with a fixed relation in amplitude and phase is a difficult task. A simple approach would be to use as many frequency generators as needed and locked them in phase. This is, however, very difficult to achieve in practice. A more practical approach is to use one generator to produce the carrier frequency and to modulate it with another signal having the desired characteristics. Here, it is possible to use a PRS as the modulating signal, even if the carrier level would than be almost nil. However, the transmitter power required would be impractically large, especially for a carrier located at 861.5 MHz. Moreover, the absence a of carrier component would increase the difficulty of coherently demodulating the signal as the technique requires.

The generator circuit of Figure 2.1 produces the signals used during the experiment. Their generation is accomplished by a quadrature phase shift keying (QPSK) modulator whose input is a sequence of modulation signals (shown in the right upper part of Figure 2.1) repeated at a rate of 32,000 sequences per second and a tone at the chosen carrier frequency. The use of a QPSK modulator allows the simultaneous production of multiple sinusoids from one highly stable frequency source. This method limits the envelope of the frequency spectrum of the transmitted power of the signal to a (sin x)/x form. The different tones generated do not have the same amplitude. Consequently only a limited number of tones located near the carrier frequency are practically usable. The carrier frequency chosen was 861.5 MHz. Two sequences of four bits fed simultaneously to the phase modulator, produced sequential positive and negative phase shifts of 90°. These 90° phase shifts allowed the generation of signals with the desired frequency separation between spectral lines. The carrier and the sequence clock were generated by high quality frequency generators locked in phase on the rubidium frequency standard. The useful signal generated was:

$$\begin{aligned} y(t) = & A\cos(2\pi f_c t + \phi_0) \\ & + 0.924\ A\cos(2\pi(f_c \pm 32\text{kHz})t + \phi_{\pm 1}) \\ & + 0.707\ A\cos(2\pi(f_c \pm 64\text{kHz})t + \phi_{\pm 2}) \\ & + \cdots \end{aligned}$$

Factor A is an amplitude constant, ϕ_n is a phase constant and $f_c = 861.5$ MHz. Only the five inner spectral lines were used, due to the basic bandwidth limitation of the receiver system (180 kHz) and the power limitations of the transmitter. The signal is shown on figure 2.2. The 32 kHz separation between the different frequencies could be modified simply by using another

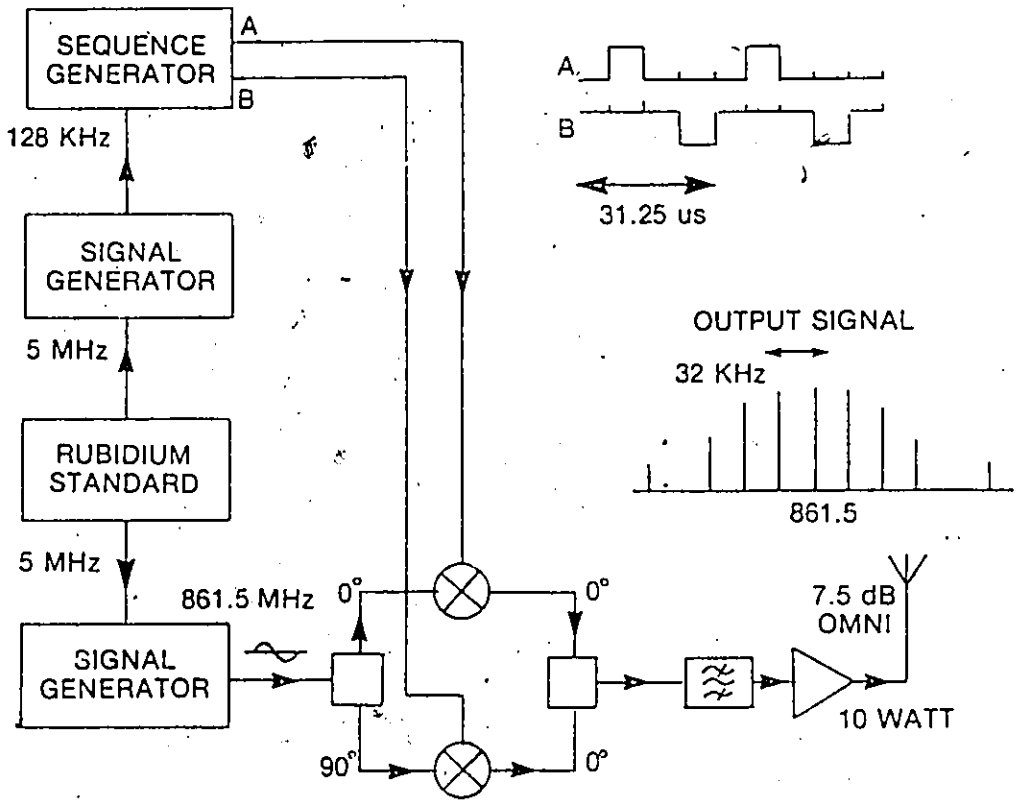

FIGURE 2.1 : Block diagram of the experimental multitone generator.

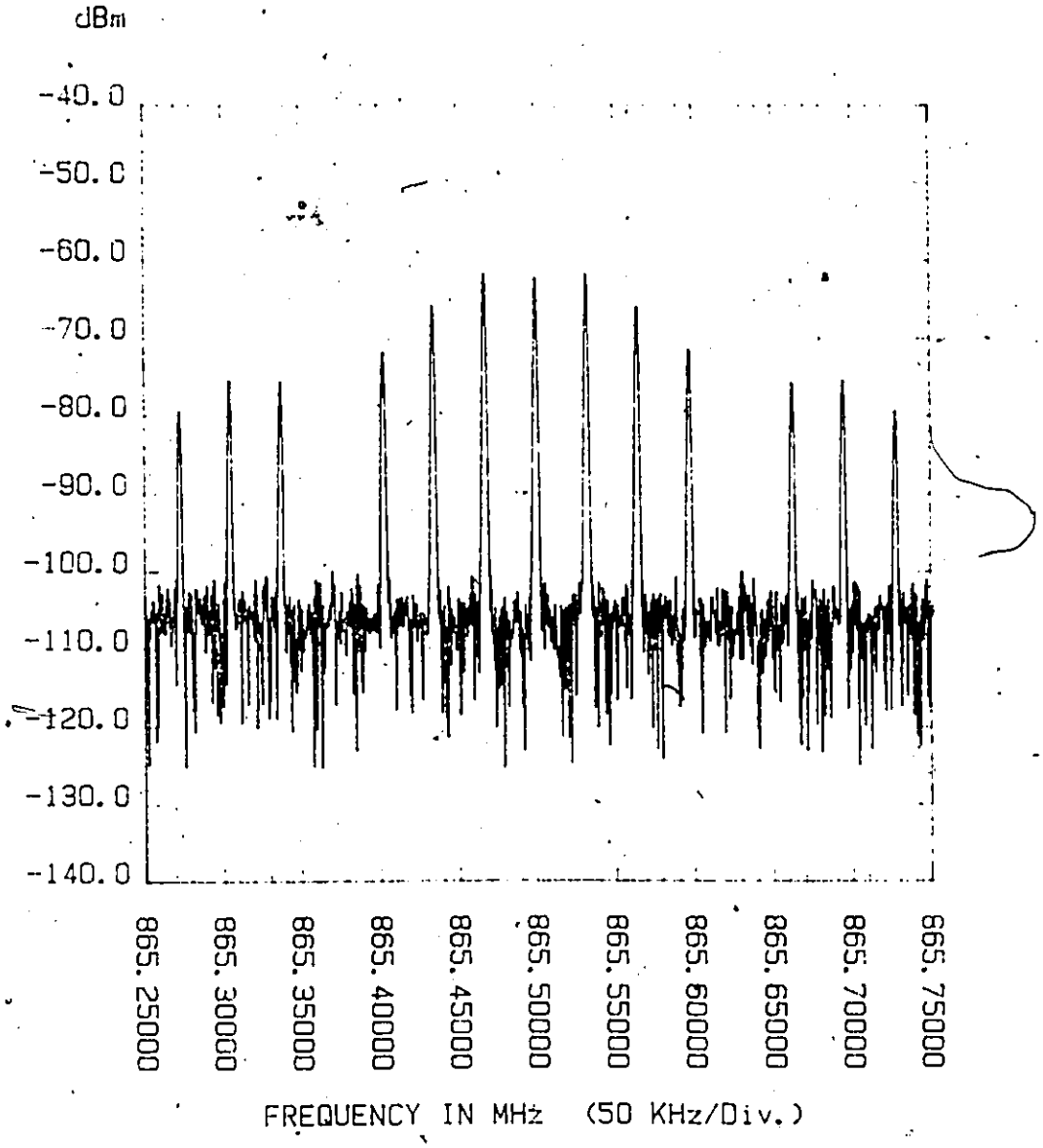

FIGURE 2.2 : The power spectrum of the transmitted signal

modulation rate. There is a one to one relation between the modulation rate and the frequency separation between two tones. The total useful signal bandwidth, after filtering at the receiver end, was 128 kHz. As a consequence, the received signal provides information about the frequency correlation function for four differents bandwidths namely 32 kHz, 64 kHz, 96 kHz and 128 kHz. For a 32 kHz separation, the correlation function $R_f(\Omega)$ was assumed to vary smoothly between the different points measured. This assumption is based on different results obtained by Cox [7], Bajwa and Parsons [6] showing a smooth correlation function for a bandwidth less than 128 kHz (Fig. 2.5).

As already noted, phase stability is provided by a rubidium standard. The two signal generators used are phase locked to it and give a stability of 5×10^{-7} Hz for a 10 ms period. In fact, such high stability is not absolutely necessary, as long as the relationship in amplitude and phase for all tones is constant for the measurement period of 1 ms. Constant relationships are the basis of the experiment. During the experiment, the received signal is measured at different points along a path. Stable phase relationships at the transmitting end enables the observation of the modifications of the signal due only to the channel. The measurement technique can stand a phase shift, as long as it is the same for all tones because it does not destroy the relationships between the different tones. This is one of the assumptions (verified by experiments) which supports the non-importance of small doppler shifts (below 15 Hz). The total transmitted power was 10 Watts and the transmitting antenna had a uniform azimuthal gain of 7.5 dB. In brief, the transmitted signal consisted of five tones located 32 kHz apart, centered at 861.5 kHz, each tone being linked to the others by fixed amplitude and phase relationships.

2.4 Demodulation of the signal

A block diagram of the receiver system, located in a mobile laboratory, is shown in Figure 2.3. A local rubidium frequency standard provided (through phase locking) the overall phase stability required by the receiver system. This frequency standard eliminated any possible problem caused by phase instability in the receiver system and allowed phase coherent measurements. The signal was received by an omnidirectional half wavelength monopole antenna. The receiver system converted the incoming signals from a center frequency of 861.500 MHz to a center frequency of 141 kHz and limited the bandwidth to 180 kHz. The signal was then sampled at a rate of 512 kHz by a 12 bit A/D converter during a period of 1 ms. From the A/D converter, the digital signal was fed to an array processor. A Fast Fourier Transform (FFT) was performed on every block of

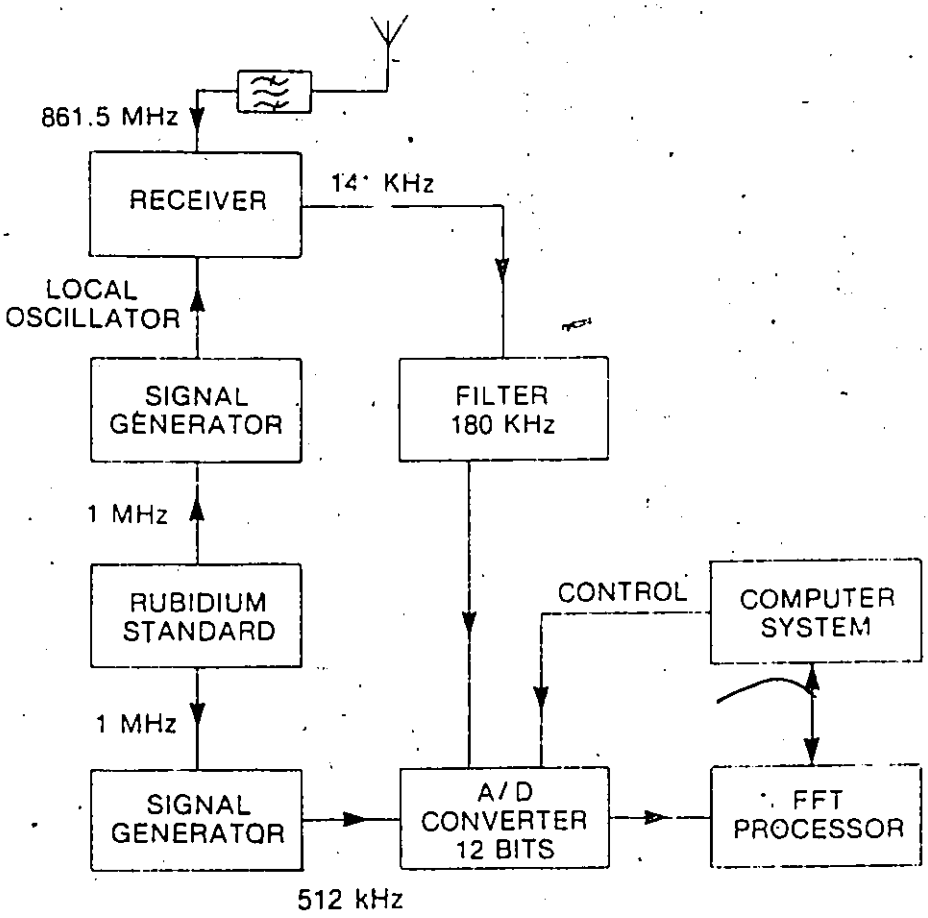

FIGURE 2.3 : Block diagram of the experimental receiver system installed in the mobile laboratory

512 samples gathered.

The use of the FFT enabled an extraction of the real and imaginary parts of each frequency component. The data obtained corresponded to a snapshot of the transfer function at 5 different frequencies, namely 861.5 MHz, 861.5 MHz ± 32kHz, 861.5 MHz ± 64 kHz. The assumption of an instantaneous view of the fading channel is based on the fact that the mobile laboratory moved a maximum of 1.0 cm during the sampling time of 1 ms (at 10m/s, 1ms corresponds to 1cm). At 861.5 MHz the wavelength is about 35 cm and a 1.0 cm path corresponds to less than 5% of a wavelength. It could be safely assumed that the channel transfer function barely changed for such a short distance.

2.5 Data acquisition

One experimental run consisted of 128 independent observations of 1 ms of the channel while the mobile laboratory was slowly moving (most of the time below 10 m/s). The 128 observations were equally spread over a total period of time of four minutes. In terms of distance, each observation was separated by few wavelengths (between 2 to 10), so that they may be regarded as independent [8]. It should be stressed here that an experimental run covered a rather large area and not a short path of few meters. A block of data thus included the effects of the local scatterers, called fast fading, as well as the effects due to large (relative to the wavelength) obstacles, called slow fading. The mean of the signal over a small distance is a random variable describes by a log-normal distribution. A special data processing is necessary to bring back data to a wide-sense stationary behaviour (all samples have the same mean). Chapter 3 describes the signal processing in detail.

Measurements were taken in the vicinity of Ottawa. The map shown in Figure 2.4 depicts the two transmitting sites used and the 9 differents areas (cross-hatched) where measurements were taken. Table 2.1 gives a short description of each environment. Here CRC stands for the Communications Research Centre, in Nepean, one of the two locations where the transmitter was located. The other location is Carleton University in Ottawa. Among the different environments tested there were rural environments with and without a line-of-sight propagation paths and also suburban and urban environments. No high urban density environment (e.g., New York) was available for study. During experiments the mobile laboratory which carried the receiving system, moved slowly following irregular paths into each zone in order to randomize the locations where measurements were taken.

TABLE 2.1 : DESCRIPTION OF DIFFERENT ENVIRONMENTS

SITE (no. of blocks)	BASE	DISTANCE	DESCRIPTION
Kanata (14)	CRC	3-6 km	Suburban,1-2 story buildings, small hills
Experimental Farm* (10)	Car. U.	1-2 km	Rural, most of the time line-of-sight
Ottawa South* (10)	Car. U.	1-3 km	Suburban, 1-3 story buildings, flat terrain
Aylmer (16)	CRC	5-8 km	Suburban,1-2 story buildings, flat terrain
Alta Vista (21)	Car. U.	1-5 km	Suburban,1-3 story buildings, small hills
Ottawa West (16)	CRC	5-8 km	Suburban, 2-3 story buildings, small hills
Carleton Heights (14)	Car. U.	2-4 km	Suburban, 1-2 story buildings, small hills
Center-Town (25)	Car. U.	3-4 km	Urban,2-20 story buildings, flat terrain
Corkstown Road (20)	CRC	3-4 km	Rural, most of the time behind a hill

* These two areas were processed together.

CRC is Communications Research Centre, Car. U. is Carleton University.

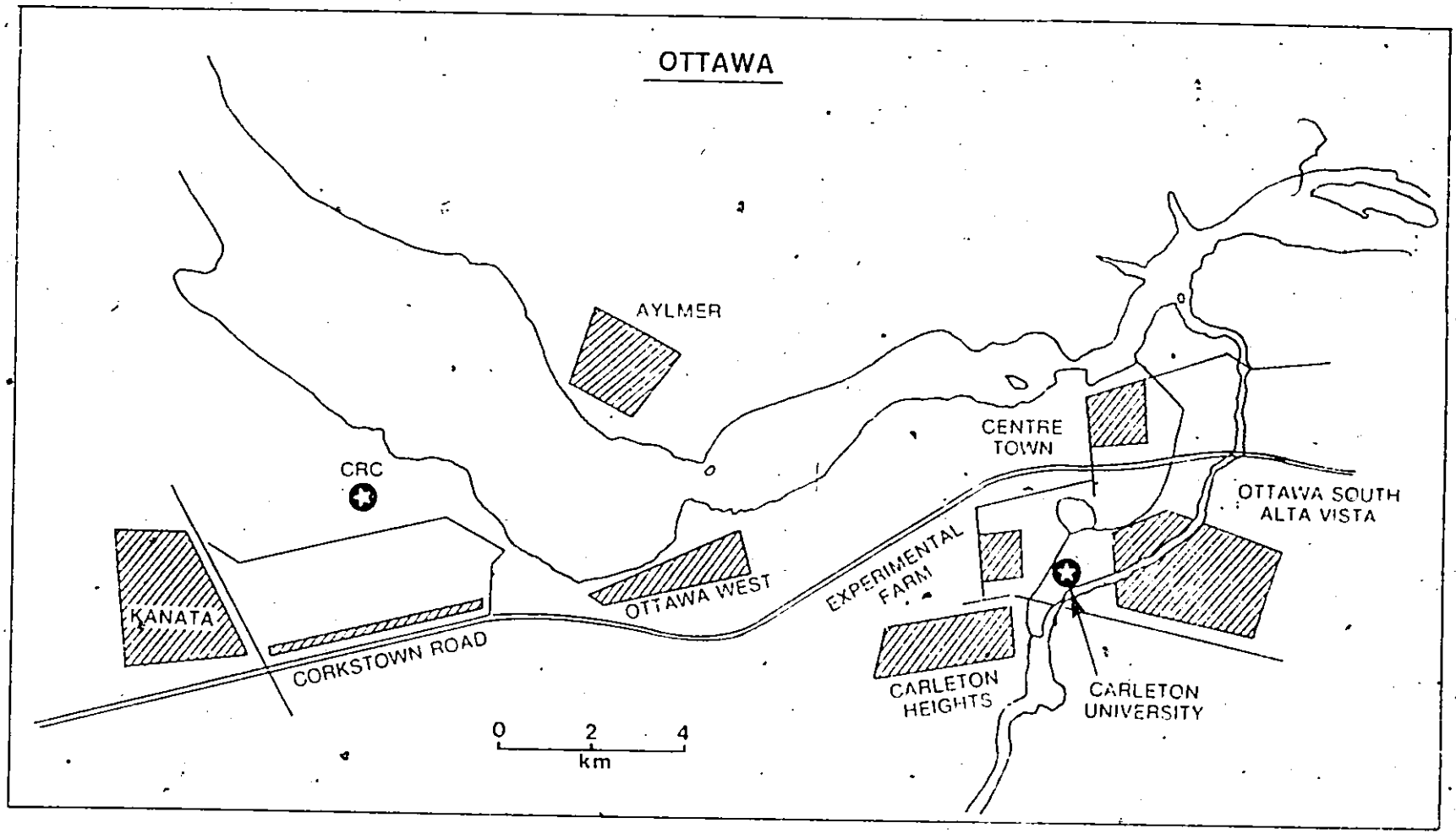

FIGURE 2.4 : Map of Ottawa. The different areas tested are filled with a cross-hatched pattern

CHAPTER 3

SIGNAL PROCESSING

3.1 Introduction

The data obtained following preliminary signal processing were grouped into blocks of 128 observations for each environment. Each observation resulted from the computation of a real FFT over 512 samples taken at a rate of 512 kHz. The signals under observation consisted of five tones located at 861.500 MHz, 861.500 MHz ± 32 kHz, 861.500 MHz ± 64 kHz. Each tone was characterized by its amplitude and its phase. Data gathered in Ottawa South and the Experimental Farm areas were grouped together to form a statistically better sample.

Doppler effects caused by the movement of the vehicle were determined to be negligible for two reasons. First, different tests using a doppler frequency shift comparable to those expected during the experiment yielded almost no change in to the results after performing the FFT. Secondly, even if the signals are slightly modified, all five signals under observation are similarly modified. Therefore, the same behaviour is observed for the different frequencies and no frequency selectivity is artificially added by the doppler effect.

If we assume that amplitude and phase behaviours are independent, the data processing for each block can be done separately for these two parameters. This procedure allowed a simpler interpretation of the results than a complex analysis would have permitted. In order to illustrate the different computations, two typical environments were chosen, namely Aylmer, a suburban area near Ottawa and Centre-Town an urban environment (downtown Ottawa).

3.2.1 Amplitude Behaviour

As already stated, data was gathered over a large area. As a consequence, the envelope of the signal received combined a fast variation due to local scatterers and a slow variation due to large obstacles. Figures 3.1 and 3.2 show two typical blocks of data. Figure 3.1 is a block of data which represents the amplitude of the carrier tone gathered in Aylmer as a function of the distance. The distance is expressed in sampling intervals. One sampling interval is the distance travelled between two samples (from 2 to 5 m) and the figures show the data gathered as the mobile moved through

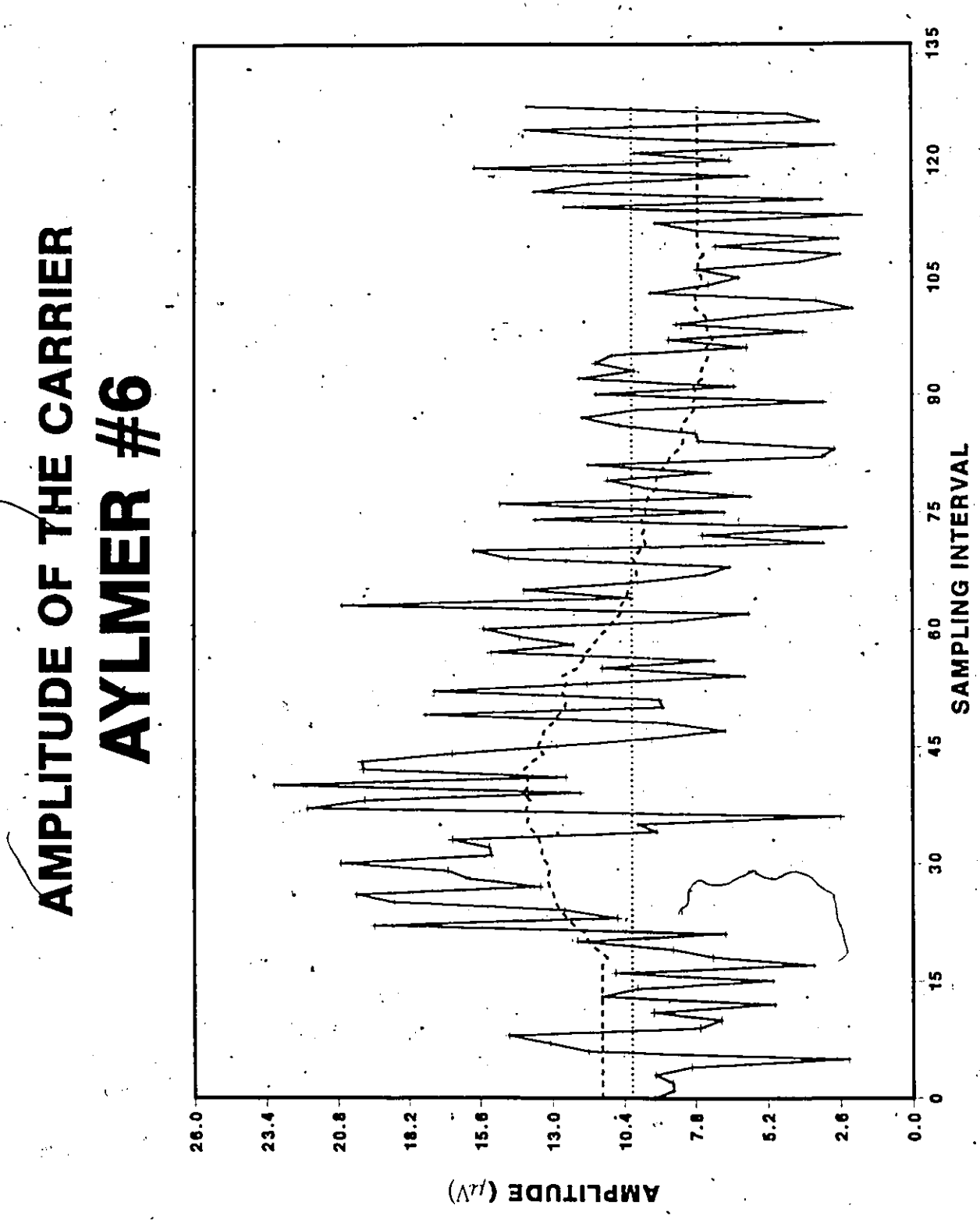

FIGURE 3.1 : Amplitude of the carrier for Aylmer area, block no. 6.

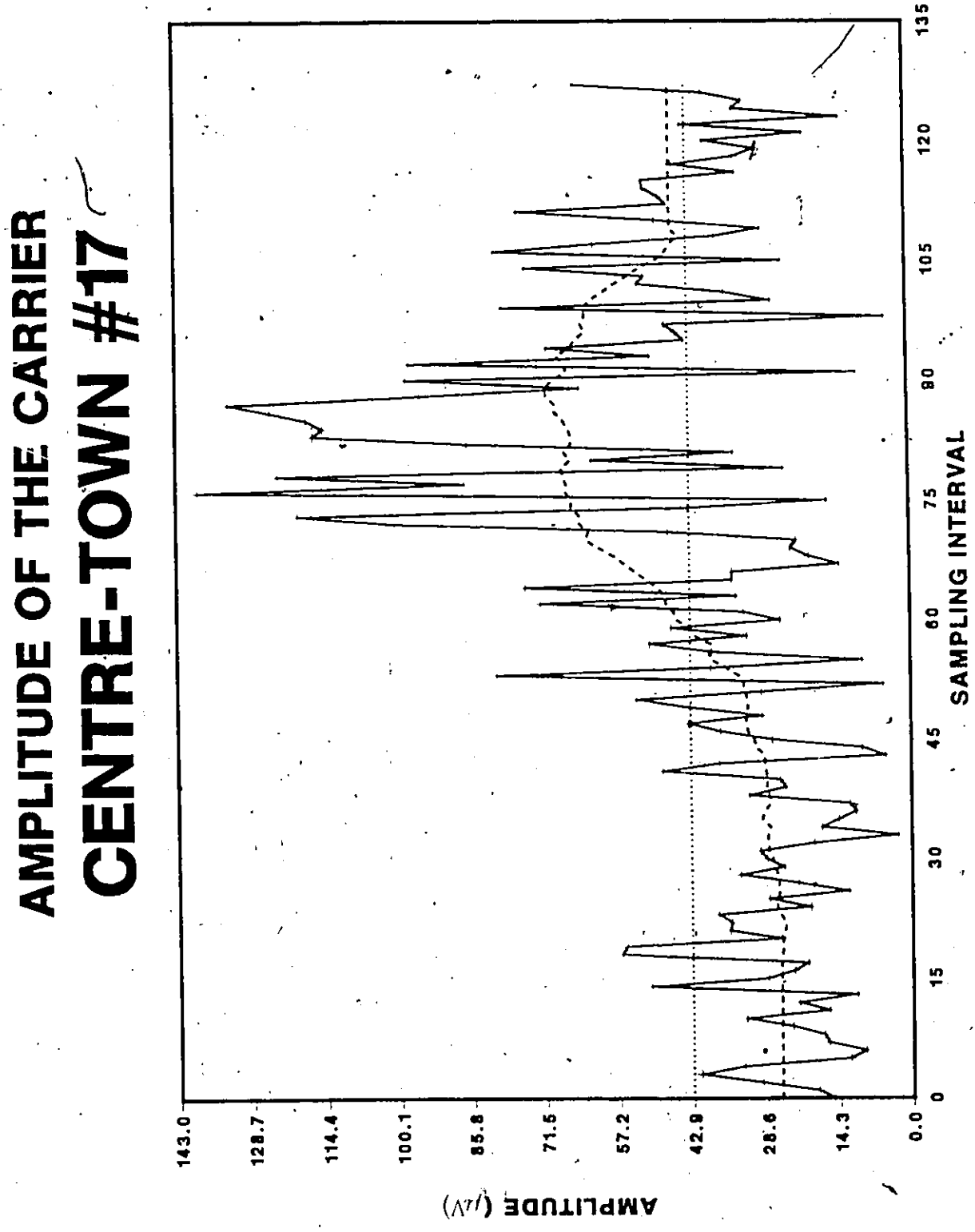

FIGURE 3.2 : Amplitude of the carrier for Centre Town area, block no. 17.

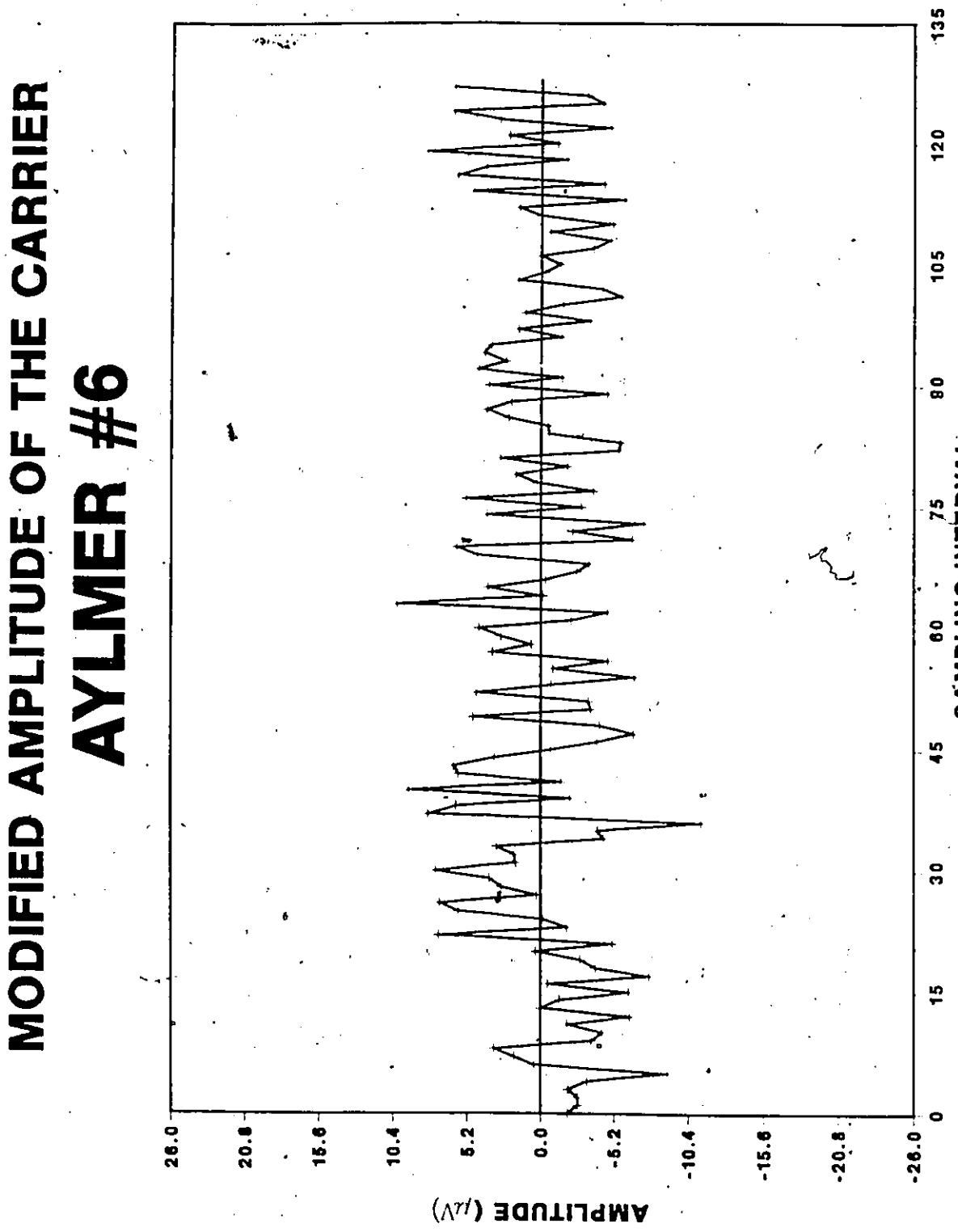

FIGURE 3.3 : Modified amplitude of the carrier for Aylmer area, block no. 6.

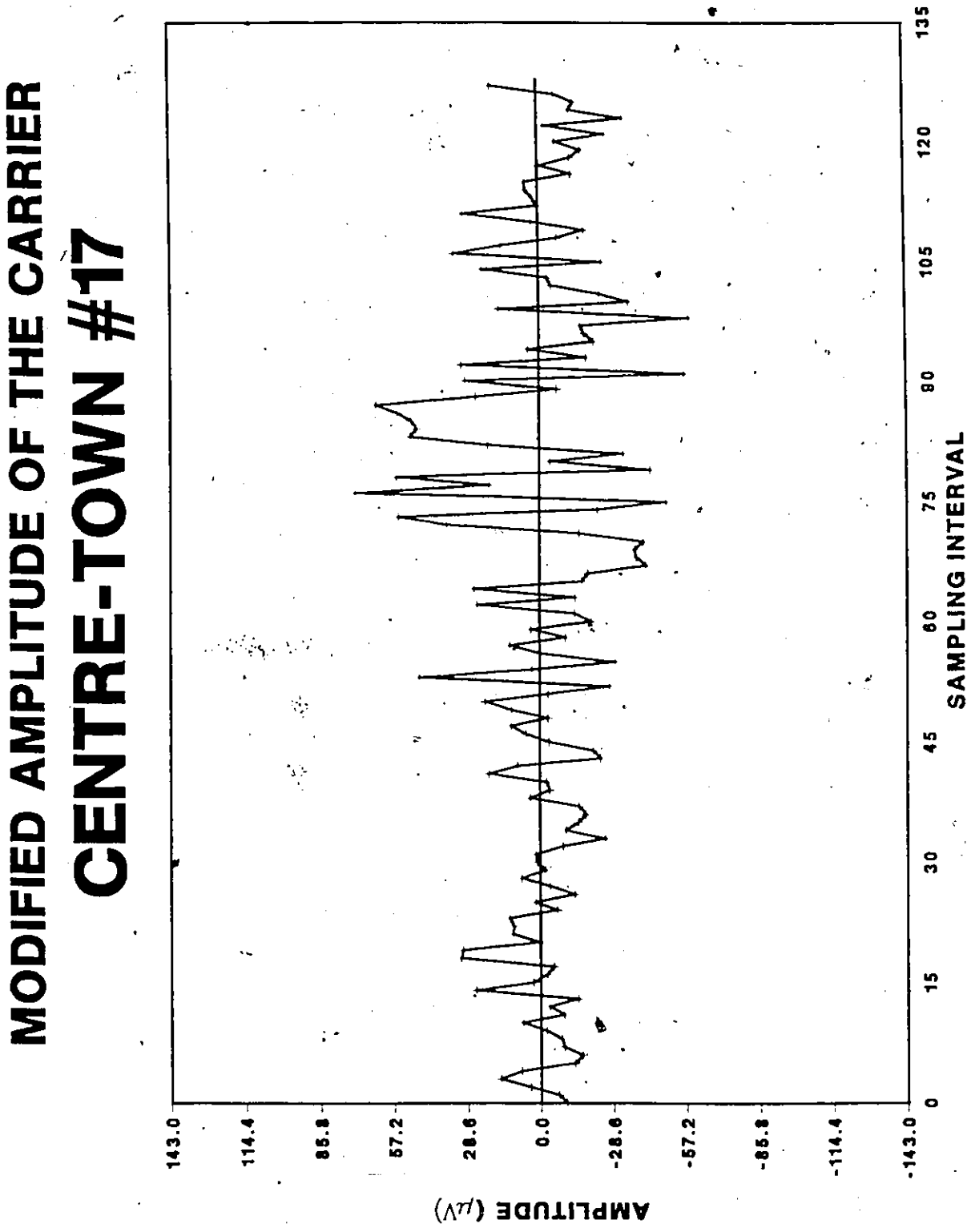

FIGURE 3.4 : Modified amplitude of the carrier for Centre-Town area, Block no. 17.

an area. **The line between each observation (a cross) doesn't indicate a knowledge of the amplitude of the signal between two points.**It is merely a convenient way to represent data. The rapid variation of the envelope is caused by the constructive and destructive sum of the different waves. The much smaller and slower variations of the local mean signal (dashed line) are also shown. This local mean is computed over a running window of 36 consecutive observations.

Figure 3.2 shows a similar behaviour of the carrier amplitude within the Center–Town area. Figures 3.1 and 3.2 represent only the carrier tone but the 4 other tones exhibit very similar behaviour. They more or less closely follow the carrier amplitude variations, depending on the degree of correlation between amplitudes.

In a first step each of the different tones is normalized with respect to a common level using the overall mean of a block. This adjustment is done to compensate for the different transmitting powers used for each of the tones. This adjustment is not really necessary because the signal power has little importance as long as it is well above the noise level. However, in so doing, it is easier to compare two tones in a qualitative manner.

The second operation removes the slow variations of the local mean. This operation brings back each observation to an equal weight. Then, no part of a block of data would bias the result because of a temporary variation of the local mean for a small period of time, see Figure 3.2 between sample 75 and 90. Also, the assumption of wide-sense stationarity is easier to satisfy when the whole block has the same mean. Thus no part of a block dominates further computations. To remove this slow variation, the local mean of the carrier is computed and subtracted from each sample. The local mean consists of a running mean computed over a window of 36 consecutive data samples. The dashed line in figures 3.1 and 3.2 represents the local mean computed for these two blocks. Longer and shorter windows have been used, and it was observed that wider windows provide better cross-correlations between tones. The choice of a window of 36 samples is based on estimates made by Lee [23] and provides a good estimate of the mean. (36 independent samples is the minimum number of samples to obtain a value of the local mean within $\pm$1dB of its real value). The running mean of the carrier is used to normalize all five tones. Figures 3.3 and 3.4 show the normalizing effect of the running mean average on the different tones. The average is then shown by a straight line.

The operation that was performed next is the computation of the cross-correlation between pairs of tones among the five tones. For each block there are 10 possible correlations, spread over four bandwidths; four at 32 kHz, three at 64 kHz, two at 96 kHz and one at 128 kHz (see

Table 3.1). Each correlation is (in turn) suitably normalized in order to allow reliable comparison between blocks of data. The end result obtained is an estimate of the coefficient of correlation. This process provides a comparison between independent observations and quantifies the difference in their behaviour from one sample to the following. Staying at the same location would result in non-independent observations. Instead of the coefficient of correlation for the amplitude, the complex coefficient of correlation might have been computed. However, in the complex coefficient of correlation phase and amplitude effects are merged together and the interpretation of the results becomes more ambiguous. Here, only the estimate of coefficient of correlation for the amplitude has been computed. It is defined as the ratio of the covariance of the amplitude divided by the product of the standard deviations of the amplitudes of selected pair of the tones. The coefficients of correlation may be grouped into a cumulative distribution for each environment (see figure 3.5 and Chapter 4). These distributions indicate the frequency selectivity as expected for different frequency separations. Evidence of the wide-sense stationarity is given in figure 3.6. The cumulative distributions of the Centre-Town area is drawn for the four frequency separations of 32 kHz. This plot indicates that results are independent of the frequency location of the two tones in the signal within the bandwidth under study.

TABLE 3.1 Sample Coefficients of Correlation (Centre-Town, 10 blocks)

No.	32 kHz				64 kHz			96 kHz		128 kHz
1	0.92	0.94	0.92	0.91	0.84	0.84	0.80	0.79	0.76	0.68
2	0.91	0.94	0.95	0.94	0.82	0.85	0.86	0.72	0.74	0.60
3	0.95	0.95	0.95	0.94	0.87	0.86	0.86	0.78	0.77	0.69
4	0.81	0.90	0.87	0.83	0.74	0.75	0.71	0.67	0.60	0.55
5	0.92	0.92	0.93	0.92	0.82	0.81	0.81	0.71	0.67	0.55
6	0.95	0.96	0.96	0.96	0.87	0.88	0.88	0.77	0.80	0.67
7	0.92	0.90	0.90	0.86	0.74	0.72	0.64	0.56	0.42	0.64
8	0.82	0.90	0.87	0.83	0.74	0.75	0.71	0.67	0.60	0.56
9	0.78	0.78	0.73	0.71	0.56	0.50	0.48	0.45	0.40	0.32
10	0.85	0.85	0.86	0.89	0.71	0.75	0.80	0.68	0.75	0.67

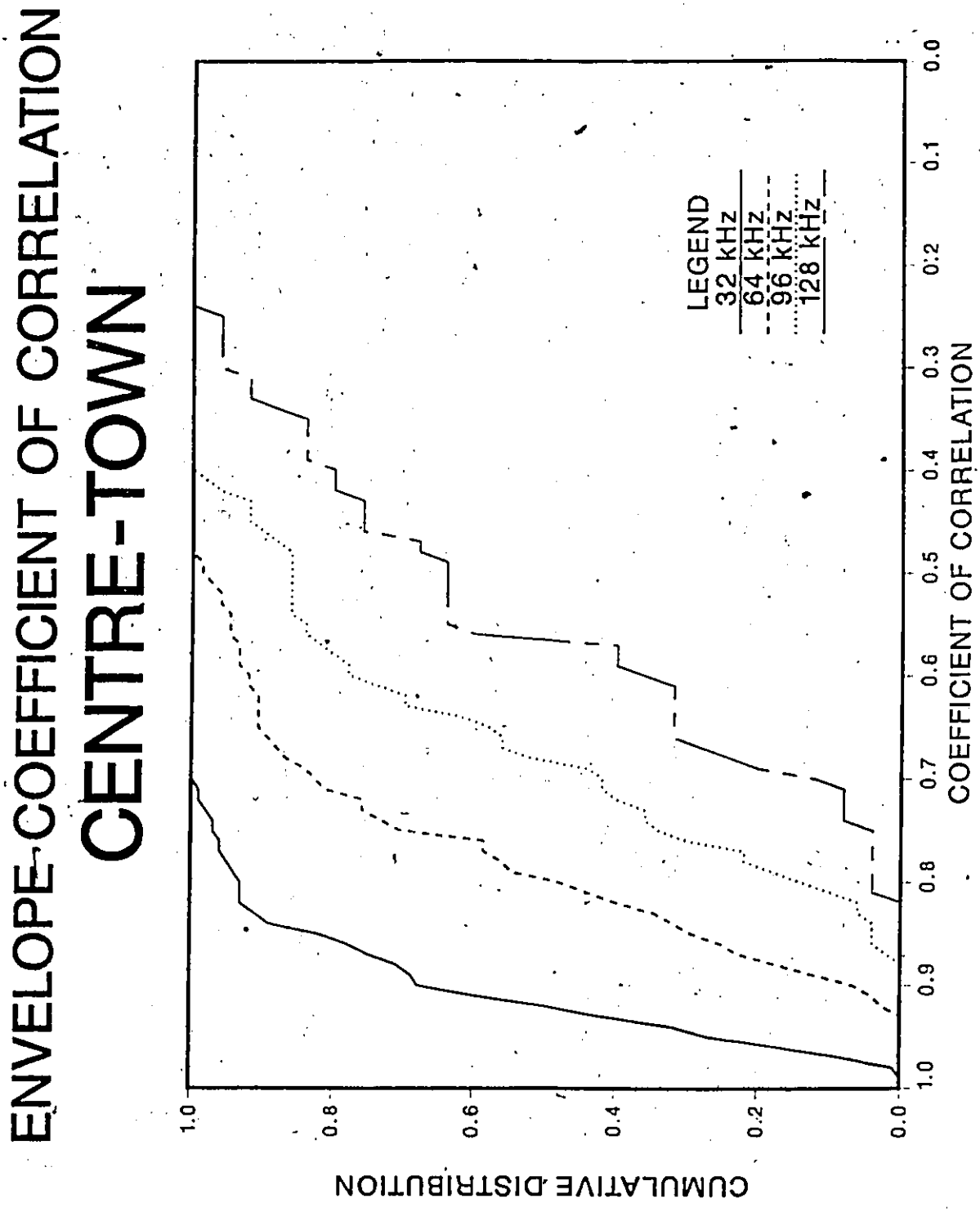

FIGURE 3.5 : Cumulative distribution of the envelope coefficient of correlation for the Centre-Town area (4 frequencies).

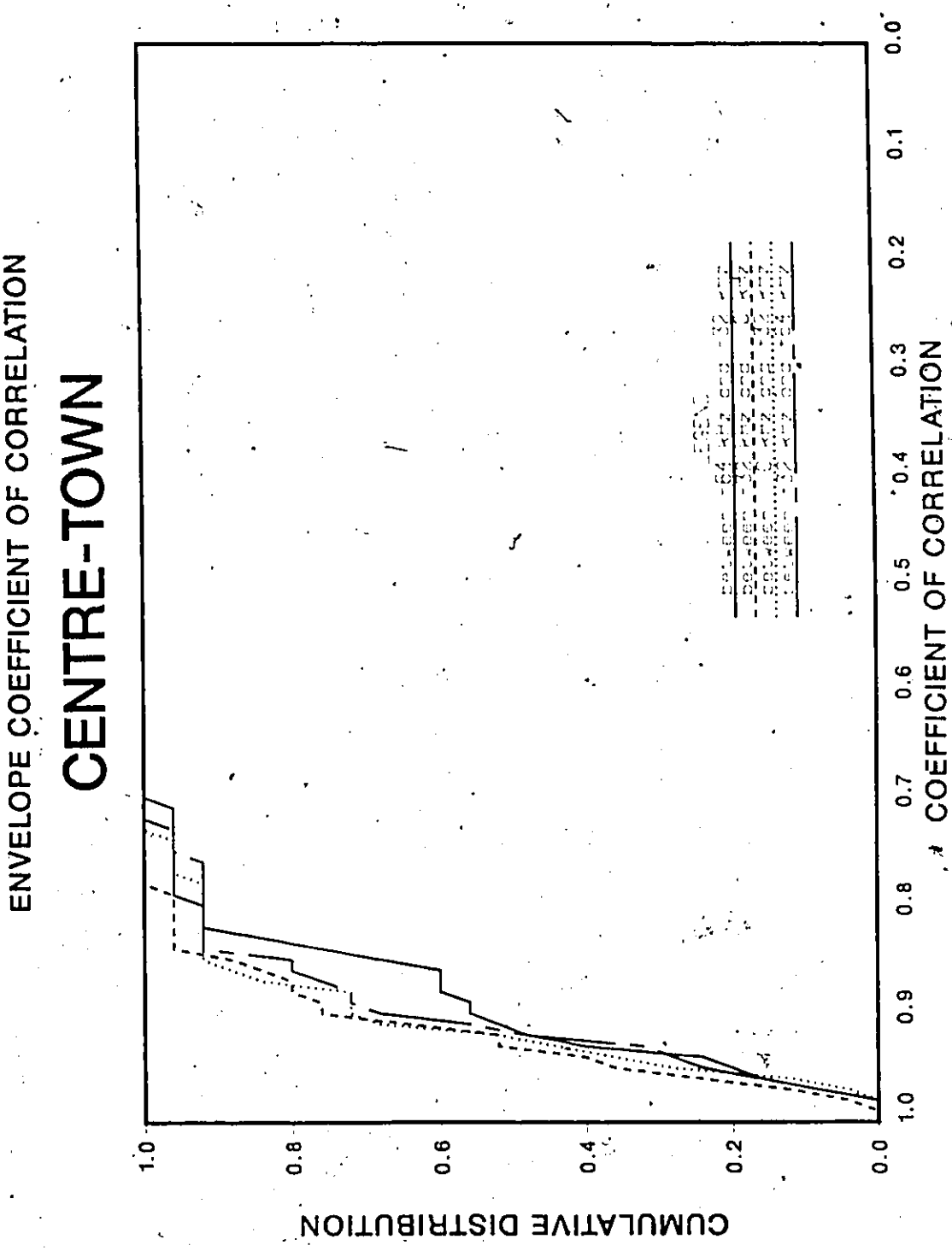

FIGURE 3.6 : Cumulative distribution of the envelope coefficient of correlation for the Centre Town area (only 32 kHz).

Finally, the four measured points of the correlation function are used to determine the coherence bandwidth. With only four points available, the exact shape of the correlation function is rather difficult to determine experimentally. A Gaussian shape correlation function was used to compute the coherence bandwidth and as an approximation of the real correlation function. This curve shape was used by Bello and Nelin [3,4,5,6] and Bailey and Linderlaub [1,24] for the computation of the probability of error of a DPSK signal. In order to use their results, this curve shape was chosen. There in no justification based on the behaviour of the channel. The following equation describes the normalized Gaussian curve used for the correlation function $R_f(\Omega)$:

$$R_f(\Omega) = \exp\left(\frac{-4\Omega^2}{B_c^2}\right)$$

Here Ω is the frequency separation and B_c corresponds to the coherence bandwidth defined as the frequency separation between the points where the coefficient of correlation is equal to e^{-1} for the Gaussian shape correlation function ajusted over the experimental points. A least square fit is then computed for each block of data. Here each coefficient of correlation is weighted by the inverse of the square of the experimental error on the measurements [28]. The error range corresponds to a 95% confidence interval. Thus the weight used is inversely proportional to the standard deviation of the measurement variable. Figures 3.7 to 3.9 show typical correlation functions thus obtained. Each measurement is drawn with its 95% confidence error bar. Error bars were computed following the method prescribed by Steel and Torrie in [30, pp.188-190].

There are no sharp distinctions between the environments in which measurements were gathered. However, the different environments can be broadly classified into three types of frequency selectivity behaviours:

1: A minimal reduction of the value of the correlation function below 128 kHz (Figure 3.7).

2: A Gaussian form of correlation function (Figure 3.8).

3: An irregular correlation function with a sharp decrease before a 32 kHz bandwidth followed by a flat level of the coefficient of correlation (Figure 3.9).

One can describe a typical environment that corresponds to each of these types of correlation function. Type 1 environment with no or little frequency selective fading is typical of a flat area with a low density housing. Line-of-sight (LOS) propagation appears to be responsible for this situation. Consequently, this kind of environment provides few propagation paths and very little diffraction. Among the sites studied; Aylmer, Kanata, Ottawa South, the Experimental Farm and the part of Corkstown Road with a LOS path exhibit this type of fading. These areas exhibit a

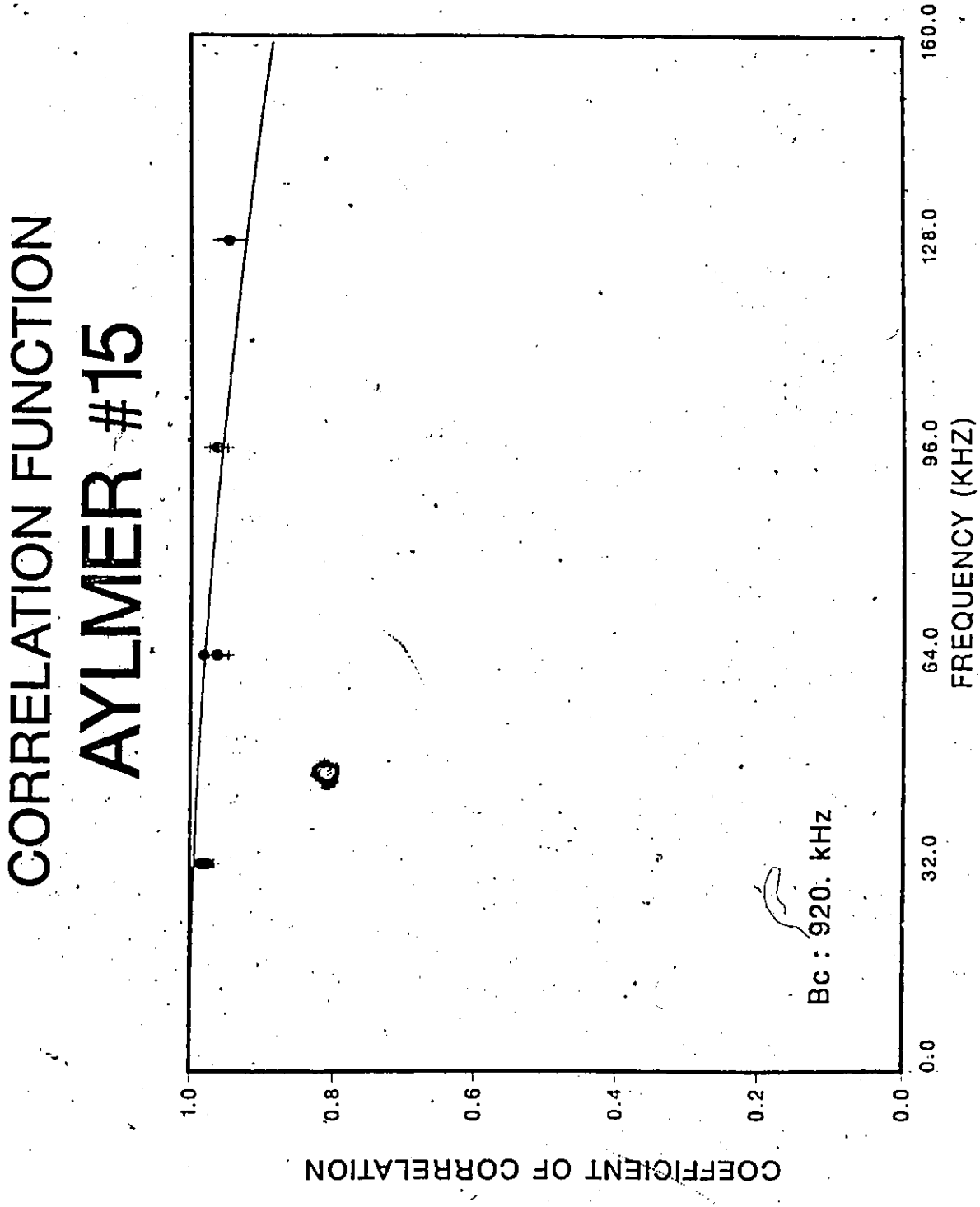

FIGURE 3.7 : Correlation function for Aylmer area block no. 15.

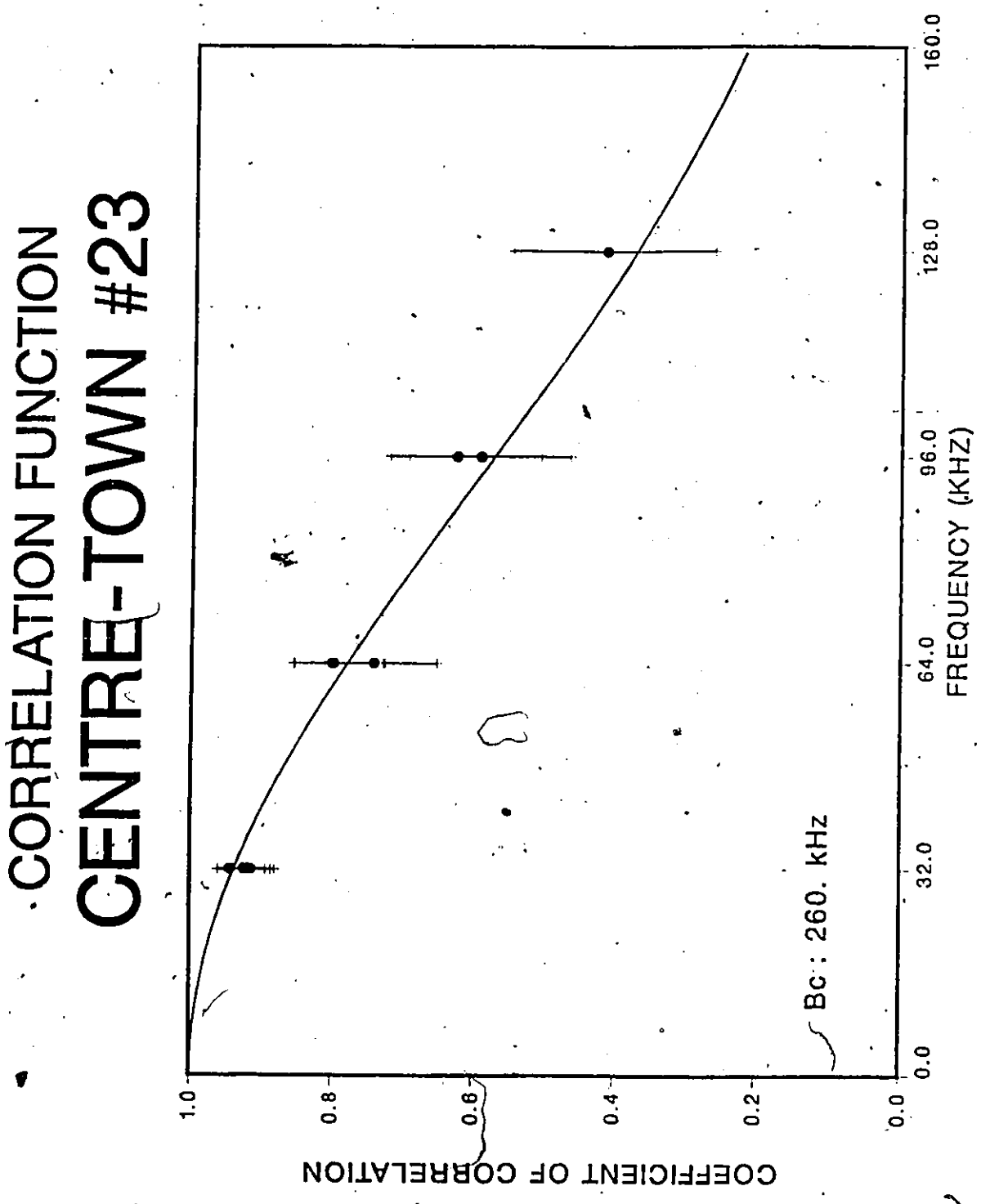

FIGURE 3.8 : Correlation function for Centre-Town area block no. 23.

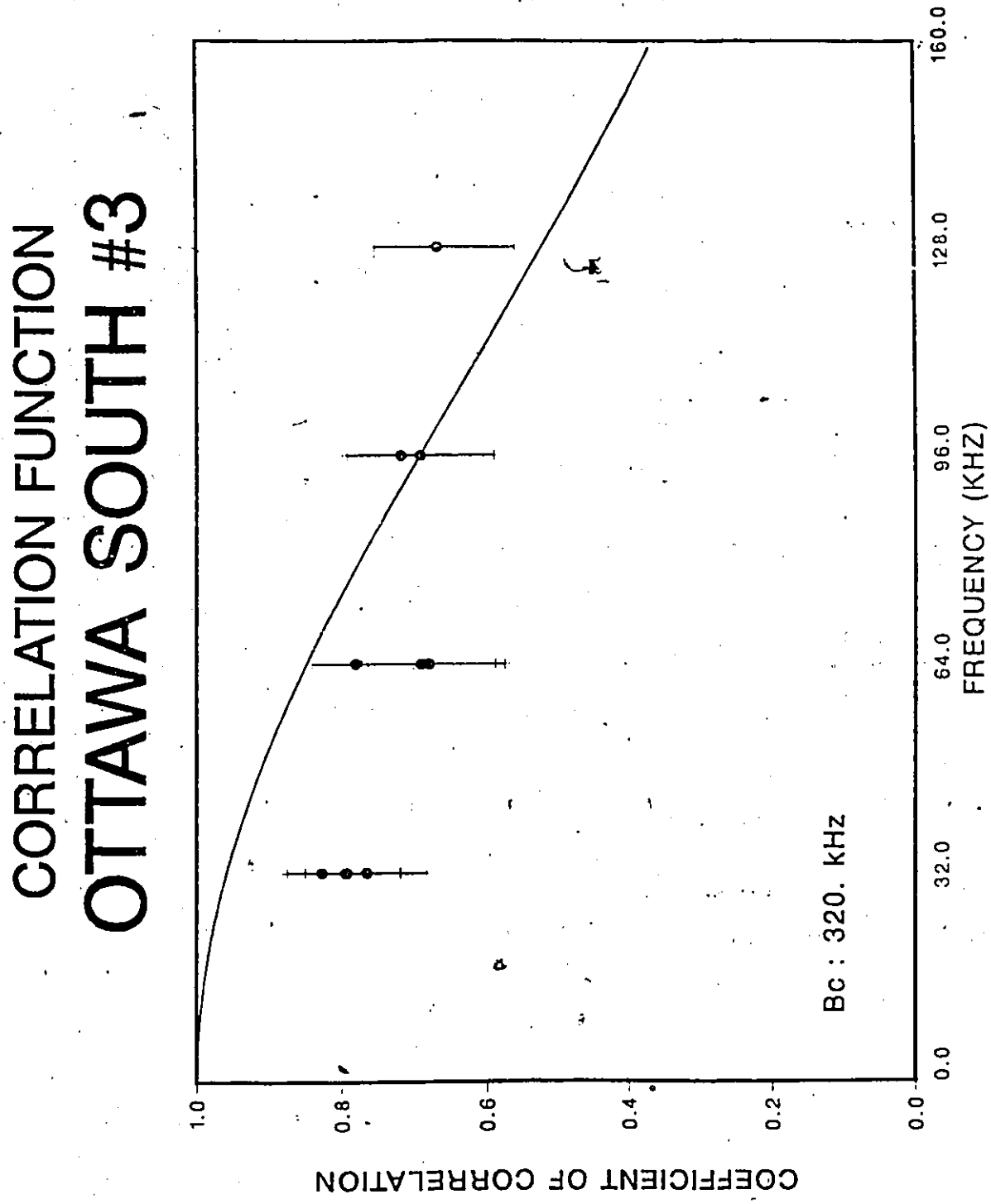

FIGURE 3.9 : Correlation function for Ottawa South area block no. 3.

wide extrapolated coherence bandwidth and have usually a very good coefficient of correlation for a bandwidth less than 128 kHz.

Type 2 correlation function is typical of an area with multiple reflections with little or no LOS propagation. The Centre-Town area corresponds to shows this situation. The correlation function is then described by a smooth Gaussian curve. Seldom, do other environments yield such a Gaussian shape.

Type 3 correlation functions correspond to the irregular case. These correlation functions usually exhibit a sharp decrease before 32 kHz followed by a flat level. This behaviour is typical of environments with a dominant diffraction path due to hills. Such a case was observed in areas such as Ottawa west, part of Alta Vista, Carleton Heights and the part of Corkstown Road located behind a hill. For these environments, the Gaussian correlation function do not apply and it should be expected that the correlation bandwidth is narrower than those computed. These curves suggest the presence of an important reflection arriving with a large delay..

3.2.2 Probability of error

The frequency selective fading causes intersymbol interference. Previous investigations have been performed on the prediction of the probability of error caused by this phenomenon. These investigations refer to envelope correlations only and they yield some interesting results.

Using the equations developed by Bello and Nelin [3,4,5,6] and by Lindenlaub and Bailey [1,24] for the probability of error (PER) caused by frequency selectivity, (see Appendix A) it is possible to obtain the cumulative distribution of the probability of error caused by frequency selectivity as a function of the SNR and the signal bandwidth.The PER was computed for the case of Differential Phase Shift Keying (DPSK) modulation. As an example, for the Centre-Town area, assuming data rates of 9600 bauds and 19200 bauds with a square waveform as data signal (see eq. A.33 and A.34), the corresponding cumulative distributions of PER for different SNR (see eq. A.40, A.41 and Table A-3) are shown in Figure 3.10.

The PER is computed from the cumulative distribution of the coherence bandwidth B_c derived from the experimental cumulative distribution of $R_f(\Omega)$ for different values of T, the bit duration ($T = 1/9,600\ s$ and $1/19,200\ s$). Referring to Figure A.2 in the Appendix A, variations of B_c affect d, the normalized error rate, defined as $1/TB_c$. In the absence of diversity, the distribution of PER is determined as a function of the distribution of B_c and of the SNR. This figure shows a constant PER value due to the noise if d is small enough. The level of error is then mainly a

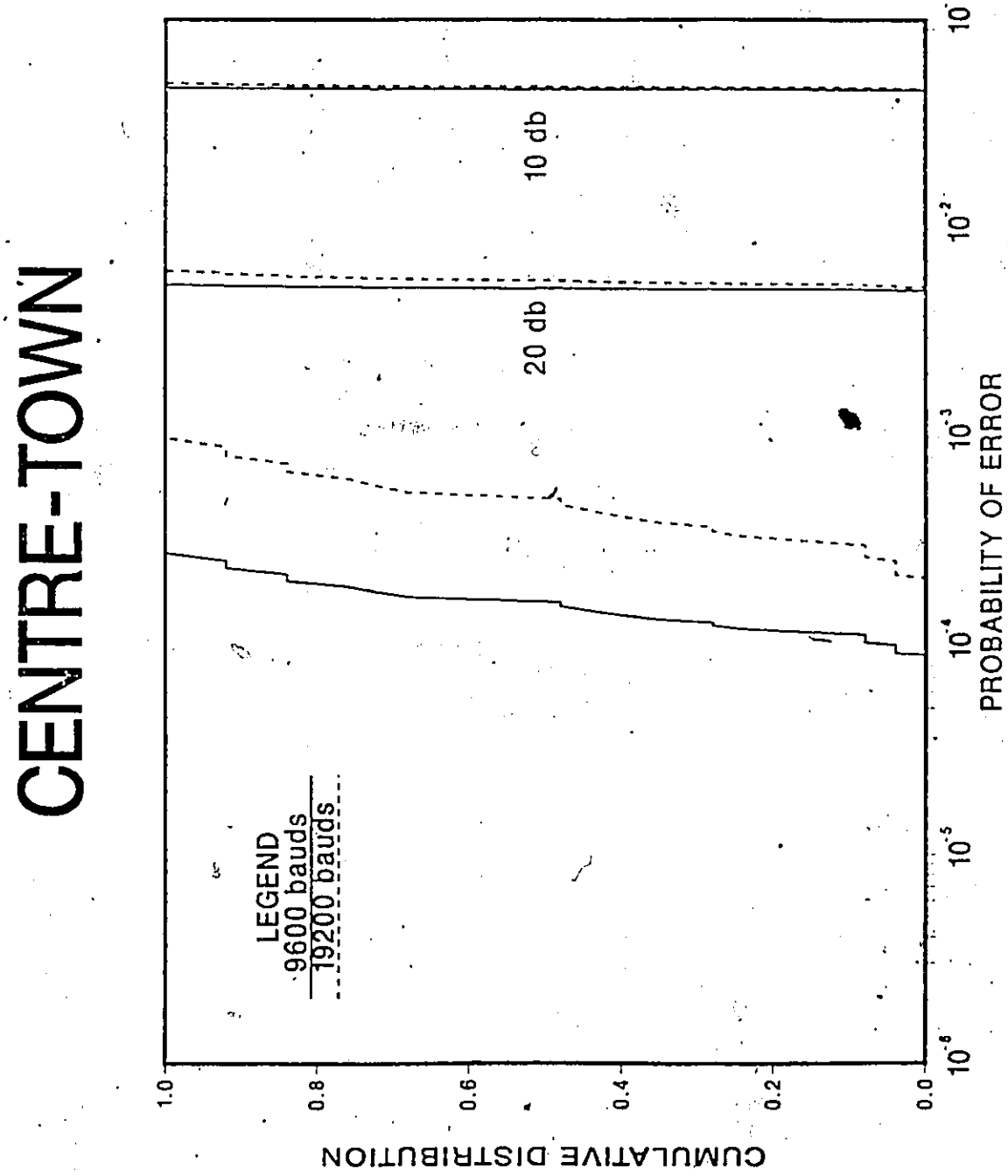

FIGURE 3.10 : Cumulative distribution of the probability of error for the Centre-Town area. Signal rate of 9600 bauds and 19200 bauds for three SNR: 10 dB, 20 dB, ∞

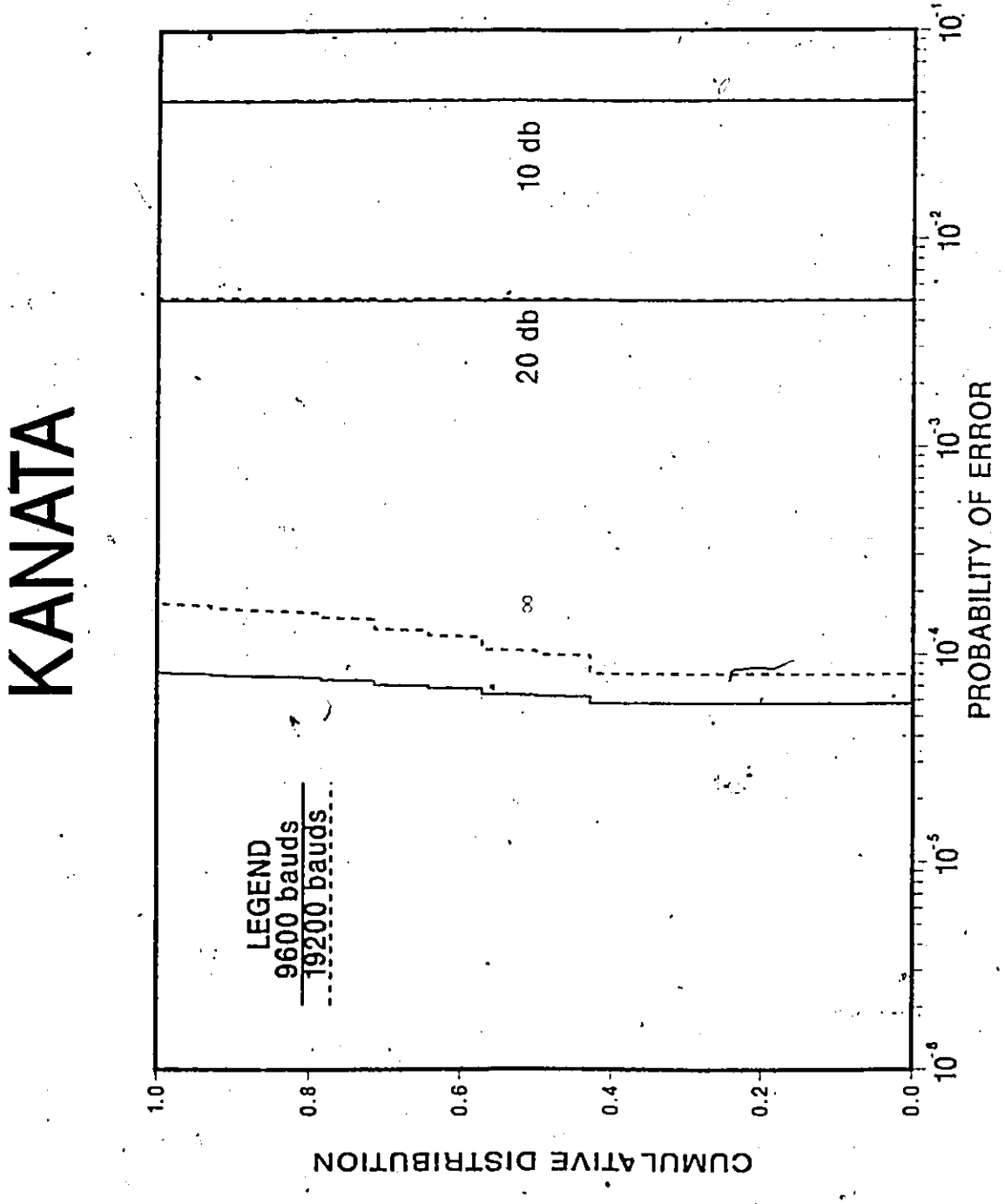

FIGURE 3.11 : Cumulative distribution of the probability of error for the Kanata area. Signal rate of 9600 bauds and 19200 bauds for three SNR: 10 dB, 20 dB, ∞

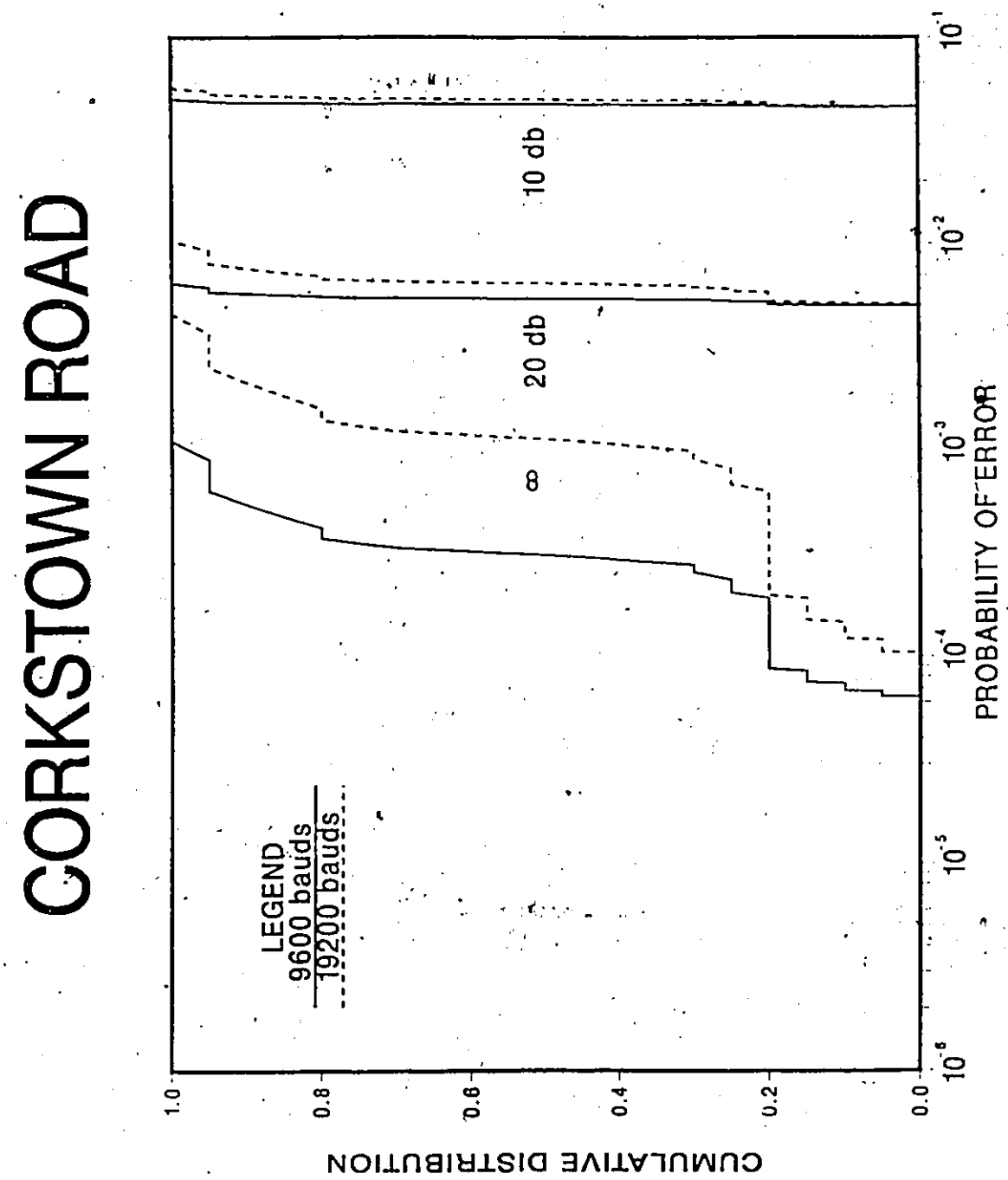

FIGURE 3.12 : Cumulative distribution of the probability of error for the Corkstown Road area. Signal rate of 9600 bauds and 19200 bauds for three SNR: 10 dB, 20 dB, ∞

function of the SNR. At the other extreme, for a larger value of d, the curve shows an irreducible error rate at any SNR caused by frequency selective fading. The PER's shown in Figure 3.10 are representative of situations encountered in a normal environment; numerous reflectors, few hills and a good SNR. There are extreme cases when the frequency selective fading is almost absent (such as in the Kanata area) or very prominent (such as in the Corkstown Road area). The PER's obtained for Kanata are shown in Figure 3.11. As one can observe, in this case, the PER cumulative distributions are lower than for the Centre–Town area (for the same infinite SNR case). A rare but extreme case prevails in the Corkstown road area (Fig. 3.12). The distortion is such that at even for SNR of 10 dB or 20 dB, the frequency selective fading has some influence on the PER. In the infinite SNR case, the PER degrades greatly and is much worse than for any of the other areas under study. This extreme case seldom arises however.

3.3 Phase Behaviour

The experiment was designed to provide both amplitude and phase information by means of coherent detection. With a rubidium frequency standard at the transmitting end and another one at the receiving end, negligible differential phase shift between the reference signal and the other tones occured during the course of an experiment. In addition, the receiver system was designed to initiate sampling always at the same position in the incoming sequence. Therefore, even if the received reference signal phase was uniformly distributed between 0^0 and 360^0, in the absence of frequency selectivity the phase relation between each tone would have remained constant.

The received signal can be represented by five rotating phasors. For the study of the phase behaviour, the central tone (861.500 MHz) is used as a phase reference. Then the four remaining tones can be considered as forming two pairs of vectors, with each pair consisting of two vectors rotating in opposite directions (with respect to the phase reference) at equal angular speeds (+32 kHz and -32 kHz, +64 kHz and -64 kHz) respectively. Observations over two bandwidths (or span of frequencies) are then possible; 64 kHz and 128 kHz. Two other bands of observation corresponding to a tone spacing of 64 kHz are possible. However, they yield statistical results similar to the central 64 kHz bandwidths. Other arrangements of tones are not suitable because of the required condition of symmetry of a pair of tones relatively to a selected phase reference. The two tones must rotate at equal but opposite angular speeds.

Figure 3.13 shows the phase behaviour of two tones (with respect to the reference, the positive direction being defined as the normal sense of rotation of each tone) for a typical block of data

in Aylmer. This sample corresponds to an environment with little frequency selective fading for a 128 kHz bandwidth. The following observations may be made:

1. As expected for a relatively 'well behaved' channel, the average phase displacement for the upper tone (+64 kHz) is equal to the average phase displacement for the lower tone (-64 kHz). This condition corresponds to a uniform time delay of the signals across the bandwidth under observation. Also the observation of the data sample by sample shows a symmetrical variation of the phase for the two tones. A more selective channel (as observed in the Centre-Town area) exhibits less symmetry.

2. Each tone exhibits sudden phase excursions in the vicinity of 90^0 and 180^0 (see circle in figure 3.13) in addition to smaller variations of phases. For the block of data of figure 3.13, these variations are relatively few. However, for areas with a narrower amplitude correlation function (smaller coherence bandwidth) such a phase behaviour is more likely. When these excursions are observed at a given time only for one tone and not for the other one, they indicate selective fading in the form of selective phase reversals of the tone frequency.

3. From the beginning of the block of data to its end (fig. 3.13), the average phase drifted slowly and uniformly by about 30^0. Since both the generation of the modulation sequences and the initiation of the signal sampling are closely synchronized (by the use of rubidium frequency standards), such a displacement may be explained by a difference in the arrival time of the modulated signals, which was due to the physical displacement of the receiver system with respect to the transmitter. For a modulating frequency of 64 kHz and a phase displacement of -30^0, the corresponding reduction in the radial distance between the transmitter and the receiver was approximately 400 m.

4. Computation of the correlation function for the phase presents difficulties. Unless random phase variations about the mean are minimal, phase ambiguities render the task of computing the coefficient of correlation of the phase almost impossible. The Centre-Town environment as opposed to the Aylmer area, typically exhibits large random phase variations (Fig. 3.14).

In order to devise a common factor of comparison of the phase behaviour between different environments, a novel approach is suggested here. Assuming a pair of tones rotating at the same angular speed, but in opposite directions relatively to a central phase reference (example: +64 kHz, -64 kHz and 0 Hz), in absence of frequency selective fading the two tones of a pair exhibit the same phase behaviour from one sample to the other. If, with respect to the reference, the positive direction is defined as the normal sense of rotation for each tone (counterclockwise for

-64 kHz and clockwise for +64 kHz), the phase of one tone changes by the same amount as the phase of the other tone. Thus, without frequency selectivity the difference between the measured phases at two adjacent observations, say points A and B, for the -64 kHz tone will be the same as for the +64 kHz tone. A measure of the frequency selectivity is to compare the two differences or changes of phases from point A to B for the two tones. A large difference between the changes of phases indicates the presence of an important selective effect while a small difference indicates its absence. The new approach is to compute the difference of these changes for a block of data and to establish statistical values for these differences for each of the environments under study. The approach is based on the differences of phases between two adjacent observations rather than on the absolute measured phase at each point because the absolute phase is not known *a priori* and therefore it is not possible to compare the received phases with the transmitted phases.

Assuming that tones 1 and 2 make up a pair of symmetrical vectors rotating at the same but opposite angular speeds, relatively to a center reference, the first step is to compute the phase shifts between the observed phase at measurement point A and the following observed phase at measurement point B.

$$\delta_{1AB} = \phi_A - \phi_B$$

$$\delta_{2AB} = \theta_A - \theta_B$$

Here δ_{1AB} and δ_{2AB} are the phase changes for tones 1 and 2 respectively, between the consecutive measurement points A and B. Angles ϕ and θ are phase angles for tones 1 and 2 respectively. Each block of measurements includes 128 phases and therefore yields 127 phase shifts for each tone. The next step is to compute the difference Δ between the phase shift of tone 1 and the corresponding phase shift of tone 2.

$$\Delta_{AB} = \delta_{1AB} - \delta_{2AB}$$

The minimum phase difference was taken for each measurement point (there is two differences because all phases are defined on a circle). The 127 values of Δ form a set where the standard deviation (stdv) is an indication of the frequency selective fading. A large standard deviation indicates an important fading and vice versa.

Figures 3.15 to 3.17 show such cumulative distributions of the phase difference between two tones for two typical areas Aylmer and Centre–Town. These distributions indicate the probability

of a phase distortion to occur between two tones. As example, in Figure 3.15 the two tones vary by the same phase $\pm 30^0$ with a probability of 80%. As expected, the Aylmer site has less phase dissymmetry (see remarks about Fig. 3.13) than the Centre-Town area. Exceptional behaviour occured, Figure 3.17 has a distribution similar to the distribution of Figure 3.16. For each environment, the standard deviations were grouped and used to form a cumulative distribution of the standard deviation of the phase diffence between two tones equally spaced from the reference (Fig. 4.17 to 4.24). Aylmer the cumulative distributions of the standard deviations for the 64 kHz and the 128 kHz bandwidths are closer than in Center-Town, which indicates the presence of a larger coherence bandwidth because it suggests a flat correlation function. A strong correspondence between the cumulative distribution of the standard deviation and the envelope correlation function was observed for each area. They show clearly, for Aylmer and Centre-Town areas, that phases have a different behaviour. The Centre-Town block has, as expected, a wider distribution.

It is important to observe here that important phase asymmetries between two tones may exist concurrently with relatively flat amplitude correlation functions of type 1. This condition implies the occurrence of intersymbol interference even in the presence of a good SNR.

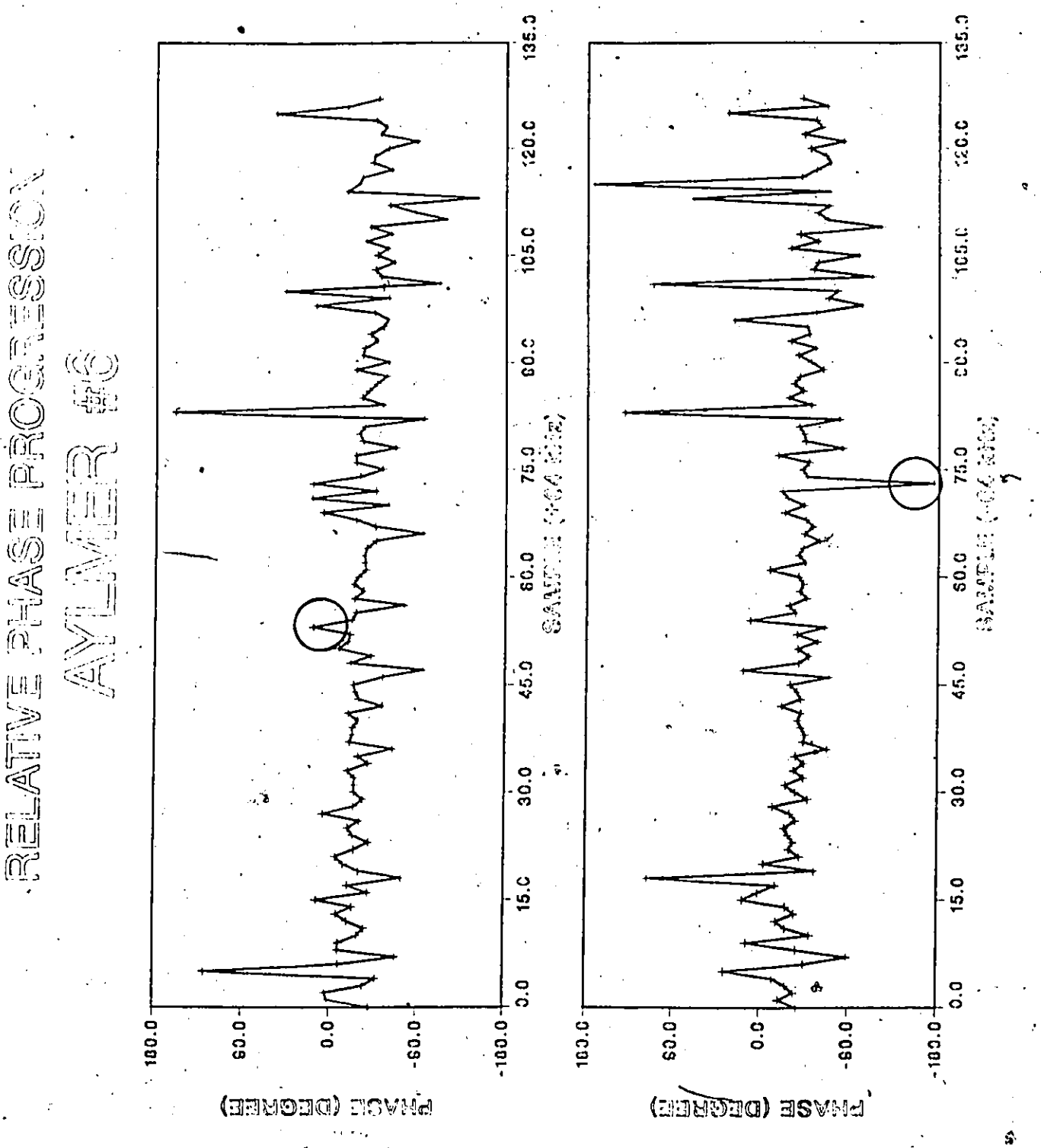

FIGURE 3.13 : Relative Phase progression for Aylmer area, block no. 6.

FIGURE 3.14 : Relative Phase progression for Centre Town area, block no. 2.

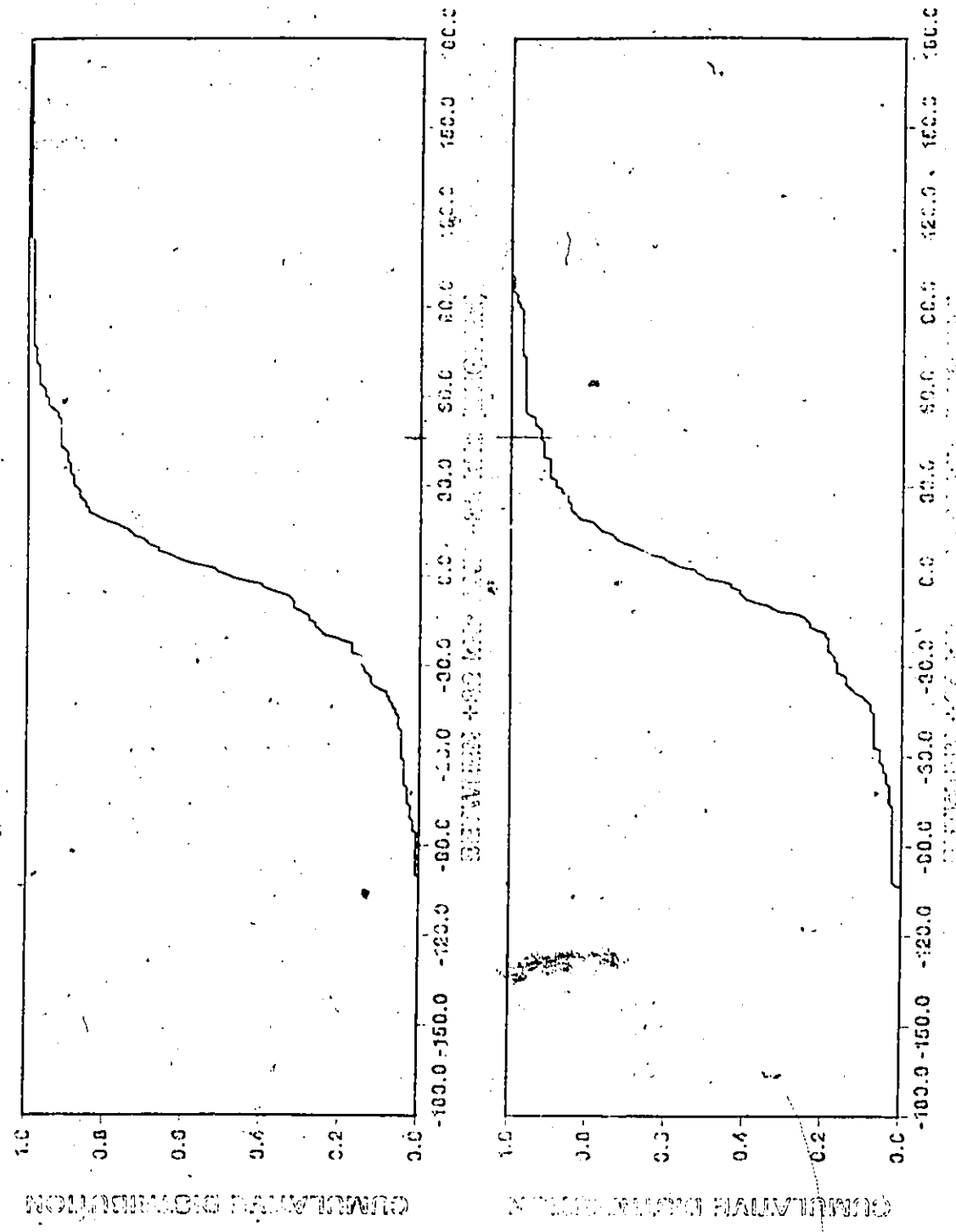

FIGURE 3.15 : Phase difference between two tones for Aylmer area, block no. 2.

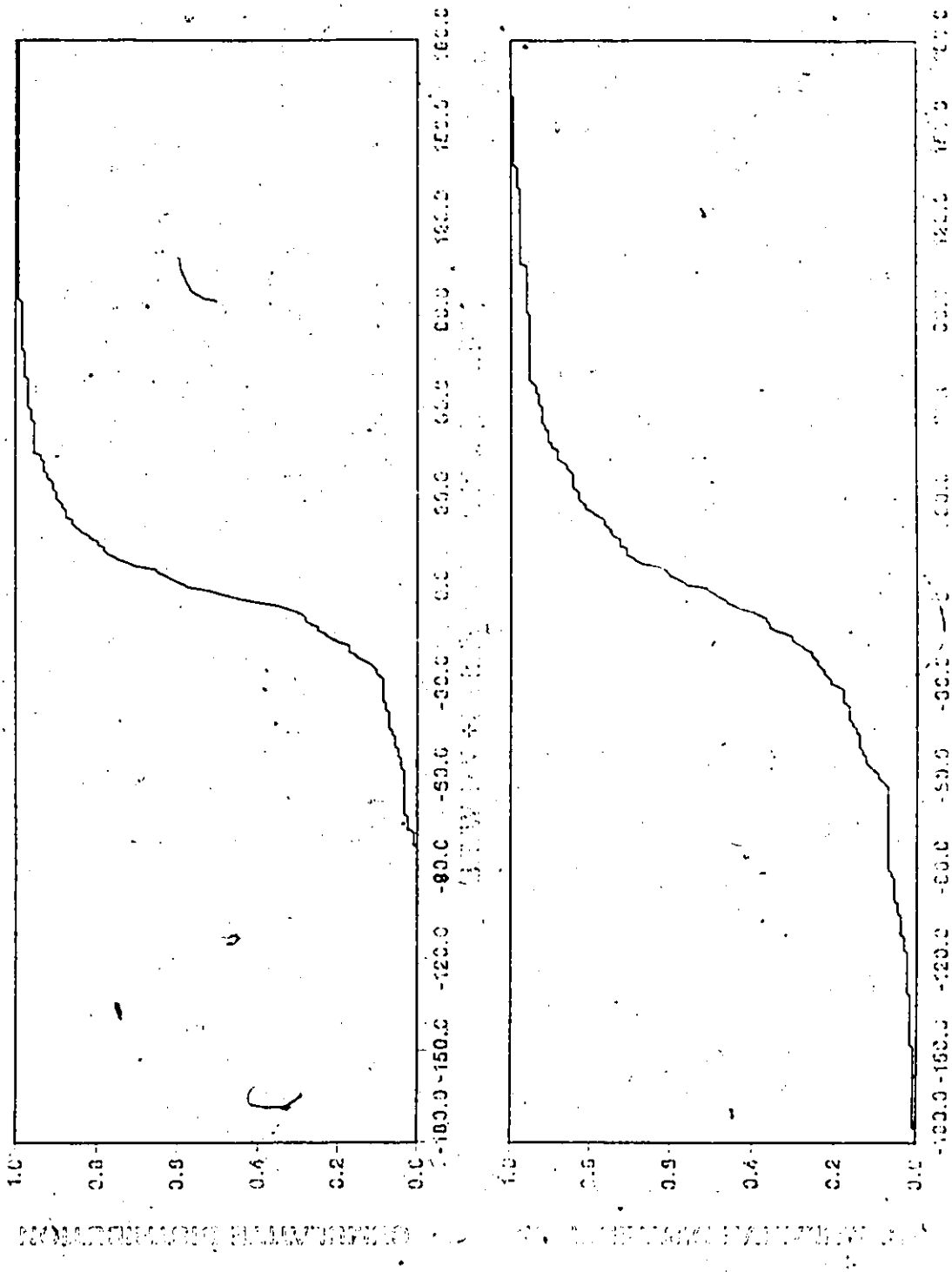

FIGURE 3.16 : Phase difference between two tones for Centre Town area, block no. 2

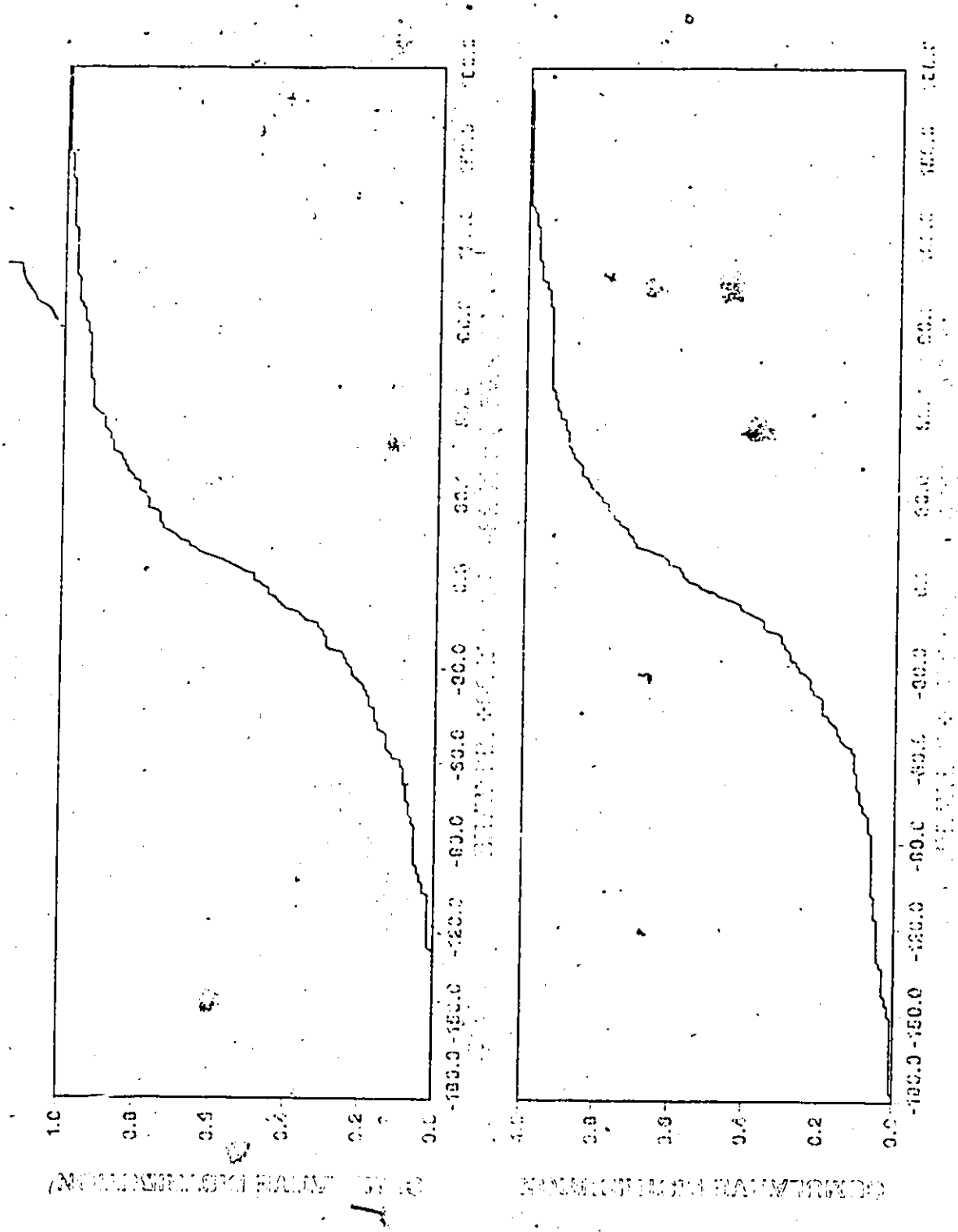

FIGURE 3.17 : Phase difference between two tones for Aylmer area, block no. 6.

CHAPTER 4

RESULTS

4.1 Introduction

This chapter contains global results for each of the eight different environments. It contains the cumulative distributions of the envelope coefficient of correlation for four different frequencies, the cumulative distributions of the coherence bandwidth ($B_c = e^{-1}$; arbitrary value used by Bello and Nelin [3,4,5,6]) and finally the cumulative distributions of the standard deviation of the phase for two frequency separations. These results agree for each environment in the sense that when the coefficient of correlation is high, the coherence bandwidth is wide and the standard deviation of the phase is small.

This chapter contains graphs derived by the signal processing described in Chapter 3. They are easy to interpret. As example the cumulative distribution of the Centre Town area (Fig. 4.5) exhibits a coefficient of correlation better than 0.8 with a probability of 0.05, 0.15, 0.5, 0.9 for respectively 128 kHz, 96 kHz, 64 kHz and 32 kHz. The coherence bandwidth is higher than 280 kHz with a probability of 0.5 and the standard deviation of the phase has a probability of 0.5 to be below 45^0 and 65^0 for respectively 64 kHz and 128 kHz.

All these results show the presence of frequency selectivity. Some areas are more subject to this phenomenon than others, especially when diffraction of the signals occured. An extreme case is the Corkstown Road area, where most of the measurements were taken behind a hill with very few reflections and some measurements with a line-of-sight component. The three plots related to this area exhibit a steep change in their cumulative distributions because of this situation.

A last remark, three similar environments show very different distributions, namely Kanata, Ottawa West and Carleton Heights areas. It seems that a slight change in housing and size of hills is enough to result in a large difference in their distributions. There is no clear explanation for this. The orientation of hills relatively to the transmitter could be an explanation. Indeed, if hills are oriented perpendicularly to the direction of the signal more diffraction occured. On the other hand, if they are oriented in the same direction of the received signal, very little diffraction occured.

4.2 Amplitude (Envelope) of the Signal.

The results of the effects of the frequency selective fading on the envelope of the signal are gathered in two groups, namely the cumulative distribution of the coefficient of correlation and the cumulative distribution of the coherence bandwidth. Table 4.1 gives the average, the standard deviation, the minimum and the maximum of the coherence bandwidth for each area. Probabilities of error for the average value of B_c are shown for two baud rates, namely 9600 and 19200.

Each block of data have resulted after data processing in 10 coefficients of correlation. For each environment, the coefficients of correlation have been grouped together. Figures 4.1 to 4.8 show the cumulative distribution of the coefficient of correlation for every frequency separation for each environment. The presence of frequency selective fading is clearly shown by these Figures.

Figures 4.9 to 4.16 show the cumulative distributions of the coherence bandwidth for the 8 different areas. The coherence bandwidth was computed as described in Chapter 3 and is defined as the frequency separation between two points equal to e^{-1} on the correlation function. A Gaussian shape is assumed for the correlation function. When B_c is higher then 1000 kHz, they are grouped together on the distribution.

4.3 Phase of the Signal

Figures 4.17 to 4.24 show the cumulative distributions of the standard deviation of the phase such as defined in Chapter 3. These distributions show clearly that even for a very good environment where the envelope coefficient of correlation is near 1, there are frequency selectivity effects appearing in the phase of the signal.

The eight areas can be sorted from the point of view of the importance of frequency selectivity, from the less selective to the most selective these areas are: Kanata, Ottawa South and Experimental Farm, Aylmer, Altavista, Centre-Town, Carleton heights, Ottawa West and finally Corkstown Road. The origins of frequency selectivity can be identified as:

1) The diffraction of the signals, certainly the most important contributor.

2) The reflection of the signals, a less important contributor. The number of reflections appears to be an important factor (the Aylmer and Centre-Town area illustrate this point well).

TABLE 4.1: Coherence Bandwidth (Results)

Site	Coherence Bandwidth (kHz).				PER ($\times 10^{-5}$)*	
	Average	St. Dev.	Min.	Max.	9600 b/s	19200 b/s
Kanata	815	226	520	1050	1.2	4.8
Exp. Farm + Ott. South	636	286	300	1050	1.9	4.8
Aylmer	580	196	250	1010	2.3	9.5
Alta Vista	383	110	210	560	5.5	22.5
Carleton Heights	310	120	160	510	8.3	34.2
Ottawa West	298	96	180	510	8.9	36.5
Center–Town	293	62	200	450	10.0	39.1
Corkstown Road	265	196	100	780	11.9	49.0

* Probability of error for a DPSK modulation. The PER values are computed from the average coherence bandwidth for an infinite SNR.

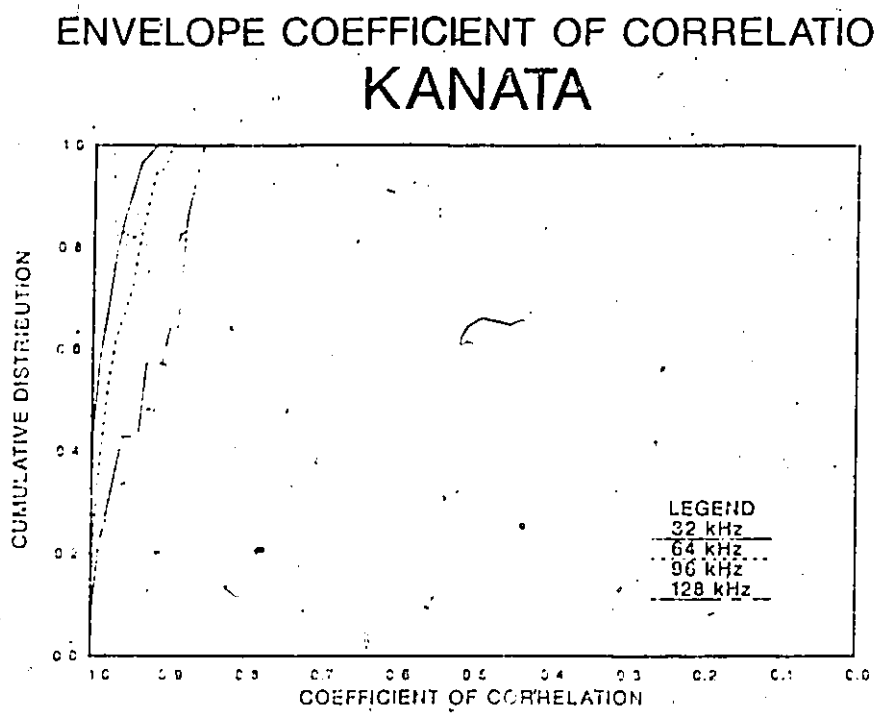

FIGURE 4.1 : Cumulative distribution of the envelope coefficient of correlation for Kanata area.

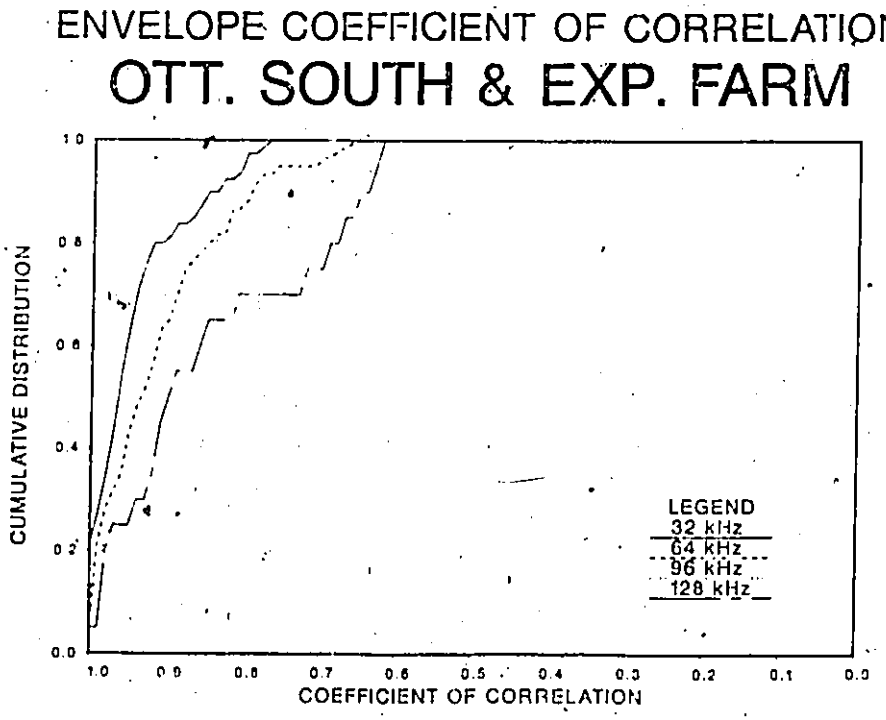

FIGURE 4.2 : Cumulative distribution of the envelope coefficient of correlation for Ottawa South & Experimental Farm area.

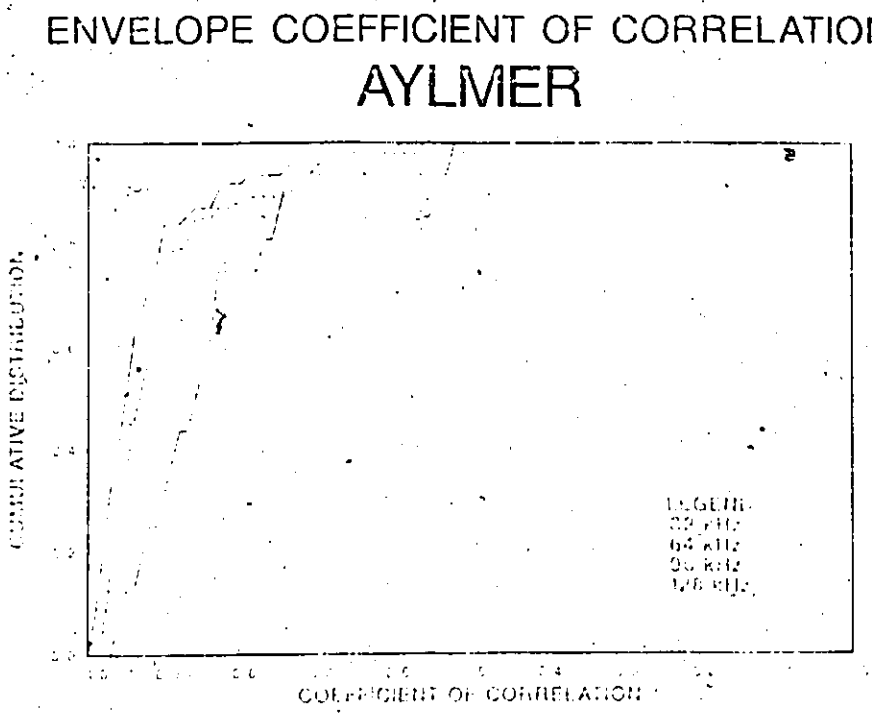

FIGURE 4.3 : Cumulative distribution of the envelope coefficient of correlation for Aylmer area

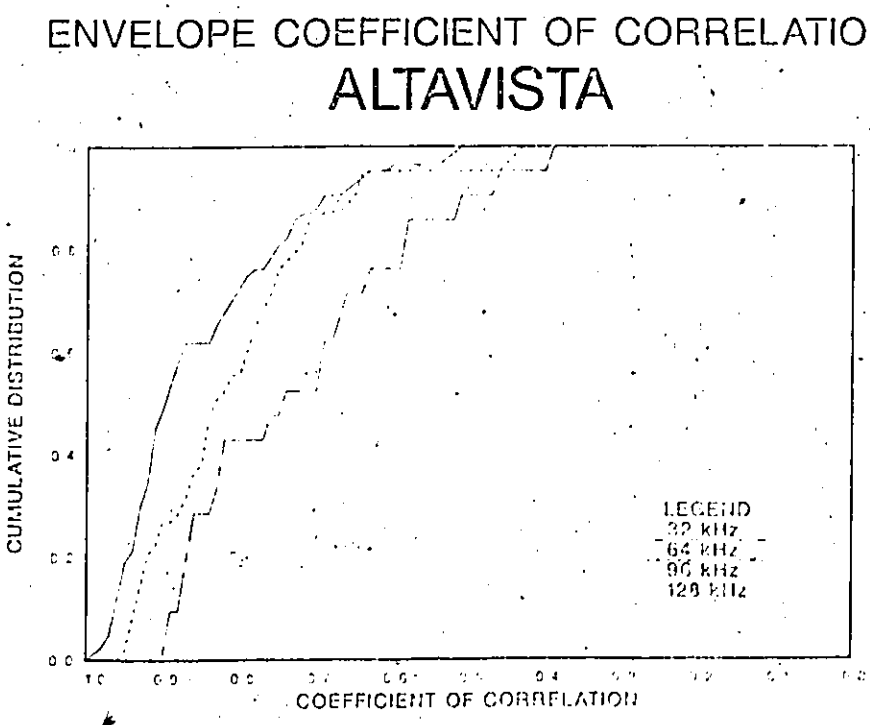

FIGURE 4.4 : Cumulative distribution of the envelope coefficient of correlation for Altavista area

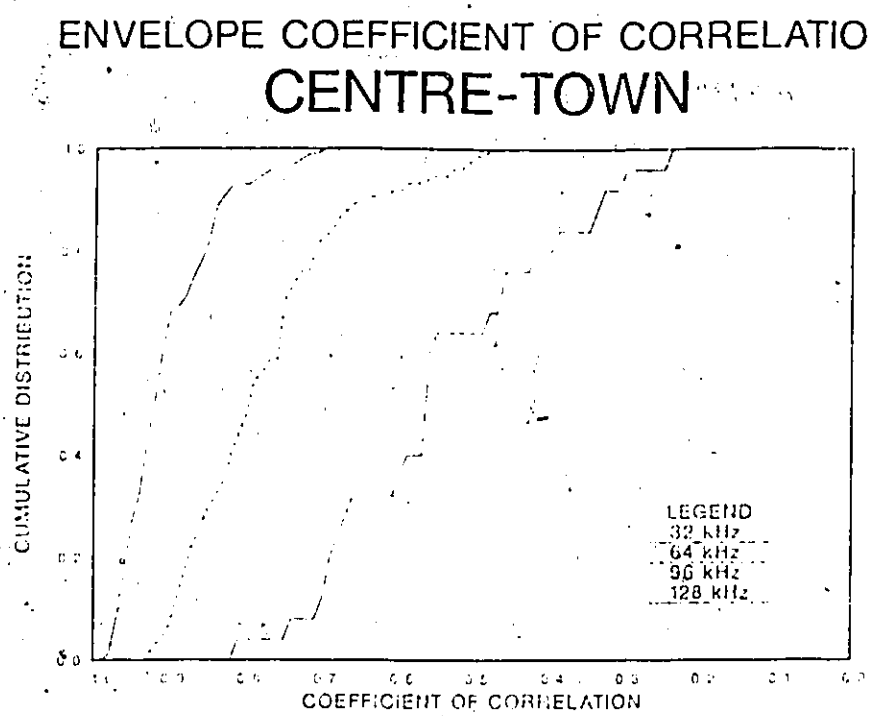

FIGURE 4.5 : Cumulative distribution of the envelope coefficient of correlation for Centre-Town area.

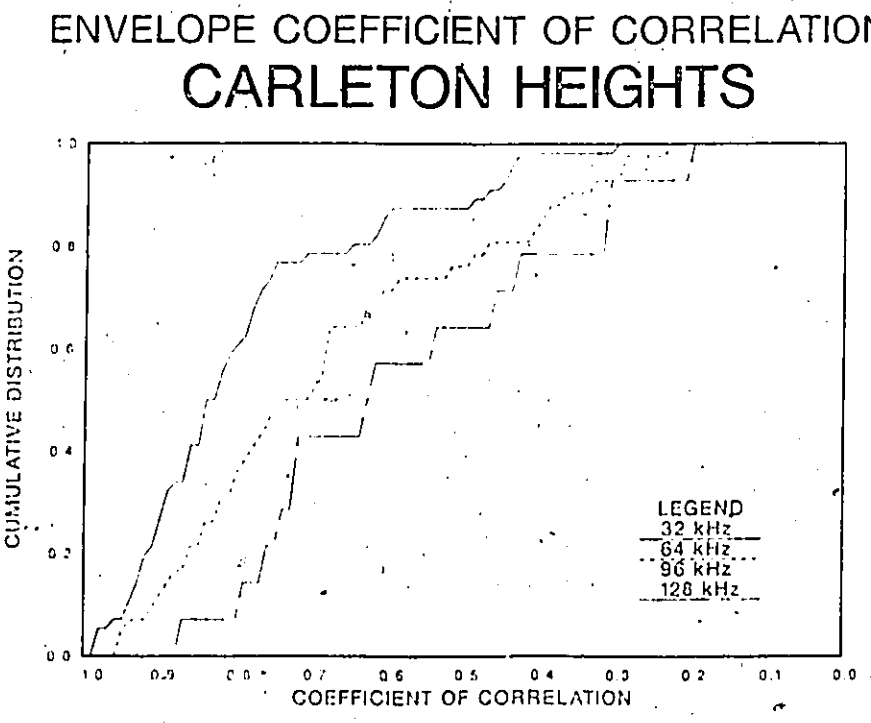

FIGURE 4.6 : Cumulative distribution of the envelope coefficient of correlation for Carleton Heights area.

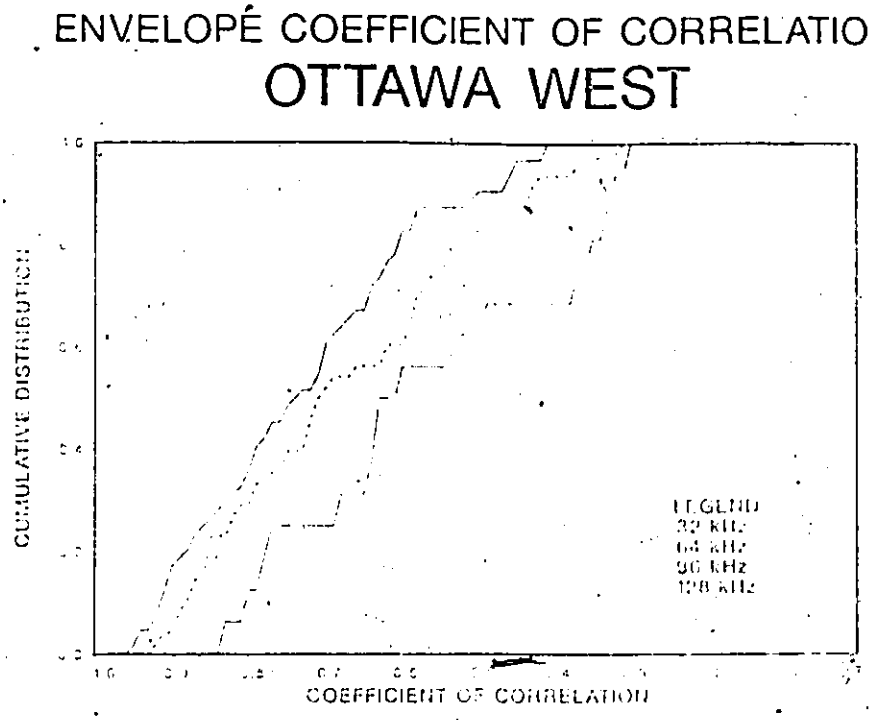

FIGURE 4.7 : Cumulative distribution of the envelope coefficient of correlation for Ottawa West area.

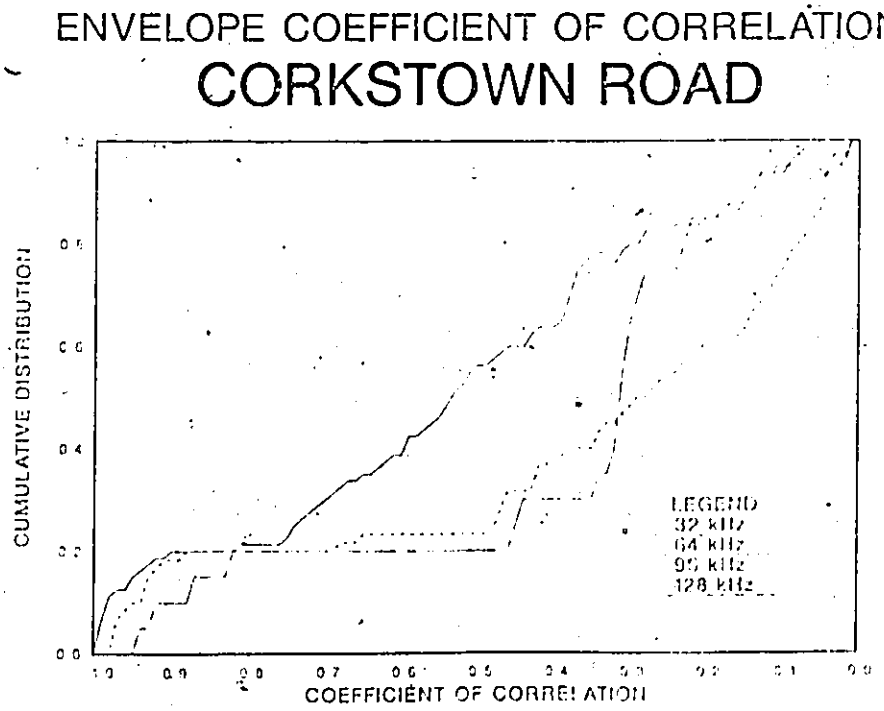

FIGURE 4.8 : Cumulative distribution of the envelope coefficient of correlation for Corkstown Road area.

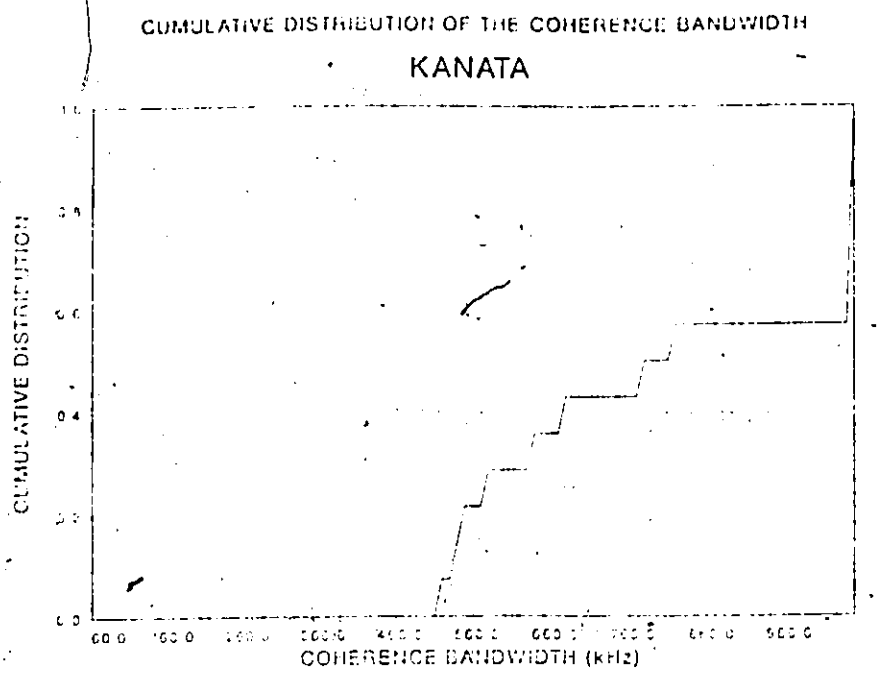

FIGURE 4.9 : Cumulative distribution of the coherence bandwidth for Kanata area

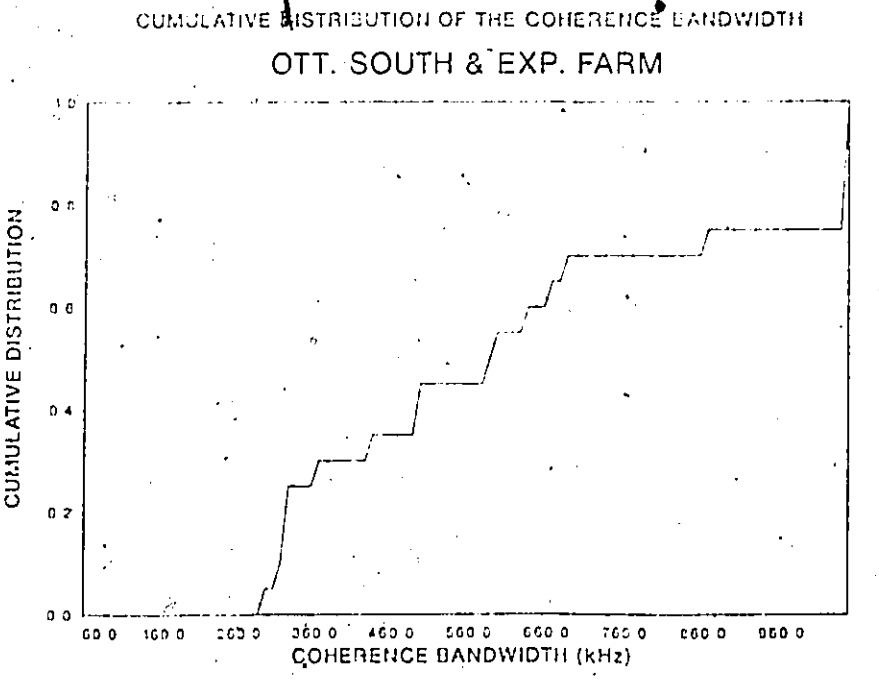

FIGURE 4.10 : Cumulative distribution of the coherence bandwidth for Ottawa South & Experimental Farm area.

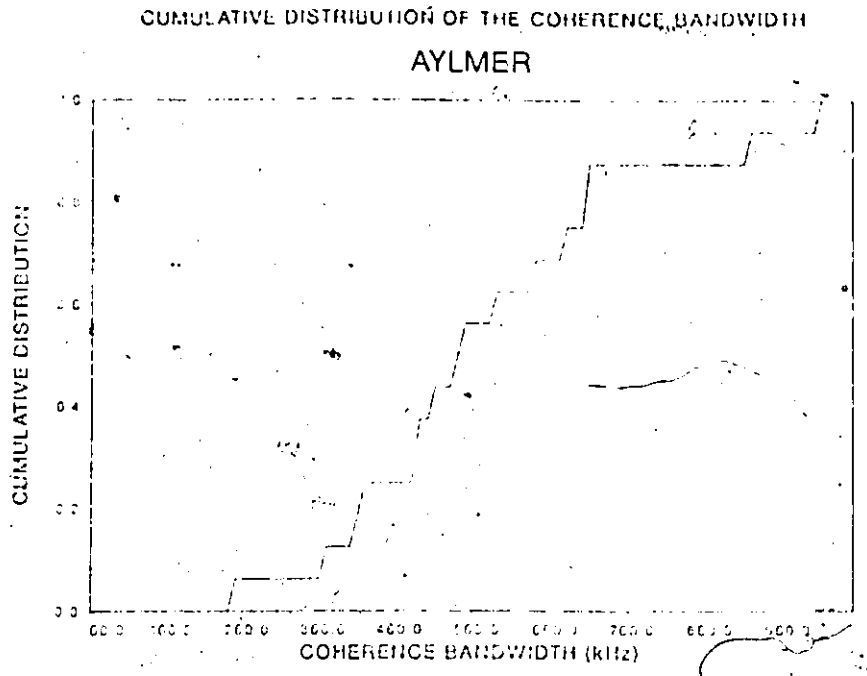

FIGURE 4.11 : Cumulative distribution of the coherence bandwidth for Altavista area

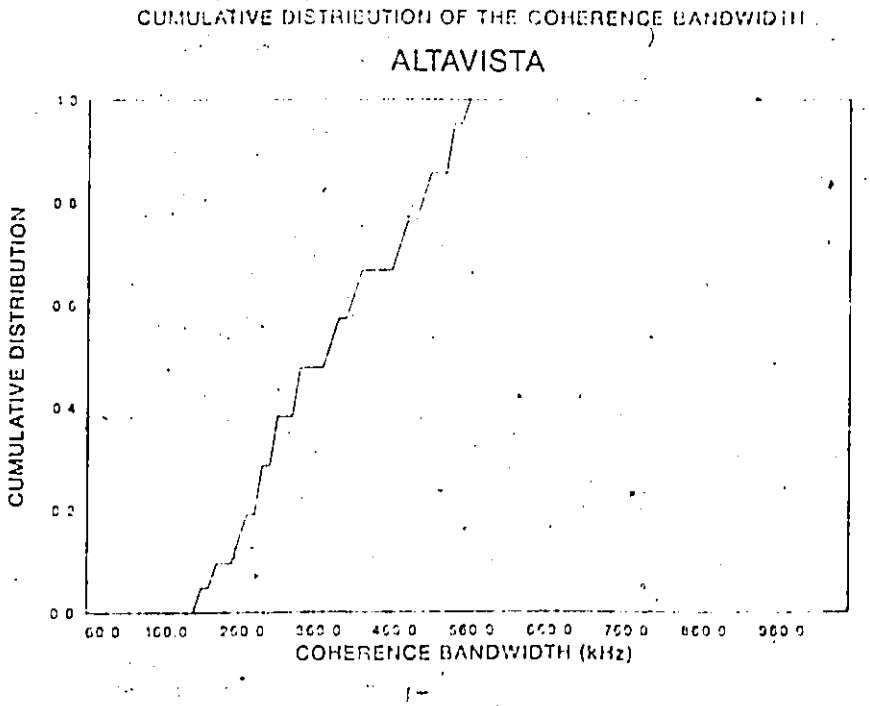

FIGURE 4.12 : Cumulative distribution of the coherence bandwidth for Aylmer area

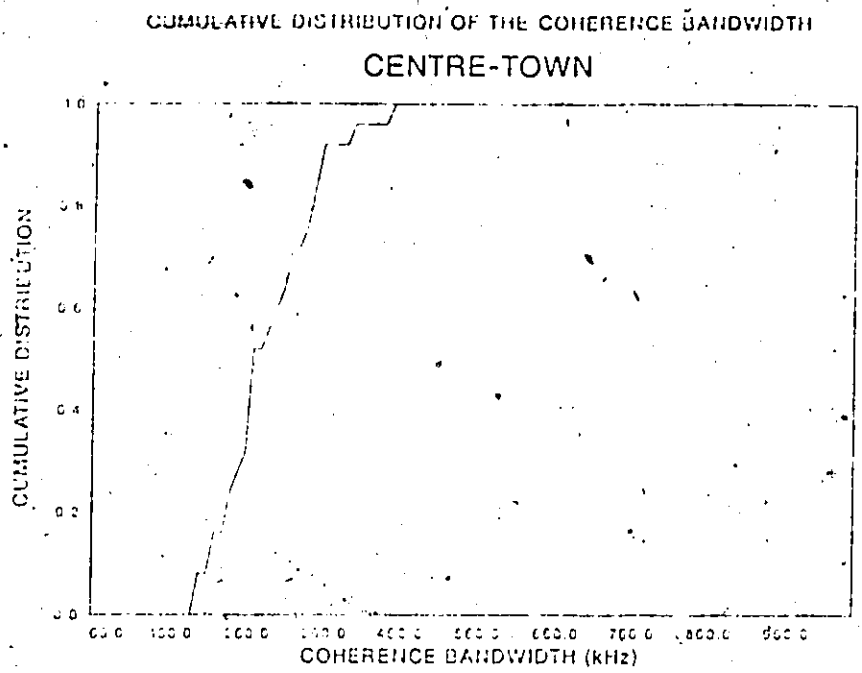

FIGURE 4.13 : Cumulative distribution of the coherence bandwidth for Centre Town area.

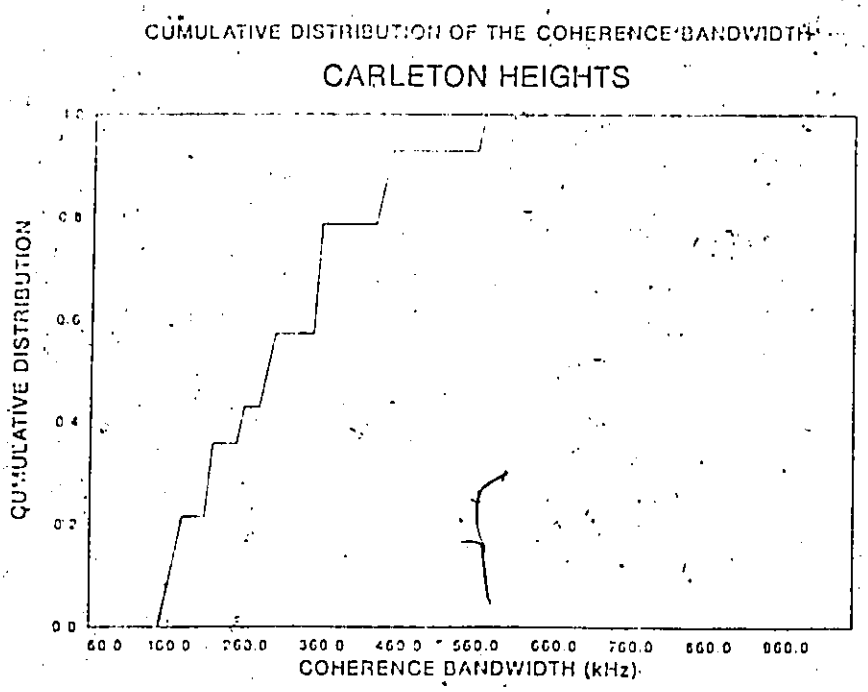

FIGURE 4.14 : Cumulative distribution of the coherence bandwidth for Carleton Heights area.

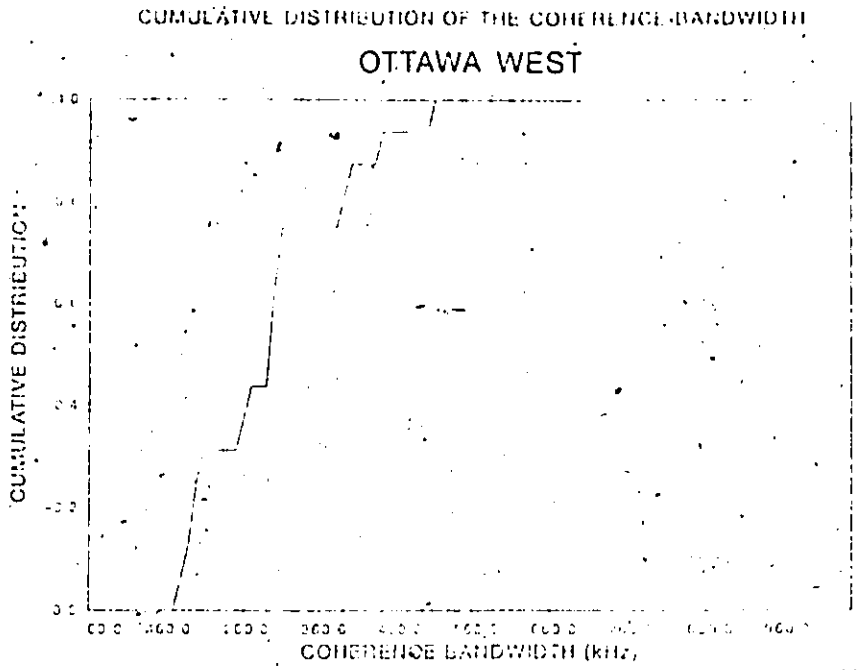

FIGURE 4.15 : Cumulative distribution of the coherence bandwidth for Ottawa West area

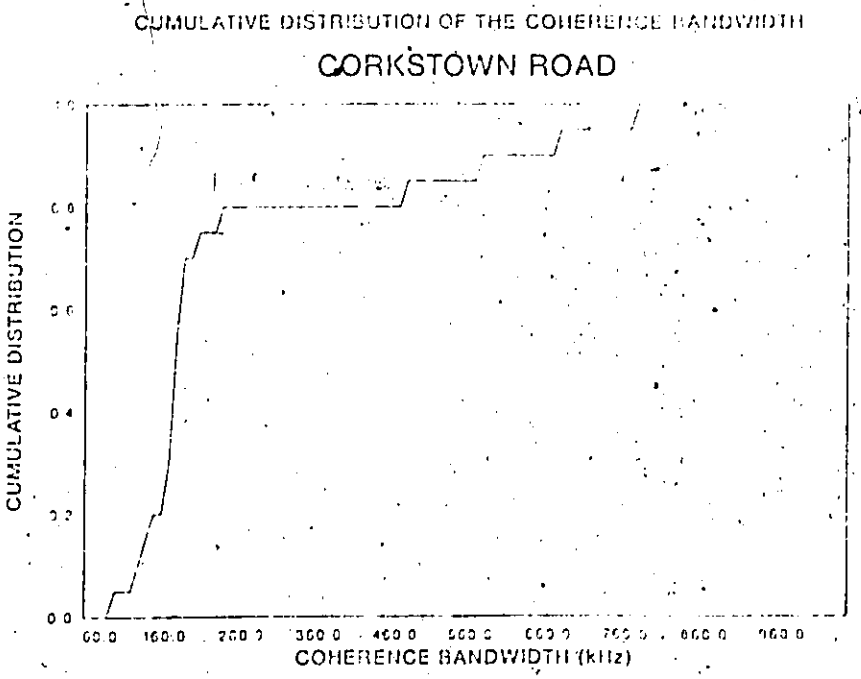

FIGURE 4.16 : Cumulative distribution of the coherence bandwidth for Corkstown Road area

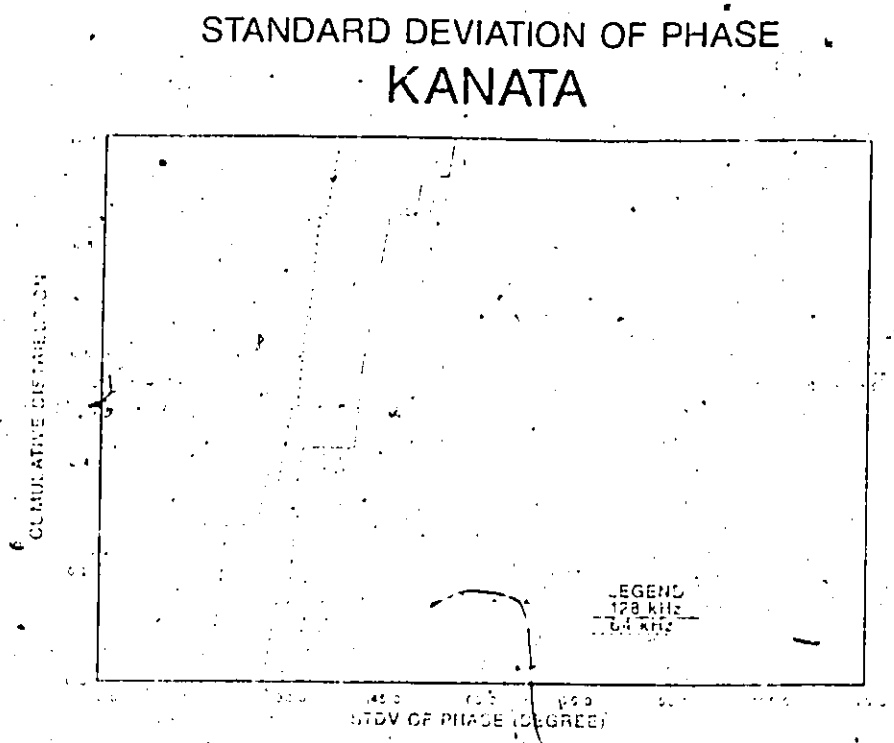

FIGURE 4.17 : Cumulative distribution of the standard deviation of the phase for Kanata area.

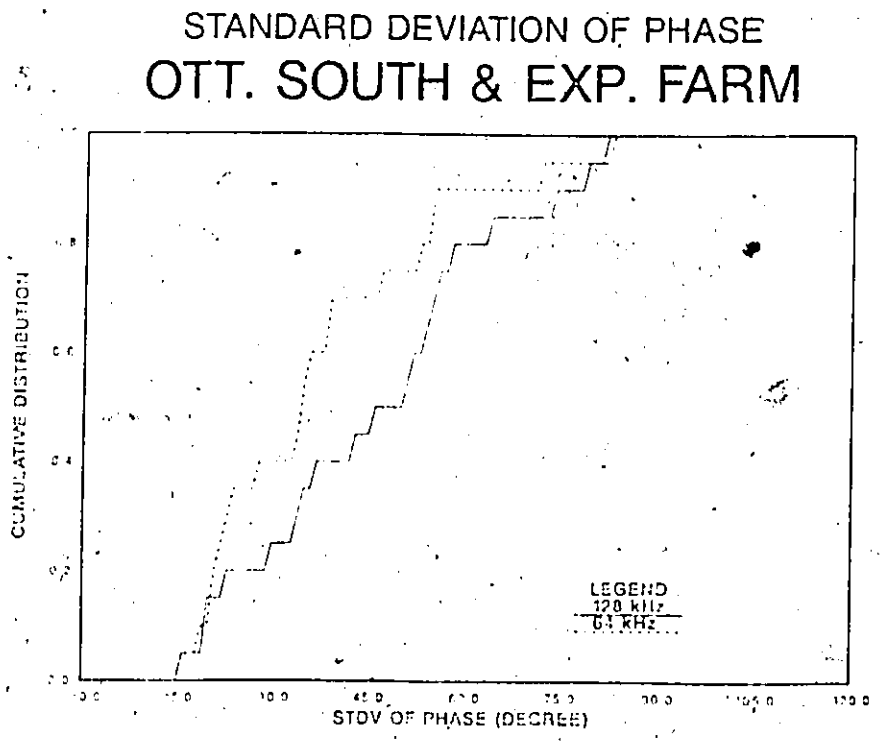

FIGURE 4.18 : Cumulative distribution of the standard deviation of the phase for Ottawa South & Experimental Farm area.

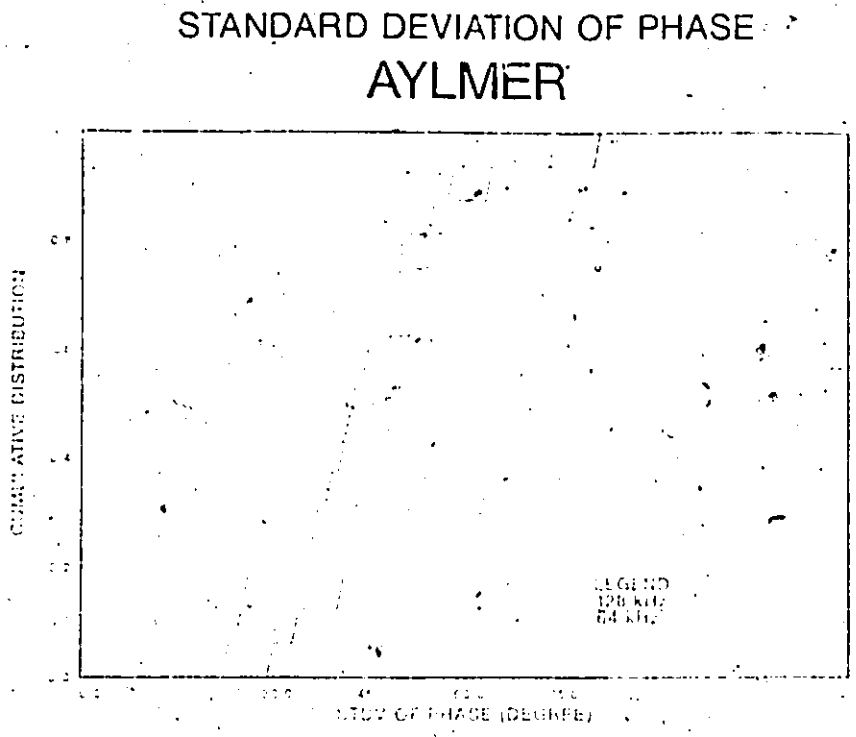

FIGURE 4.19 : Cumulative distribution of the standard deviation of the phase for Aylmer area

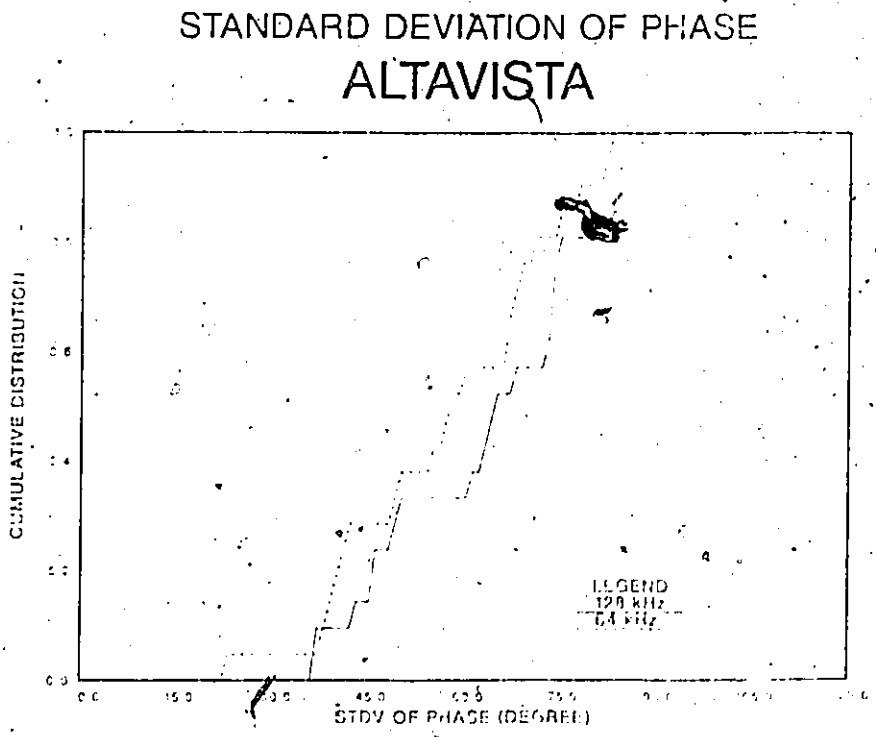

FIGURE 4.20 : Cumulative distribution of the standard deviation of the phase for Altavista area

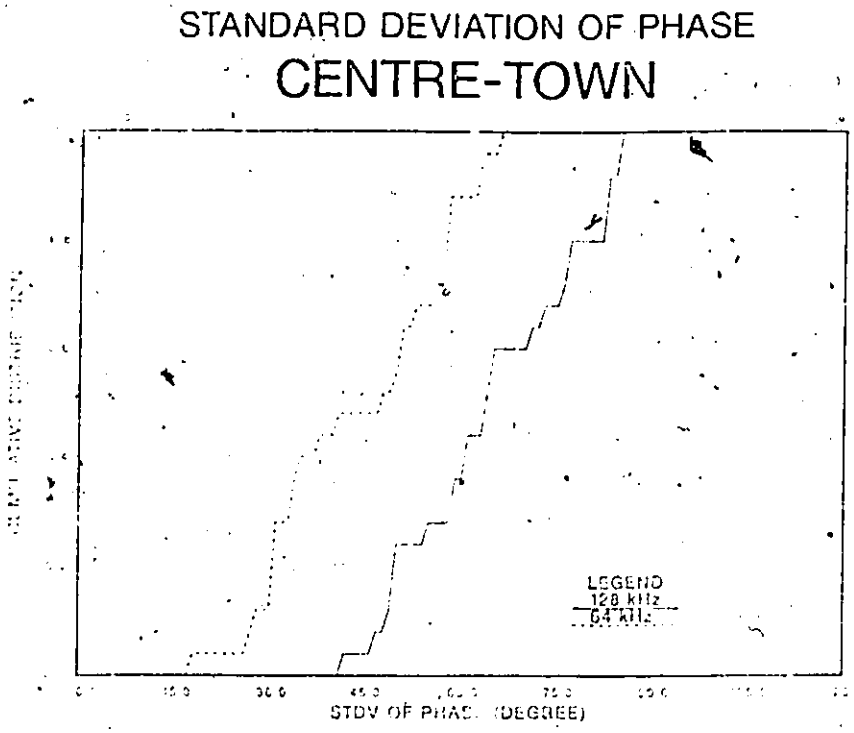

FIGURE 4.21 : Cumulative distribution of the standard deviation of the phase for Centre-Town area.

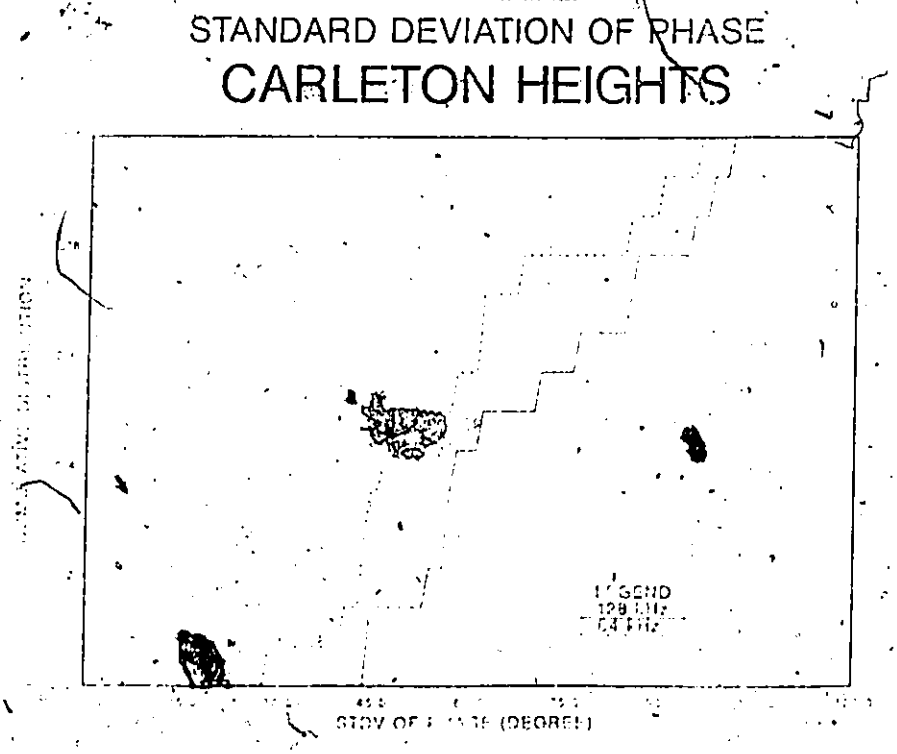

FIGURE 4.22 : Cumulative distribution of the standard deviation of the phase for Carleton Heights area

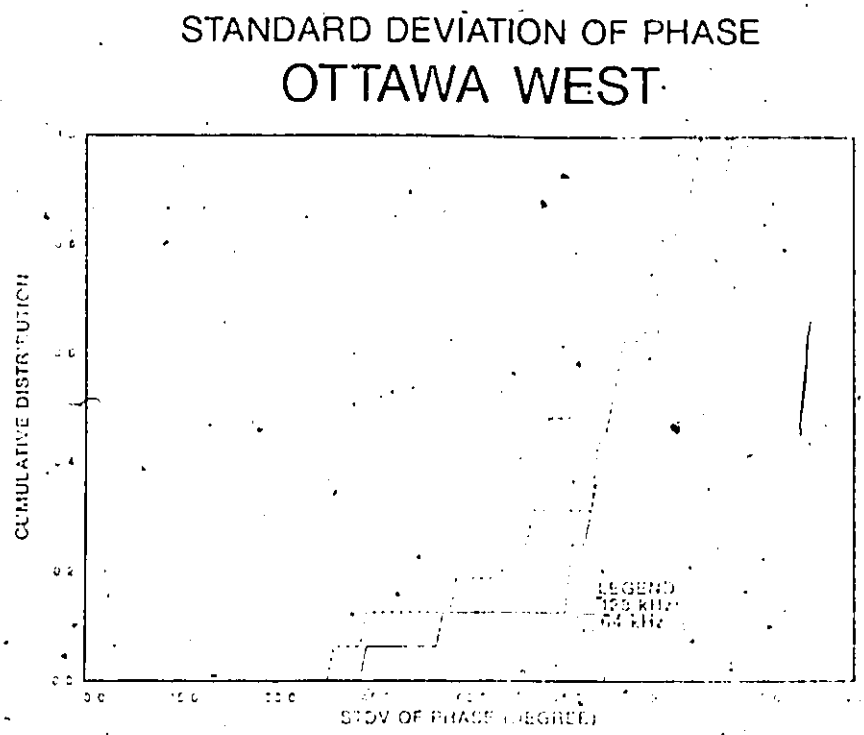

FIGURE 4.23 : Cumulative distribution of the standard deviation of the phase for Ottawa West area.

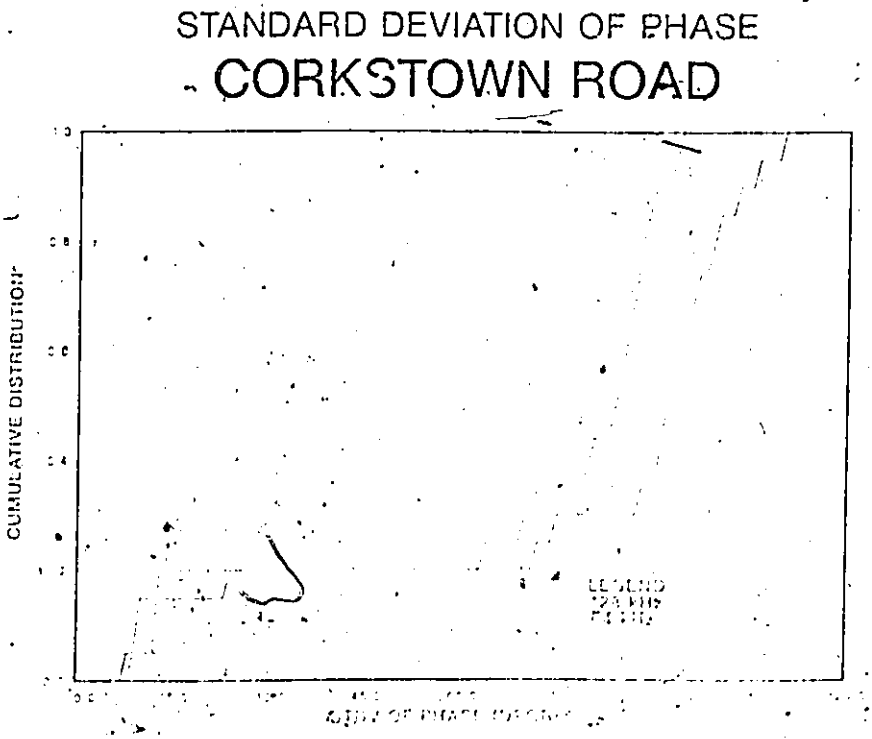

FIGURE 4.24 : Cumulative distribution of the standard deviation of the phase for Corkstown Road area.

CHAPTER 5

CONCLUSION

The multitone technique described in this thesis, both in its implementation and its application, affords a novel way to probe the mobile radio channel frequency selective behaviour. On the other hand, the power spectrum of the signal is limited to a $((\sin\ x)/x)^2$ form and the bandwidth studied is rather limited. While this current implementation of the multitone method provides only five useful spectral lines, longer sequences could be designed to produce a larger number of equally spaced spectral lines over the same bandwidth. Also, the frequency separation between two tones and therefore the bandwidth studied could be changed with an adjustment of the generating sequence rate and few modifications to the receiving equipment. The technique is rather flexible for a small and a medium bandwidth. Moreover, amplitude and phase behaviours of the signal are measurable. The multitone technique offers a great degree of precision to measure the correlation for a specific frequency separation and it would be instructive to pursue other experiments using a larger number of more closely spaced spectral lines in the order to obtain a higher degree of definition over the bandwidth under study.

In spite of the fact that frequency selectivity has been studied for a small bandwidth as compared to other techniques (5 to 10MHz), interesting results have been gathered. It was determined that distortion is ever present and changes as a function of the environment. From the results of the experiment, some major contributors to frequency selective fading were determined. Among the most disturbing factors appear to be hills and the number of reflectors presents (high buildings, river, etc.). For a small bandwidth a large number of reflectors does not seem to destroy the signal from the point-of-view of the frequency selectivity. In comparison, diffraction effects would appear to have a major influence as the presence of hills along the propagation path between the transmitter and mobile receiver has been shown to cause important frequency selective fadings. In view of the strong influence of diffraction phenomena, it would be interesting to conduct similar measurements at much greater distances (far in the excess of 10 km) where the diffraction effects over the horizon might be dominant. It is also the first time that results show the cumulative distribution for a specific bandwidth for different environments over a large area rather than a small path.

Three types of frequency selective behaviours have been observed for the envelope of the signal; 1: A little reduction of the value of the correlation function over 128 kHz. 2: A Gaussian

form of correlation function. 3: An irregular correlation function with a sharp decrease before a 32 kHz bandwidth followed by a flat level of correlation. Moreover, for each site, the coherence bandwidth has been computed. The results are summarized in Table 2. These curves suggest the presence of an important reflection arriving with a large delay and therefore an important intersymbol interference between consecutive symbols.

The effects of the frequency selective fading on PER become important only for very high SNR. At SNR of 10 or 20 dB, the PER is relatively constant at 4.6×10^{-2} or 5.0×10^{-3} respectively and relatively independent of frequency selective fading. For an infinite SNR the PER ranges from 1.2×10^{-5} to 11.9×10^{-5} for 9600 bauds and from 4.8×10^{-5} to 49.0×10^{-5} for 19200 bauds.

The results of the present experiment indicate that, most of the time, narrow band analog communications will not be seriously affected by frequency selective fading distortions. On the other hand, ever present phase distortion may cause intersymbol interference during digital communications and therefore increase the bit error rate.

APPENDIX

Bit Error Probability for a Frequency Selective Channel

The following equations are excerpted from the papers of Bello and Nelin [3,4,5,6] and Lindenlaub and Baily [1,24].

The computation of the Probability of Error (PER) of one bit is derived for a Differential Phase Shift Keing (DPSK) modulation scheme. The expressions obtained at the end of the Appendix may not be generalized for other type of digital modulation schemes. However, the development method is the same for other types of modulation. The signal is assumed to be corrupted only by an additive white noise and the clock recovery is assumed to be perfect, an impossible task for a practical system. The demodulator consists of by a differentially coherent matched filter receiver with L diversity branches as shown in figure A-1. The other assumptions are that only two possible signals $s_0(t)$ and $s_1(t)$ are transmitted. The transmitted bit is assumed to be encoded into the change (bit = 0) or lack of change (bit = 1) of two adjacent pulses. The signal is transmitted through a channel corrupted by frequency selective fading and is received by a differentially coherent filter receiver.

The received signal, in the frequency domain, is expressed by

$$Y_k(f) = S(f)T_k(f) + N_k(f) \tag{A.1}$$

where $S(f)$ is the transmitted signal ($S_0(f)$ or $S_1(f)$), $T_k(f)$ is the channel transfer function, $N_k(f)$ is the spectrum of the complex envelope of the additive Gaussian noise and k is the index denoting the diversity branches. The complex envelope of the sample output of the undelayed matched filter receiver is (see Fig.A-1)

$$V_k = \int_{-\infty}^{\infty} [S(f)T_k(f) + N_k(f)][S_1^*(f) - S_0^*(f)]df \tag{A.2}$$

and the output of the delayed matched filter receiver is

$$U_k = \int_{-\infty}^{\infty} e^{-j2\pi fT}[S(f)T_k(f) + N_k(f)][S_1^*(f) - S_0^*(f)]df \tag{A.3}$$

here * denotes the complex conjugate.

The input to the threshold device is a random variable q given by

$$q = \sum_{k=1}^{L} [U_k^* V_k + U_k V_k^*] \tag{A.4}$$

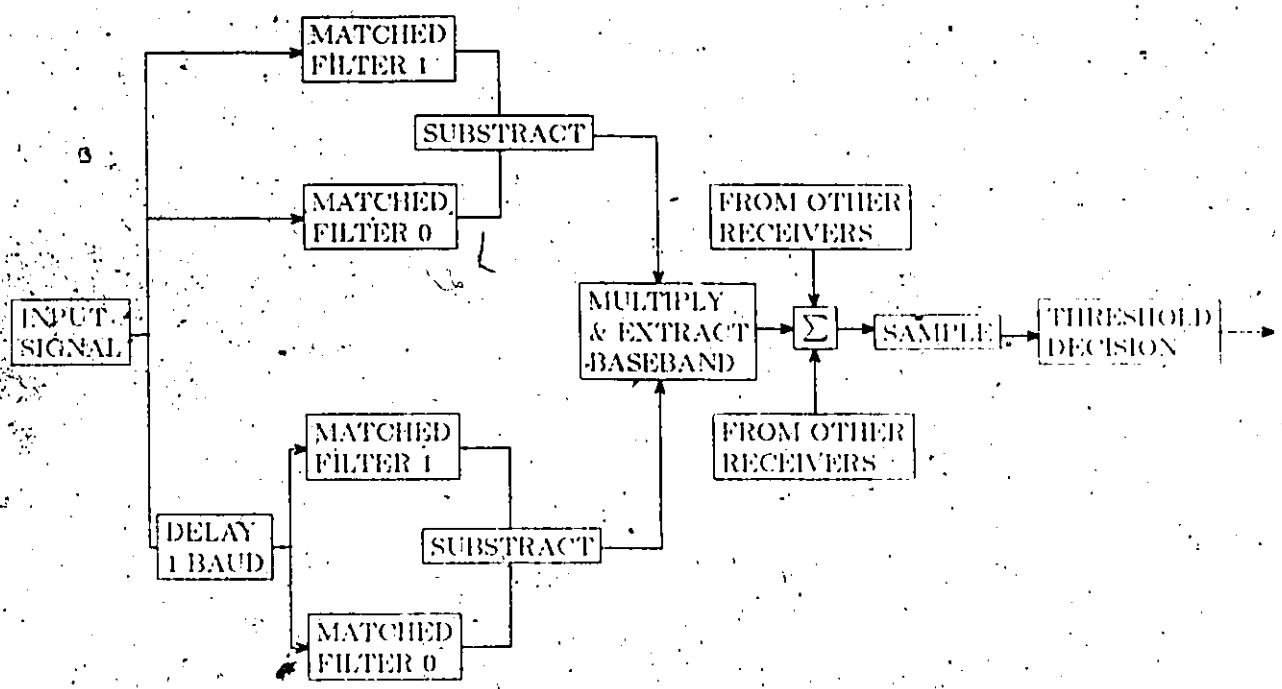

FIGURE A.1 (a) : Block diagram of differentially coherent matched filter

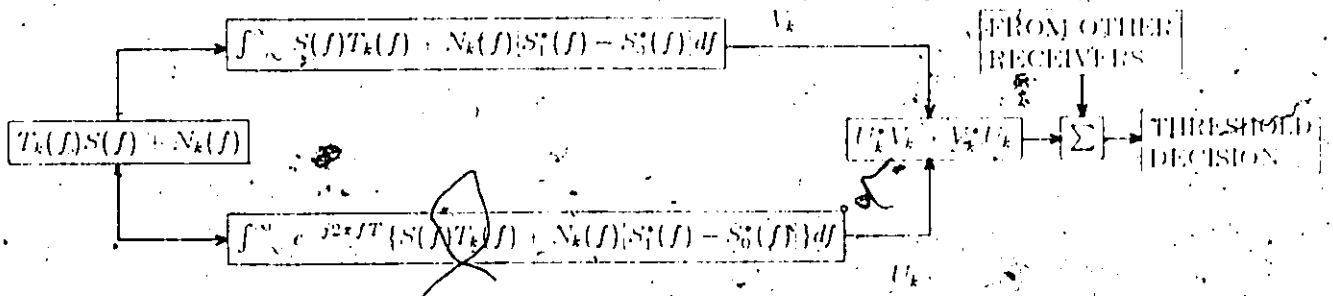

FIGURE A.1 (b) : Mathematical operations in a differentially coherent matched filter receiver.

where L is the maximum number of receiver branches. The threshold is set at 0. If $q > 0$ the bit received is a 1 and if $q < 0$ the bit received is a 0. U_k and V_k are complex-valued Gaussian random variables. Equation (A.4) is a special case of the quadratic form

$$q = \sum_{k=1}^{L} a|U_k|^2 + b|V_k|^2 + cU_k^* V_k + c^* U_k V_k^* \tag{A.5}$$

where a, b, c, c^* are constant.

It was shown by Bello and Nelin [3] that the probability that q is superior to 0 and inferior to 0 are respectively:

$$Pr(q > 0) = \left[\frac{1+\gamma}{2}\right]^L \sum_{m=0}^{L-1} \frac{1}{(2+\gamma)^m} C_m^{L-1+m} \equiv F_L(\gamma) = G_L\left(\frac{-\gamma}{1+\gamma}\right) \tag{A.6}$$

and

$$Pr(q < 0) = \left[\frac{1}{2+\gamma}\right]^L \sum_{m=0}^{L-1} \left[\frac{1+\gamma}{2+\gamma}\right]^m C_m^{L-1+m} \equiv G_L(\gamma) \tag{A.7}$$

where C means the mathematical operation of combination and the parameter γ is given by

$$\gamma = \frac{\frac{-(p_{11}+p_{00})}{\det P}}{\sqrt{\left[\frac{p_{11}+p_{00}}{2\det P}\right]^2 - \frac{1}{\det P}} + \frac{p_{11}+p_{00}}{2\det P}} \tag{A.8}$$

with

$$P = \begin{bmatrix} p_{11} & p_{10} \\ p_{10}^* & p_{00} \end{bmatrix} = \begin{bmatrix} m_{11} & m_{10} \\ m_{10}^* & m_{00} \end{bmatrix} \begin{bmatrix} a & c \\ c^* & b \end{bmatrix} \tag{A.9}$$

and

$$m_{11} = \overline{|U_k|^2}; \quad m_{10} = \overline{U_k^* V_k}; \quad m_{00} = \overline{|V_k|^2}. \tag{A.10}$$

The overline indicates an ensemble average and det is the determinant of matrix P. For the differentially coherent receiver $a = b = 0$ and $c = 1$ It follows that γ simplifies to

$$\gamma = \frac{2(m_{10}+m_{10}^*)}{\sqrt{(m_{10}+m_{10}^*)^2 + 4(m_{11}m_{00} - |m_{10}|^2)} - (m_{10}+m_{10}^*)} \tag{A.11}$$

where m_{rs}, for r and $s = 0$ or 1, is expressed by

$$m_{rs} = \int\int \overline{[S^*(f)T_k^*(f) + N_k^*(f)][S(l)T_k(l) + N_k(l)]} e^{j2\pi(f-l)\tau} [S_1(f) - S_0(f)][S_1^*(l) - S_0^*(l)] df\, dl \tag{A.12}$$

If we set the correlation function of the channel $R(\Omega)$ as

$$R(\Omega) = \overline{T_k^*(f) T_k(f+\Omega)} \tag{A.13}$$

where Ω is the frequency separation between two tones and express the noise as

$$\overline{N_k^*(f_1)N_k(f_2)} = 4N_0\delta(f_1 - f_2) \tag{A.14}$$

where N_0 is the noise power in the channel, then

$$m_{rs} = \int_{-\infty}^{\infty} R(\Omega)\lambda_{rs}(\Omega)d\Omega + 4N_0 b\delta_{rs} \tag{A.15}$$

where

$$\lambda_{rs}(\Omega) = \int_{-\infty}^{\infty} S^*(f)e^{j2\pi rfT}[S_1(f)-S_0(f)]\cdot S(f+\Omega)e^{-j2\pi s(f+\Omega)T}[S_1^*(f+\Omega)-S_0^*(f+\Omega)]df \tag{A.16}$$

$$b = \int_{-\infty}^{\infty} |S_1(f) - S_0(f)|^2 df \tag{A.17}$$

and

$$\delta_{rs} = \begin{cases} 1; & r = s \\ 0; & r \neq s \end{cases} \tag{A.18}$$

If we define

$$B_r(\tau) = \int_{\infty}^{\infty} S^*(f)e^{j2\pi rfT}[S_1(f) - S_0(f)]e^{j2\pi f\tau}df \tag{A.19}$$

then

$$\lambda_{rs}(\Omega) = \int_{\infty}^{\infty} B_r(\tau)B_s^*(\tau)e^{j2\pi\Omega\tau}d\tau \tag{A.20}$$

and if one substitutes A.20 in A.15

$$m_{rs} = \int_{-\infty}^{\infty} p(\tau)B_r(\tau)B_s^*(\tau)d\tau + 4N_0 b\,delta_{rs} \tag{A.21}$$

where $p(\tau)$ is the Fourier transform of $R(\Omega)$, then

$$p(\tau) = \int_{\infty}^{\infty} R(\Omega)e^{-j2\pi\tau\Omega}d\Omega \tag{A.22}$$

If bit '1' is transmitted by a lack of change and bit '0' is transmitted by a change of two adjacent pulses, then the two error probabilities of concern are given by

$$\begin{aligned} p_0 &= \frac{1}{2}Pr[q > 0 | s(t) = s_1(t+T) + s_0(t); -T < t < T] \\ &+ \frac{1}{2}Pr[q > 0 | s(t) = s_0(t+T) + s_1(t); -T < t < T] \end{aligned} \tag{A.23}$$

which is the probability of error of decoding bit '0' while bit '1' is transmitted, and by

$$\begin{aligned} p_1 &= \frac{1}{2}Pr[q < 0 | s(t) = s_0(t+T) + s_0(t); -T < t < T] \\ &+ \frac{1}{2}Pr[q < 0 | s(t) = s_1(t+T) + s_1(t); -T < t < T] \end{aligned} \tag{A.24}$$

which is the probability of error of decoding bit '1' while bit '0' is transmitted. As already stated, the frequency selective fading caused by the channel introduces excessive intersymbol interference which results in an erreducible PER. If the degree of frequency selective fading is small enough, intersymbol interference effects need to be considered only from pulses adjacent to the interval of time $-T < t < T$. Assuming that 1's and 0's have equal probabilities of being transmitted, the probability p_0 that a '1' may be detected when a transition is transmitted (a '0') can be expressed as

$$p_0 = \frac{1}{8}\sum_{a=0}^{1}\sum_{b=0}^{1}\sum_{c=0}^{1} p_{ab\bar{b}c} \tag{A.25}$$

where

$$p_{ab\bar{b}c} = Pr[q > 0 | s(t) = s_{ab\bar{b}c}(t)] \tag{A.26}$$

Also $s_{ab\bar{b}c}(t)$ is equal to that portion of $s(t)$, the transmitted signal corresponding to the transmission of the bit sequence $ab\bar{b}c$. Here a, b, c represent the transmitted waveform, either $s_0(t)$ or $s_1(t)$. The transmission of a '0' is a change of waveform expressed by $\bar{b}$. The probability that a '0' is detected when no transition (a '1' is transmitted) occurred is

$$p_1 = \frac{1}{8}\sum_{a=0}^{1}\sum_{b=0}^{1}\sum_{c=0}^{1} p_{abbc} \tag{A.27}$$

$$p_{abbc} = Pr[q < 0 | s(t) = s_{abbc}(t)] \tag{A.28}$$

or expressed in terms of γ (equ. A.6 to A.10)

$$p_0 = \frac{1}{8}\sum_{a=0}^{1}\sum_{b=0}^{1}\sum_{c=0}^{1} F_L(\gamma_{ab\bar{b}c}) \tag{A.29}$$

$$p_1 = \frac{1}{8}\sum_{a=0}^{1}\sum_{b=0}^{1}\sum_{c=0}^{1} G_L(\gamma_{abbc}) \tag{A.30}$$

These general expressions of error probabilities are now specialized for a DPSK signal with a channel having a Gaussian shaped frequency correlation function defined as

$$R(\Omega) = 2\sigma^2 \exp[-4\Omega^2/B_c^2] \tag{A.31}$$

with its time domain equivalent

$$r(\tau) = \sigma^2\sqrt{\pi}B_c \exp[-(\pi B_c \tau/2)^2] \tag{A.32}$$

Here B_c is defined as the frequency spacing between the $1/e$ points on the frequency correlation curve. This definition of the coherence bandwidth is more easily applicable to computation. The

quantity σ^2 is equal to the average power that would be received when a sinusoid of unity peak value is transmitted.

Because of the assumption that intersymbol interference effects are caused only by adjacent bits only, $p(\tau)$ must have negligible value for $|\tau| > T$. This means that the data rate $1/T$ must be sufficiently small compared to B_c. If we define the normalized data rate as $d = 1/TB_c$, then provided $d < \pi/4 = 0.7854$, 99.5% of $p(\tau)$ area is concentrated in the interval $|\tau| < T$.

Consider now the specific example where

$$s_1(t) = \sqrt{\frac{2E}{T}}; \quad 0 < t < T \tag{A.33}$$

$$s_0(t) = -\sqrt{\frac{2E}{T}}; \quad 0 < t < T \tag{A.34}$$

As established by Bello in [5] the error probabilities p_0 and p_1 are not symmetrical if frequency selectivity is present. However, because of symmetrical conditions in DPSK the PER caused by the sequence of symbols $abcd$ is equal to the PER caused by other sequences of symbols.

$$p_{abcd} = p_{\overline{abcd}} \tag{A.35}$$

$$p_{dcba} = p_{abcd} \tag{A.36}$$

therefore

$$p_0 = \frac{1}{4}[p_{0101} + p_{1100} + 2p_{0100}] \tag{A.37}$$

$$p_1 = \frac{1}{4}[p_{0110} + p_{1111} + 2p_{0111}] \tag{A.38}$$

and the total system probability of error if we suppose $s_1(t)$ and $s_0(t)$ equally probable is given by

$$P_e = \frac{1}{2}[p_0 + p_1]. \tag{A.39}$$

provided we defined an 'equivalent' Signal-to-Noise Ratio (SNR) ρ as

$$\rho_{abbc} = \gamma_{abbc} \tag{A.40}$$

$$\rho_{\overline{abbc}} = \frac{-\gamma_{abbc}}{1 + \gamma_{abbc}} \tag{A.41}$$

These equations are related to the real SNR of the received signal defined as $\rho = \sigma^2 E/N_0$ (see Table A-3). The general conditional error probability is expressed as

$$p_{abcd} = G(\rho_{abcd}) \tag{A.42}$$

$$p_1 = \frac{1}{4}[G_L(\rho_{0101}) + G_L(\rho_{1100}) + 2G_L(\rho_{0100})] \qquad (A.43)$$

$$p_0 = \frac{1}{4}[G_L(\rho_{0110}) + G_L(\rho_{1111}) + 2G_L(\rho_{0111})] \qquad (A.44)$$

The B function (equ. A.19) corresponding to a specific received signal sequence S_{abcd} is conveniently designated as

$$B_\tau^{abcd}(\tau) = \int_{-\infty}^{\infty} s_{abcd}(t - \tau T)[s_1(t+\tau) - s_0(t+\tau)]dt \qquad (A.45)$$

For the case we are considering, s_0 and s_1 are real and anticorrelated, so (A.45) becomes

$$B_\tau^{abcd} = 2\int_{-\infty}^{\infty} s_{abcd}(t - \tau T)s(t+\tau)dt \qquad (A.46)$$

where $s_1(t) = -s_0(t) = s(t)$. To compute the moments $m_{\tau\sigma}^{abcd}$ we use the following equation

$$m_{\tau\sigma}^{abcd} = \int_{-\infty}^{\infty} p(\tau)B_\tau^{abcd}(\tau)B_\sigma^{abcd}(\tau)d\tau + 32EN_0\delta_{\tau\sigma} \qquad (A.47)$$

The following steps will be used to determine p_e, the system probability of error :

1. Determine $B_\tau^{abcd}(\tau); a, b, c, d; \tau = 0, 1$ from equ. (A.46) for a value of τ in the interval $(-T, T)$, since only such value of τ is relevant when the intersymbol interference is caused only by adjacent pulses.

2. Determine $m_{\tau\sigma}^{abcd}$ with a chosen correlation function, namely a Gaussian correlation function for the present case, with equation (A.47).

3. Compute γ_{abcd} from equation (A.11) and find ρ_{abbc} and $\rho_{\bar{a}\bar{b}\bar{b}c}$.

4. Compute $G_L(\rho_{abcd})$ from equation (A.7) for the value used in (A.43) and (A.44)

5. Compute p_0, p_1 and finally p_e.

The values of B_τ^{abcd} , $m_{\tau\sigma}^{abcd}$ and ρ_{abcd} are in table A-1 to A-3. These values are from [24]. The curves of PER are drawn in figure A-2. This figure shows clearly that even with an infinite SNR there is an irreducible error rate present in any DPSK mobile radio communications. Others types of correlation functions and/or signals can be used [24], but it is not the aim of this study. Meanwhile it is worthy to rewrite some conclusions from Lindenlaub and Bailey [24].

1. A bandlimited or compact spectrum should be preferable to one whose spectrum is 'spread out' when using a random channel communication system near its irreducible error probability.

2. The system performance is not as sensitive to the shape of the channel frequency correlation function as it is to the shape of the transmitted signal.

The remark 2 is linked to the remark 1 in the sense that a 'smooth' signal produces a narrower spectrum than a square wave.

TABLE A-1: VALUES OF B_τ^{abcd}

$$
\begin{aligned}
B_0^{1111}(\tau) &= 4E && , \ |\tau| < T \\
B_1^{1111}(\tau) &= 4E && , \ |\tau| < T \\
B_0^{0110}(\tau) &= \begin{cases} 4E(1+2\tau/T) \\ 4E \end{cases} && \begin{matrix} , -T < \tau \leq 0 \\ , \ 0 < \tau < T \end{matrix} \\
B_1^{0110}(\tau) &= \begin{cases} 4E \\ 4E(1-2\tau/T) \end{cases} && \begin{matrix} , -T < \tau \leq 0 \\ , \ 0 < \tau < T \end{matrix} \\
B_0^{0111}(\tau) &= 4E && , \ |\tau| < T \\
B_1^{0111}(\tau) &= B_1^{0110}(\tau) && , \ |\tau| < T \\
B_0^{0101}(\tau) &= 4E(-1+2|\tau|/T) && , \ |\tau| < T \\
B_1^{0101}(\tau) &= 4E(-1-2|\tau|/T) && , \ |\tau| < T \\
B_0^{1100}(\tau) &= -B_1^{0110}(\tau) && , \ |\tau| < T \\
B_1^{1100}(\tau) &= B_0^{0110}(\tau) && , \ |\tau| < T \\
B_0^{0100}(\tau) &= B_0^{1100}(\tau) && , \ |\tau| < T \\
B_1^{0100}(\tau) &= B_1^{0101}(\tau) && , \ |\tau| < T
\end{aligned}
$$

TABLE A-2: VALUES OF m_{rs}^{abcd}

$$
\begin{aligned}
m_{00}^{1111} &= 32E(\sigma_0^2 E + N_0) \\
m_{11}^{1111} &= m_{00}^{1111} \\
m_{10}^{1111} &= 32\sigma_0^2 E^2 \\
m_{00}^{0110} &= 32\sigma_0^2 E^2(1 - 4c_1 d + 4c_2 d^2) + 32EN_0 \\
m_{11}^{0110} &= m_{00}^{0110} \\
m_{10}^{0110} &= 32\sigma_0^2 E^2(1 - 4c_1 d) \\
m_{00}^{0111} &= m_{00}^{1111} \\
m_{00}^{0111} &= m_{00}^{0110} \\
m_{10}^{0111} &= 32\sigma_0^2 E^2(1 - 2c_1 d) \\
m_{00}^{0101} &= 32\sigma_0^2 E^2(1 - 8c_1 d + 8c_2 d^2) + 32EN_0 \\
m_{11}^{0101} &= m_{00}^{0101} \\
m_{10}^{0101} &= -32\sigma_0^2 E^2(1 - 8c_1 d + 8c_2 d^2) \\
m_{00}^{1100} &= m_{00}^{0110} \\
m_{11}^{1100} &= m_{00}^{0110} \\
m_{10}^{1100} &= -m_{10}^{0110} \\
m_{00}^{0100} &= m_{00}^{0110} \\
m_{11}^{0100} &= m_{00}^{0101} \\
m_{10}^{0100} &= -32\sigma_0^2 E^2(1 - 6c_1 d + 4c_2 d^2)
\end{aligned}
$$

where $c_1 = 1/\pi\sqrt{\pi}$ and $c_2 = 1/\pi^2$.

TABLE A-3 : VALUES OF ρ_{abcd}

$$\rho_{1111} = 2\rho$$

$$\rho_{0110} = \frac{2\rho(1-4c_1 d)}{1+\rho(4c_2 d^2)}$$

$$\rho_{0111} \approx \frac{2\rho(1-2c_1 d)}{(1+\rho)(1-2c_1 g(\rho)d + 2d^2[c_2 g(\rho) - c_1^2 g^2(\rho)]) - \rho(1-2c_1 d)}$$

$$\rho_{0101} = 2\rho(1-8c_1 d + 8c_2 d^2)$$

$$\rho_{1100} = \rho_{0110}$$

$$\rho_{0100} \approx \frac{2\rho(1-6c_1 d + 4c_2 d^2)}{(1+\rho)(1-6c_1 g(\rho)d + 2d^2[3c_2 g(\rho) - c_1^2 g^2(\rho)]) - \rho(1-6c_1 d + 4c_2 d^2)}$$

where $\rho = \frac{\sigma^2 E}{N_0}$, $d = \frac{1}{TB_c}$, $c_1 = \frac{1}{\pi\sqrt{\pi}}$, $c_2 = \frac{1}{\pi^2}$, $g(\rho) = \frac{\rho}{1+\rho}$

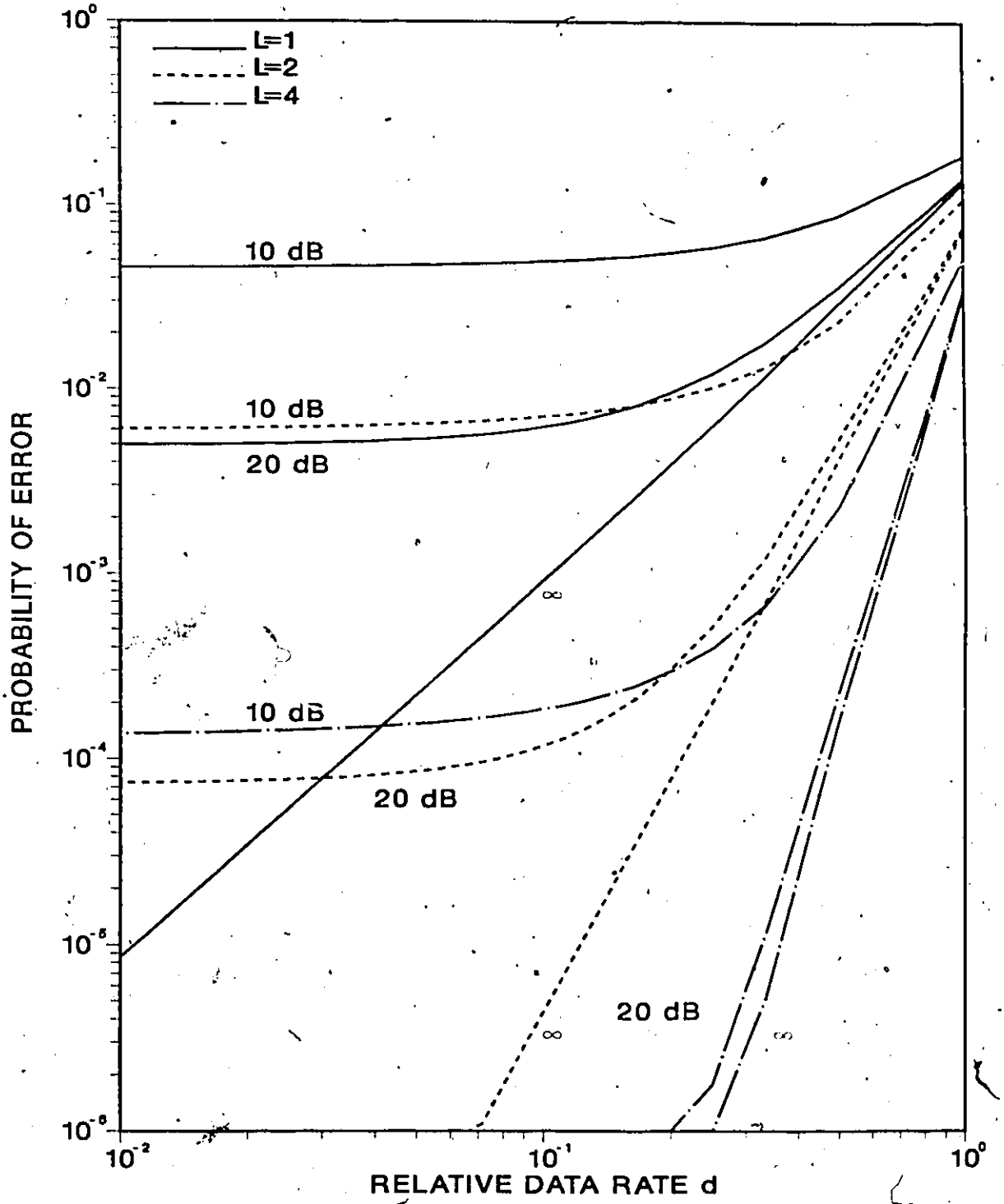
L=1
L=2
L=4
10 dB
10 dB
20 dB
10 dB
20 dB
20 dB
PROBABILITY OF ERROR
RELATIVE DATA RATE d
10^{0}
10^{-1}
10^{-2}
10^{-3}
10^{-4}
10^{-5}
10^{-6}
10^{-2}
10^{-1}
10^{0}

BIBLIOGRAPHY

1. Bailey, C.C. and Lindenlaub, J.C. 'Further Results Concerning the Effect of Frequency Selective Fading on Differentially Coherent Matched Filter Receivers', *IEEE Trans. on Communications Technology*, pp. 749-750, Oct. 1968.

2. Bajwa, A.S. and Parsons, J.D. 'Small Area Characterisation of UHF Urban and Suburban Mobile Radio Propagation', *IEE Proc.*, Vol. 129, Pt. F, No. 2, pp. 102-109, April 1982.

3. Bello, P.A. and Nelin, B.D. 'The Influence of Fading Spectrum on the Binary Error Probabilities of Incoherent and Differentially Coherent Matched Filter Receivers', *IRE Trans. on Communications Systems*, Vol. CS-10,pp. 160-168, June 1960.

4. Bello, P.A. and Nelin, B.D. 'Predetection Diversity Combining with Selectively Fading Channels', *IRE trans. on Communications Systems*, pp. 32-42, March 1962.

5. Bello, P.A. and Nelin, B.D. 'The Effect of Frequency Selective Fading on the Binary Error Probabilities of Incoherent and Differentially Coherent Matched Filter Receivers', *IEEE Trans. on communications Systems*, Vol. CS-11, pp. 170-186, June 1963.

6. Bello, P.A. and Nelin, B.D. 'Correction to " The Effect of Frequency Selective Fading on the Binary Error Probabilities of Incoherent and Differentially Coherent Matched Filter Receivers"', *IEEE Trans. on Communications Technology*, Vol. COM-12, pp. 230-231, Dec. 1964.

7. Bello, P.A. 'Measurement of the Complex Time-Frequency Channel Correlation Function', *Radio Science Journal of Research*, Vol. 68D, no 10, pp. 1161-1165, Oct. 1964.

8. Bello, P.A. 'Characterization of Randomly Time-Variant Linear Channels', *IRE trans. on Communications Systems*, pp. 366-393, Dec. 1978.

9. Bossé, E. *Simulation du canal de propagation pour les communications radio-mobile en milieu urbain, Thèse de Maitrise*, Université Laval, Québec, Canada, juin 1981.

10. Bultitude, R.J.C. *Measurement, Characterization and Modelling of 800/900 MHz Mobile Radio Channels for Digital Communications*, PhD Proposal, Carleton University, Sept. 1984.

11. Clarke, R.H. 'A Statistical Theory of Mobile-Radio Reception', *BSTJ*, pp.957-1000, July-August 1968.

12. Cox, D.C. 'Delay Doppler Characteristics of Multipath Propagation at 910 MHz in a Suburban Mobile Radio Environment', *IEEE Trans. on Antennas and Propagation*, Vol AP-20, No. 5,

pp. 625-635, Sept. 1972.

13. Cox, D.C. 'Time- and Frequency-domain Characterizations of Multipath Propagation at 910 Mhz in a Suburban Mobile-Radio Environment', *Radio-Science*, Vol. 7, No. 12, pp. 1069-1077, Dec. 1972.

14. Cox, D.C. and Leck, R.P. 'Correlation Bandwidth and Delay Spread Multipath Propagation Statistics for 910 MHz Urban Mobile Radio Channels', *IEEE Trans. on Communications*, Vol. COM-23, No. 11, pp. 1271-1280, NOv.1975.

15. Cox, D.C. 'Multipath Delay Spread and Path Loss Correlation for 910 MHz Urban Mobile Radio Propagation', *IEEE trans. on Vehicular Technology*, Vol. UT-26, No. 4, pp. 340-344, Nov. 1977.

16. Delisle, G. et al, *Etude des problemes de propagation associés aux stations emettrices et mobiles terrestres en milieu urbain*, Université Laval, Rapport LT-80-8223, pp. 18-26, Mars 1980.

17. French, R.C. 'Radio Propagation in London at 462 MHz', *The Radio and Electronic Engineer*, Vol. 46, No. 7, pp.333-336, July 1976.

18. French, R.C. 'Error Rate Predictions and Measurements in the Mobile Radio Data Channel', *IEEE Trans. on Vehicular Technology*, Vol. VT-27, No. 3, pp. 110-116, Aug. 1978.

19. Gans, M.J. 'A Power-Spectral Theory of Propagation in the Mobile-Radio Environment', *IEEE Trans. on Vehicular Technology*, Vol. VT-21, No. 1, pp. 27-38, Feb. 1972.

20. Hensen, F. and Meno, F.I. 'Mobile Fading - Rayleigh and Lognormal Superimposed', *IEEE trans, on Vehicular Technology*, Vol. VT-26, pp. 332-335, Nov. 1977.

21. Jakes, W. et al., *Microwave Mobile Communications*, Wiley-Interscience, 1974.

22. Lee, W.C.Y. *Mobile Communications Engineering.* New York: McGraw-Hill, 1982.

23. Lee, W.C.Y. 'Estimate of Local Average Power of a Mobile Radio Signal', *IEEE Trans. on Vehicular Technology*, Vol VT-34, pp.22-27, Feb. 1985.

24. Lindenlaub, J.C. and Bailey, C.C. *Digital Communication Systems Subject to Frequency Selective Fading*, School of Electrical Engineering, Perdue University, Lafayette, Ind., Tech. Rept. TR-EE67-17, Nov. 1967.

25. Papoulis, A. *Probability, Random Variables, and Stochastic Processes*, McGraw-Hill, 1965.

26. Parsons, J.D. and Bajwa, A.S. 'Wideband Characterisation of Fading Mobile Radio Channels', *IEE Proc.*, Vol. 129, Pt. F, No. 2, pp. 95-101, April 1982.

27. Proakis, J.G. *Digital Communications*, McGraw-Hill, 1983.

28. Pugh E.M. and Winslow, G.H. *The Analysis of Physical Measurements*, Addison-Wesley, 1966.

29. Schmid, H.F. 'A Prediction Model for Multipath Propagation of Pulse Signals at VHF and UHF Over Irregular Terrain, *IEEE trans. on Antennas and Propagation*, Vol AP-18, no. 2, pp. 253-258, March 1970.

30. Steel,R.G.D. and Torrie,J.H. *Principles and Procedures of Statistics*, McGraw-Hill, 1960.

31. Suzuki, H. 'A Statistical Model for Urban RAdio Propagation', *IEEE Trans. on Communications*, Vol. COM-25, No. 7, pp. 673-680, July 1977.

32. Turin, G.L. et al., 'A Statistical Model of Urban Multipath Propagation', *IEEE Trans. on Vehicular Technology*, Vol. VT-21, No. 1, pp. 1-9, Feb. 1972.